UNIVERSITY OF CALGARY

In-Situ Upgrading of Heavy Oil

by

Hai-Ying Helen Xu

A THESIS

SUBMITTED TO THE FACULTY OF GRADUATE STUDIES

IN PARTIAL FULFILMENT OF THE REQUIREMENTS FOR THE

DEGREE OF MASTER OF SCIENCE IN CHEMICAL ENGINEERING

DEPARTMENT OF CHEMICAL & PETROLEUM ENGINEERING

CALGARY, ALBERTA

JANUARY, 2001

ABSTRACT

Low temperature oxidation (LTO) of hydrocarbon liquids generally results in a more viscous end product; this has clearly been shown in the literature of the past 30 years. However, under the right conditions, LTO can be used to achieve viscosity reduction in heavy oils. The In-situ Combustion Group at the University of Calgary conceived of a two stage LTO process whereby oil is contacted with air, first at low, then at elevated temperatures. The first, low temperature step incorporates oxygen into some of the hydrocarbons, yielding labile bonds that should break at low temperatures. Once these free radicals are formed, the second step promotes bond cleavage at higher temperatures, resulting in shorter chain hydrocarbons. In a field situation, this process would be analogous to first injecting air into a formation at low temperature, then starting a steam soak or steam flood.

Experimental runs carried out on Athabasca bitumen examined the effects of oxygen partial pressure, temperature, reaction time, and the presence of rock and brine on the two-step process. On completion of each experiment, the gas composition was determined using gas chromatography, water acidity (pH) was measured, and the hydrocarbon products were analyzed for coke and asphaltenes contents, viscosity, and density. Some instances of viscosity reduction have been observed; these are linked to lower oxygen partial pressures, higher second stage temperatures and longer run times. This thesis discusses the experimental work, and estimates the optimum conditions for successful viscosity reduction of a given heavy oil.

ACKNOWLEDGMENTS

This Project would not have been possible to successfully complete without the direct support of several individuals. In particular, the author would like to sincerely thank Dr. R. Gordon Moore, the project supervisor, Dr. Nancy Okazawa, Dr. S.A. (Raj) Mehta, Mr. Mark Hancock, Ms. Elizabeth Zalewski, Mr. Matt Ursenbach, Dr. Cathy Laureshen, and Mr. Don Mallory of the In-situ Combustion Research Group at the University of Calgary, and to all the other members of the faculty, staff and fellow graduate students in the Department of Chemical and Petroleum Engineering at the University of Calgary who directly or indirectly helped with the project. The author would like to thank all family and friends who provided much moral support throughout the entirety of the project. The financial assistance provided by the Natural Sciences and Engineering Research Council of Canada (NSERC) and the Department of Chemical and Petroleum at the University of Calgary is also gratefully acknowledged.

TABLE OF CONTENTS

LIST OF TABLES

LIST OF FIGURES

NOMENCLATURE

A : pre-exponential factor, for Arrhenius Equation, mol/(m^3·Pa·s)

A_1: an empirical parameter in Andrade Equation, Pa·s

B : an empirical parameter in Andrade Equation, K

DTA: Differential Thermal Analysis

E_a : activation energy, J/mol

EDX: Energy Dispersive X-ray

EOS: Equation of State

ETS: Elevated Temperature Soak

GC: Gas Chromatography

H : Henry's law constant, (m^3·kPa)/kmol

k : reaction rate constant, $(mol/m^3)^{1-n} \cdot s^{-1}$

LTS: Low Temperature Soak

m_{oil}: mass of the input oil, g

n_{O2} : number of moles of oxygen, mol

n_{CO2} : number of moles for the product CO_2, mol

n_{CO} : number of moles for the product CO, mol

$n_{CnH2n+2}$: number of moles for the product hydrocarbon gas, mol

n : order of the reaction

P : total absolute pressure, kPa

PDSC: Pressure Differential Scanning Calorimetry

P_{H2O}: steam partial pressure at LTS, kPa

P_{HC}: hydrocarbon partial pressure, kPa

P_{O2} : oxygen partial pressure, kPa

P_{O2}^{0} : initial oxygen partial pressure, kPa

R : universal gas constant, J/mol·K

r : rate of the reaction, $mol/m^3 \cdot s$

SARA: Saturates, Aromatics, Resins, Asphaltenes analysis

T : temperature in absolute unit, K

TGA: Thermal Gravity Analysis

t : time, s

μ_o : oil viscosity, mPa·s

V_b : volume of the oil in the cell, m^3

V_g : volume of gas in the cell, m^3

WGSR: water gas shift reaction

y_{N2}^{0} : initial mole fraction of nitrogen obtained from the GC

y_{N2}: mole fraction of nitrogen obtained from the GC

y_{O2}^{0}: initial mole fraction of oxygen obtained from the GC

y_{O2}: mole fraction of oxygen obtained from the GC

y_{CO2}: mole fraction of the produced CO_2 obtained from the GC

y_{CO}: mole fraction of the produced CO obtained from the GC

$y_{CnH2n+2}$: mole fraction of the produced hydrocarbon gas obtained from the GC

z_m: compressibility factor of vapor phase

CHAPTER ONE INTRODUCTION

Heavy oil and oil sands are important hydrocarbon resources that are destined to play an increasingly important role in the oil supply of the world, and North America in particular. The heavy oil resources of the world total over 10 trillion barrels, nearly three times the conventional oil in place in the world. The oil sands of Alberta alone contain over three trillion barrels of oil. The importance of heavy oil can be appreciated by the fact that nearly 10% of the oil production in the USA and over 30% in Canada is from heavy oil and oil sands resources (Farouq Ali, 1999).

The important question is: how much of this oil is recoverable and what technique could be applied? With current production technologies only a small fraction of the available reserves can be recovered. In Alberta, recovery is low – 5 to 20% in better areas – because the main recovery method is cyclic steam stimulation (Farouq Ali, 1999). Therefore, new and improved recovery methods are required to more fully exploit this vast resource.

Many techniques have been used to assist the producer in the production and handling of heavy oil. The injection of energy by downhole combustion, steam drive, cyclic steam stimulation and steam assisted gravity drainage are the most common techniques. Thermal methods aim at reducing oil viscosity in order to increase its mobility, through the application of heat.

Thermal methods currently used by industry can be divided into two broad categories based on the changes that occur in the oil properties. The first category, and by far the most common in use today, includes those processes that, through the application of heat, cause viscosity reduction by increased molecular agitation, rather than by appreciable compositional changes in the oil. Hot water and steam flooding are examples of this kind of process. Although a great deal of research has been performed in developing and improving methods in this area, field experience has shown that the heat losses to the reservoir environment generally make them thermally inefficient.

The second category includes those processes whereby enough energy is supplied to extensively crack the heavy hydrocarbon molecules into lighter, less viscous species. An example of a process in this category is in-situ combustion. In-situ combustion involves injecting air or oxygen into the reservoir to burn a portion of the oil, which provides the heat required to reduce the viscosity of the remaining oil. As oxygen is injected and the in-situ oil ignited, a combustion front forms, pushing the oil towards a production well. This technique offers many theoretical advantages if the operational characteristics of the process are incorporated in the design and operation of the field project. The method has, however, seen only limited practical use in the petroleum industry.

One of the main difficulties encountered in the application of in-situ combustion processes is the Low-Temperature Oxidation or LTO reaction, where oxygen bypasses the front without reacting with it. Instead, the oxygen will react with reservoir oil ahead

of the front where the temperatures are lower than 300°C. Typically, the by-products of LTO reactions are oxidized hydrocarbons that have an increased polarity. This makes them more viscous and thus detrimental to the in-situ combustion process.

Because of the major impact of LTO on the performance of an in-situ combustion project, a significant number of investigations have been carried out on the nature and effect of LTO reactions. Due to the number of hydrocarbon components involved, only general reaction mechanisms have been identified. The available reaction mechanisms, however, provide a reasonable description of how LTO affects the chemical structures of the components making up a given oil.

Based on the available literature and their own experience in this area, the In-situ Combustion Group at the University of Calgary conceived a two-stage LTO process whereby oil is contacted with air, first at low, and then at elevated, temperatures. The low temperature step incorporates oxygen into some of the hydrocarbons, yielding labile bonds that should break at relatively low temperatures. Once initiating free radicals are formed, the second step promotes bond cleavage at higher temperatures, which results in shorter chain hydrocarbons. In a field situation, this process would be analogous to first injecting air into a formation at the native reservoir temperature, and then starting a high temperature steam flood. A preliminary experimental program to investigate this novel theory is described in this thesis.

CHAPTER TWO THEORETICAL BACKGROUND

2.1 LITERATURE REVIEW

A number of references are available which describe low-temperature oxidation measurements on crude oils. Dabbous and Fulton (1971) reported oxygen uptake rates and product gas compositions for a number of low temperature oxidation measurements on different oils. They also reported the presence of residual hydrocarbons following these tests. Burger and Sahuquet (1972) and Fassihi et. al (1986) described the product gas compositions that resulted when air was passed through an oil-saturated core while the core was heated under a linear heating schedule from room temperature to 500 °C. Thermogravimetric analysis (TGA), differential thermal analysis (DTA) and differential scanning calorimetry (DSC) studies have been reported by a number of authors [Bae (1977), Drici and Vossoughi (1985), Kharrat and Vossoughi (1985), Vossoughi, Bartlett and Willhite (1985), and Verkoczy and Jha (1985)] to provide useful information on the oxidation and fuel laydown characteristics of crude oils. These studies were generally aimed at providing screening tests for crude oil behaviour rather than kinetics models for describing oxygen uptake rates. They do not provide any information regarding the effect of oxidation on the oil composition.

Warren et al. (1959), Adegbesan et al. (1983), Babu and Cormack (1983, 1984), Phillips and Hsieh (1985), and Millour et al. (1987) have reported low-temperature oxidation data for Athabasca bitumen. Oxygen uptake rates for crude oils other than Athabasca bitumen have been described by Burger (1976), Tadema and Weijdema

(1970), Smith and Perkins (1973), Dabbous and Fulton (1971), and Meyers et al.(1986). Studies on the LTO of Athabasca bitumen described by Babu and Cormack (1984), show a decline in the aromatic content, an increase in asphaltenes content, and a stable saturates content. The same authors report a steady increase in coke production with the extent of oxidation. The overall trend is for a conversion from aromatics to resins, from resins to asphaltenes, and from asphaltenes to coke. This transformation to heavier, more polar components results in increased viscosities and densities.

It is well known [Emmanuel (1967)] that during any low-temperature oxidation process, liquid hydrocarbons undergo complicated chain reactions, which generally yield heavier and less reactive compounds. These reactions are applied in the air blowing techniques used in the asphalt industry [Lockwood (1959), Moschopedis and Speight (1977)]. It has been accepted that LTO causes undesirable changes in the chemical and physical properties of oil. It is a result of the changing oil composition, which occurs due to low-temperature oxidation reactions that gas phase data alone are of limited utility for developing an understanding of the oxidation process.

Moschopedis and Speight (1977), Adegbesan et al. (1983) and Millour et al. (1987) provided analytical data to illustrate the compositional changes occurring during low-temperature oxidation of Athabasca bitumen. Adegbesan et al. oxidized Athabasca bitumen in the absence of core and water by using various concentrations of oxygen. Compositional analyses were performed on the liquid products following specific oxidation times at each of a number of isotherms. In addition to the usual oxygen uptake

models, Adegbesan et al. presented a number of models describing the relationships between whole bitumen, coke, asphaltenes and maltenes. The experimental approach of Adegbesan was very similar to that developed by Hayashitani (1978) for studying the thermal cracking kinetics of Athabasca bitumen.

Because of the vast number of hydrocarbon species involved in the make-up of any oil, it is exceedingly difficult to characterize all of the individual oxidation reactions. Thus, generalized approaches have traditionally been used. As part of a kinetic study of the in-situ combustion processes, Burger and Sahuquet (1972) presented a generalized reaction scheme consisting of five basic oxidation reactions at the same temperature. The reactions include:

1) Oxidation to a carboxylic acid;

$$R - \underset{\underset{H}{|}}{\overset{\overset{H}{|}}{C}} - H + \frac{3}{2}O_2 \Rightarrow R - \underset{\underset{OH}{|}}{\overset{\overset{O}{\|}}{C}} + H_2O \qquad (2.1)$$

2) Oxidation to an aldehyde;

$$R - \underset{\underset{H}{|}}{\overset{\overset{H}{|}}{C}} - H + O_2 \Rightarrow R - \underset{\underset{H}{|}}{\overset{\overset{O}{\|}}{C}} + H_2O \qquad (2.2)$$

3) Oxidation to a ketone;

$$R - \underset{\underset{H}{|}}{\overset{\overset{H}{|}}{C}} - R' + O_2 \Rightarrow R - \overset{\overset{O}{\|}}{C} - R' + H_2O \qquad (2.3)$$

4) Oxidation to an alcohol;

$$R - \underset{\underset{R''}{|}}{\overset{\overset{R'}{|}}{C}} - H + \frac{1}{2}O_2 \Rightarrow R - \underset{\underset{R''}{|}}{\overset{\overset{R'}{|}}{C}} - O - H \qquad (2.4)$$

5) Oxidation to a hydroperoxide;

$$R - \underset{\underset{R''}{|}}{\overset{\overset{R'}{|}}{C}} - H + O_2 \Rightarrow R - \underset{\underset{R''}{|}}{\overset{\overset{R'}{|}}{C}} - O - O - H \qquad (2.5)$$

Based on an extensive experimental program, Adegbesan et al. (1987) used a more generalized approach, separating the LTO products into six separate pseudocomponents including: saturates, aromatics, resins 1, resins 2, asphaltenes, and coke. These pseudocomponents were then lumped into three functional groups (maltenes, resins, and asphaltenes / coke) of increasing molecular mass, for use in developing kinetic models of the process.

In some circumstances, however, it may be beneficial to subject oil to LTO. Cram and Redford (1977) reported improved results when injecting air/steam mixtures as opposed to steam alone in experiments involving the production of Athabasca oil in a 3-

D reservoir simulator apparatus. Their experimental results showed that certain air/steam combinations could result in better recovery rates and thermal efficiencies than steam alone, at comparable volumes of steam injected, when the process was carried out in the low temperature oxidation region. The authors believed that the heat contribution generated by the exothermic oxidation reactions has a significant effect on the oil recovery.

Isothermal low temperature oxidation studies which generated the data reported by Millour et al. (1987) confirmed that the low temperature oxidation reactions resulted in an increase in the viscosity of the oxidized oil; however, it was found that the oxidized oil samples underwent accelerated thermal cracking in terms of the rate of formation of the pseudo-component fractions compared to unoxidized samples of the same oil when subjected to the same reaction conditions (Millour et al. (1985)). Another finding of the isothermal low temperature oxidation study was that the presence of caustic in the aqueous phase resulted in a reduction in, or in the absence of, coke formation under reaction conditions where coke was normally formed. Based on the results of the cracking studies on oxidized oil samples and the modification of the low temperature oxidation products that resulted from the presence of caustic, it was postulated that air in the presence of caustic could provide a method for in-situ upgrading of heavy oils. A systematic study to evaluate this concept was undertaken by Wichert (1995).

Wichert's study was based on the concept that the presence of caustic can accelerate the oxidation of hydrocarbons allowing oxygen to be incorporated into the oil

structure at lower than expected temperatures. Since bonds involving oxygen tend to break more easily (i.e. at lower temperatures), free radical initiators can be generated more readily. Wichert postulated that, if the amount of caustic were strictly controlled, it would be possible for cracking-type bond scission reactions to dominate over undesirable polymerization type of oxidation reactions at lower-than-usual temperatures. While Wichert observed several instances of viscosity reduction, he concluded that even in the presence of caustic, it was not possible to achieve significant upgrading at the low temperatures without converting a significant proportion of the initial oil to coke (Wichert, 1995). As a result of Wichert's work, it was postulated by co-workers at the University of Calgary that splitting the process into two distinct steps would offer the most positive upgrading results. The first step would involve oxidation at low temperature, the second step would include heating to steam flood temperatures.

The presence of water is one condition that may be of importance. Lee and Noureldin (1989) reported that when the LTO of oil was carried out in the presence of water, the undesirable effects appear to be alleviated, as evidenced by a sharp decrease in the amount of coke formed. The viscosity and the acidity of the produced oil both declined. The process is accompanied by considerable CO_2 production, probably from the decarboxylation of acids produced by LTO. The lack of coke formation when water is present implies that less condensed, oxidized products are generated under aqueous conditions.

Water in the liquid or vapour phase may participate in the pyrolysis reactions. Such reactions are called aquathermolysis [Hyne (1984), Baviere (1997)]. Moreover, the presence of water may also encourage the formation of heteroatomic compounds concentrated in the solid phase. Baviere (1997) reported no change in the oxygen content of the oil phase during the process of heating the oil at 350 °C for 200 hours.

It is believed that the rock matrix, particularly the clays can have a catalytic effect on oxygen addition and oxygen induced cracking reactions. Depending on the composition of the reservoir matrix, the mineral phase itself can be affected by temperature and the presence of a water phase. Transition metals may also have a catalytic effect (Figure 2-1, Baviere, 1997).

It has generally been reported that clay minerals have a catalytic effect on cracking reactions, especially with regards to the formation of coke (Baviere, 1997). However, unpublished work performed by the In-Situ Upgrading Group at the University of Calgary has shown that the minerals have various effects on the compositional changes associated with cracking reactions.

In summary, the extent of LTO reactions that occur within a given reservoir depends on the reactivity of the oil, which is, in turn, a function of the oil composition, the nature of the core matrix and brine, the initial reservoir temperature, and the oxygen partial pressure.

Overall:

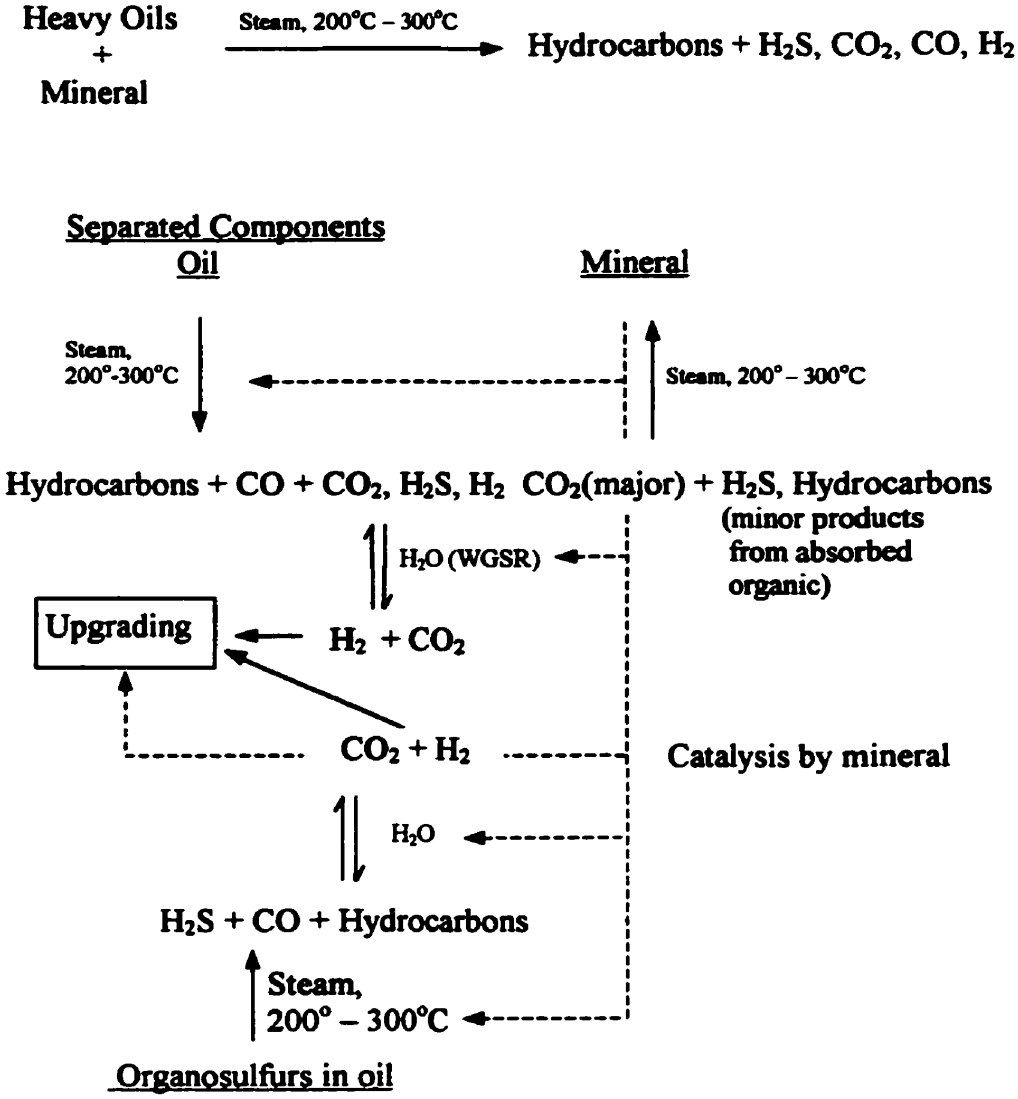

Figure 2.1: Aquathermolysis (Baviere, 1997)

2.2 RESEARCH OBJECTIVES

The current study, based mainly on the observations made during the aforementioned oxidation work carried out at the University of Calgary, investigated a process for viscosity reduction of heavy oils using a two-stage LTO process. The first stage consisted of contacting the oil with air at low temperatures in order to add oxygen into the hydrocarbon bond structures. This was followed by a treatment at elevated temperatures (typical of a relatively low pressure steam flood) that initiated free radical formation, especially at the oxygen sites. The desired result of the propagation of cleavage reactions was the generation of shorter chain (lighter) hydrocarbons. For the purposes of this thesis, the first stage of this process will be referred to as the Low Temperature Soak (LTS) and the second stage as the Elevated Temperature Soak (ETS).

The objective of this experimental program was to systematically investigate the effect of varying certain conditions on the two-step process, such as temperature, oxygen partial pressure, reaction time, and the presence of rock and brine, and furthermore, to estimate the optimum conditions for successful viscosity reduction of a given heavy oil. The ultimate goal of the work was to develop a process that would improve oil recovery and oil quality when applied in a field situation.

CHAPTER THREE EXPERIMENTAL

3.1 APPARATUS

The experimental apparatus is schematically shown in Figure 3.1. Figure 3.2 shows the detailed schematic of the reaction vessel. The specialised apparatus was designed and constructed in 1993 for the Wichert's study (Wichert, 1996). It consists of ten identical high-pressure three-phase batch reactors, each with inner volumes of 250 mL that can be operated simultaneously. Each cell is equipped with six-inch long type-K thermocouples in order to continuously monitor the inner gas and liquid temperatures. The cells are also attached to a high-pressure two-way valve. On one side of the valve is a quick-connect pressure fitting, which allows for the charging and sampling of the gas phase in the reactor. On the other side of the valve is a fitting that is used to attach a pressure transducer for continuous pressure measurement. A third port on each cell is included for pressure relief and is attached to a 28.6 MPa rupture disk. A quartz glass liner is used for each cell to protect the steel wall from brine corrosion. Figures 3.3 and 3.4 show photographs of the unassembled and assembled reactor cells, respectively.

Heat is supplied with flexible silicone strip heaters that are coiled around the outer surface of each cell. A thermocouple is inserted between the cell wall and the heater and used as the input signal in a PID control loop. Heater control and data acquisition is accomplished with a PC computer and National Instruments "Labview" process control software. Figure 3.4 also shows a reactor vessel with heat tape installed.

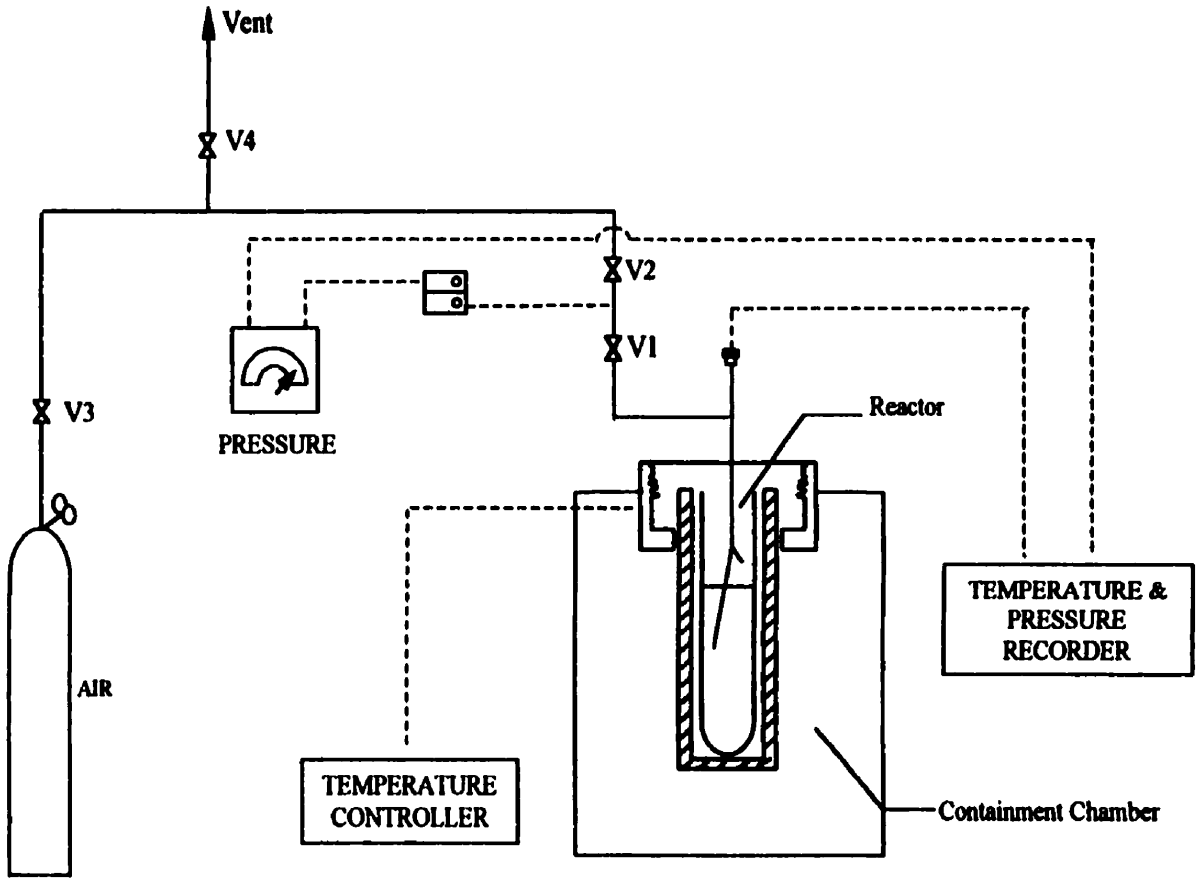

Figure 3.1: Schematic Drawing of Reaction Apparatus.

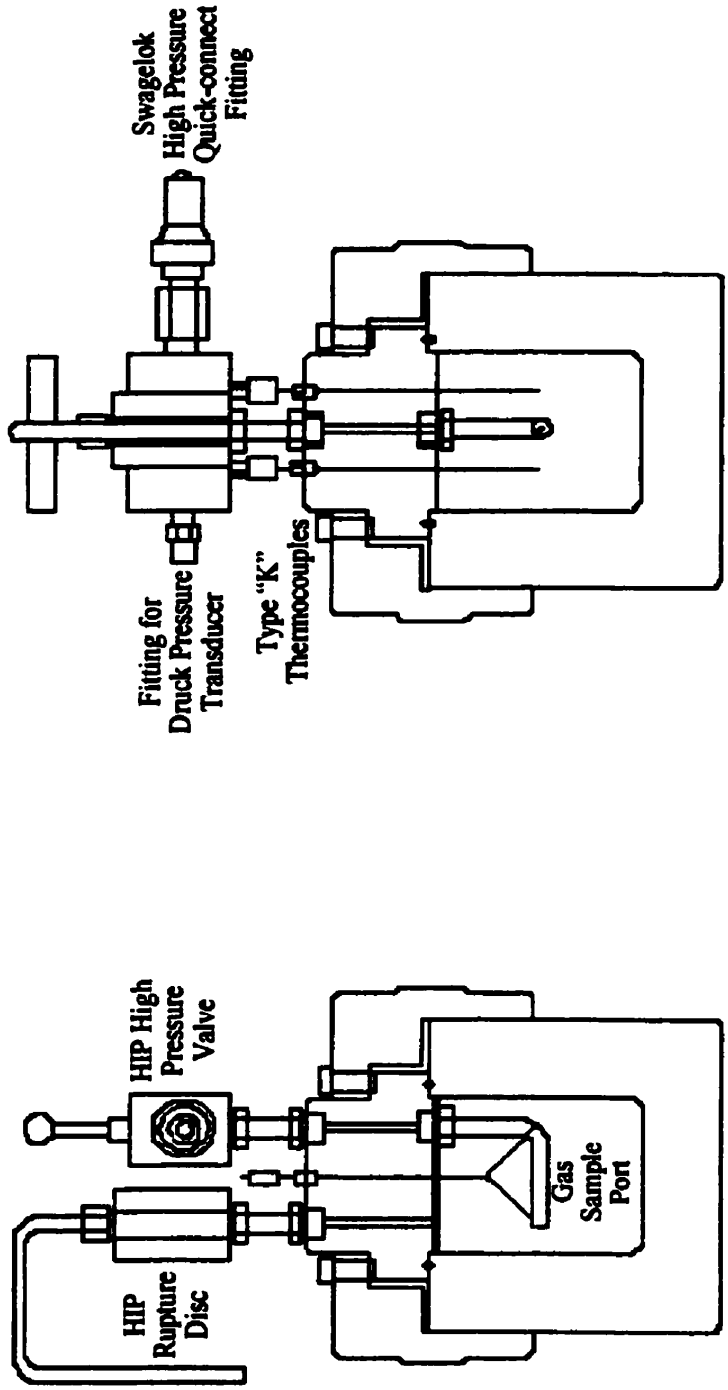

Figure 3.2 Schematic Diagram of a Pressure Cell

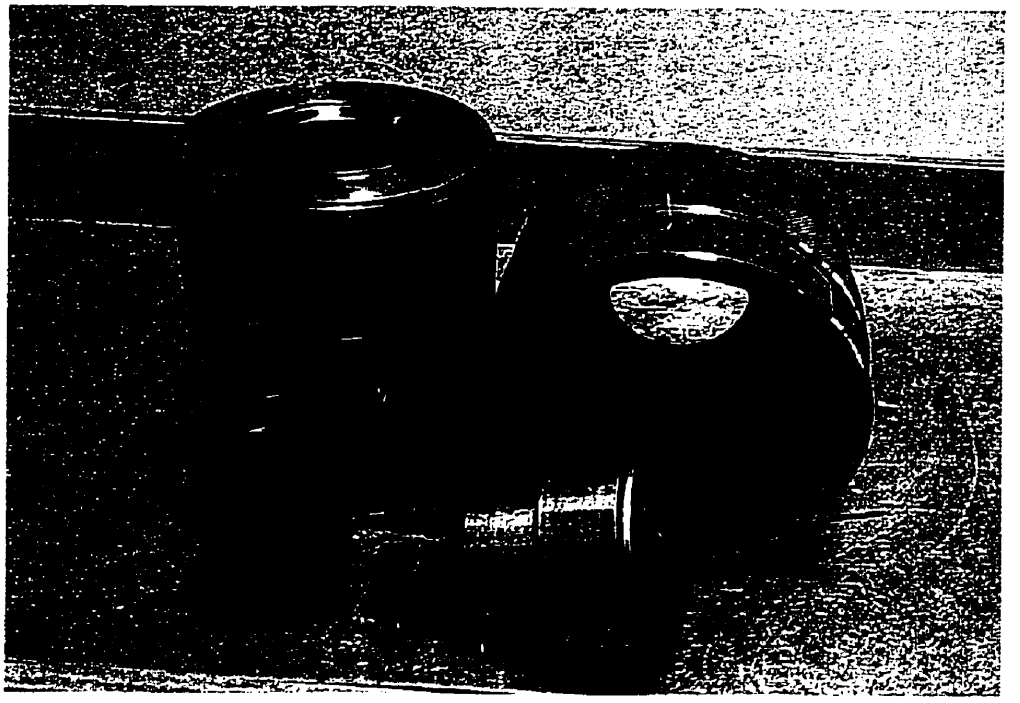

Figure 3.3: Unassembled Pressure Cell

Figure 3.4: Assembled Pressure Cells

A photograph of the heater control and data acquisition system appears in Figure 3.5.

Once the cells are filled, assembled, and heaters attached, they are mounted into individual bays on one of two rocker arms. Each bay is insulated with kaolinite wool. Each rocker arm is capable of holding five cells at once. Both arms are located inside a containment chamber, and are equipped with individual electric motor and transmission assemblies. The arms can be rotated approximately 10~30 degrees from the vertical, and rocking speeds can be varied from 0 to 11 rpm. Figure 3.6 shows a schematic diagram of the chamber showing the orientation of the rocker arms (Wichert, 1996). Photographs of the chamber and rocker arms appear in Figure 3.7 and 3.8. Figure 3.9 shows the containment chamber. The motor assemblies are mounted on the outside of the chamber, as shown in the photograph in Figure 3.10.

3.2 Experimental Materials

The materials used to formulate the synthetic reservoir core were as follows:

Heavy oil: The heavy oil used in this study was steam produced Athabasca bitumen from the Underground Test Facility (UTF) – Devon Mine operated by Northstar Petroleum near Fort McMurray, Alberta in 1998. The oil properties are provided in Table 3.1.

Brine: Table 3.2 lists the composition of the brine, which was synthetic Athabasca brine with a salinity of 1.6 % and a pH of 8.55

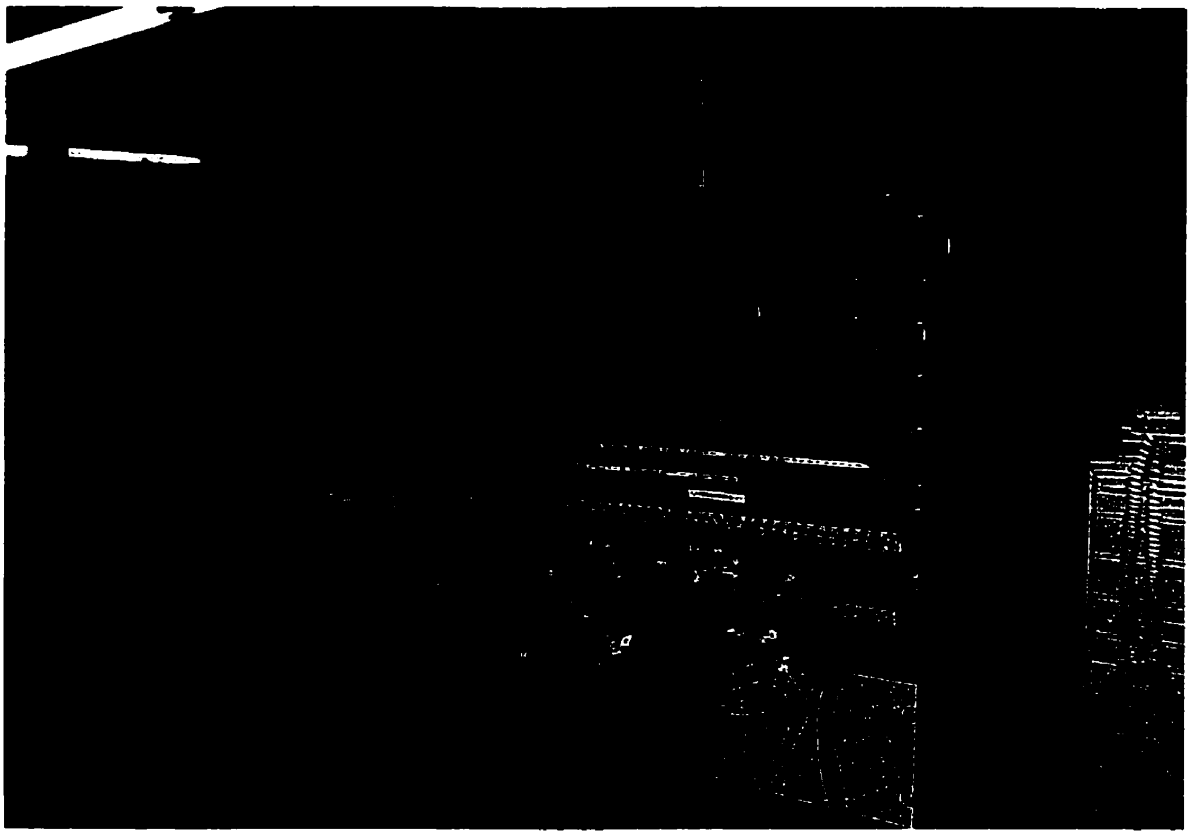

Figure 3.5: Control and Data Acquisition System

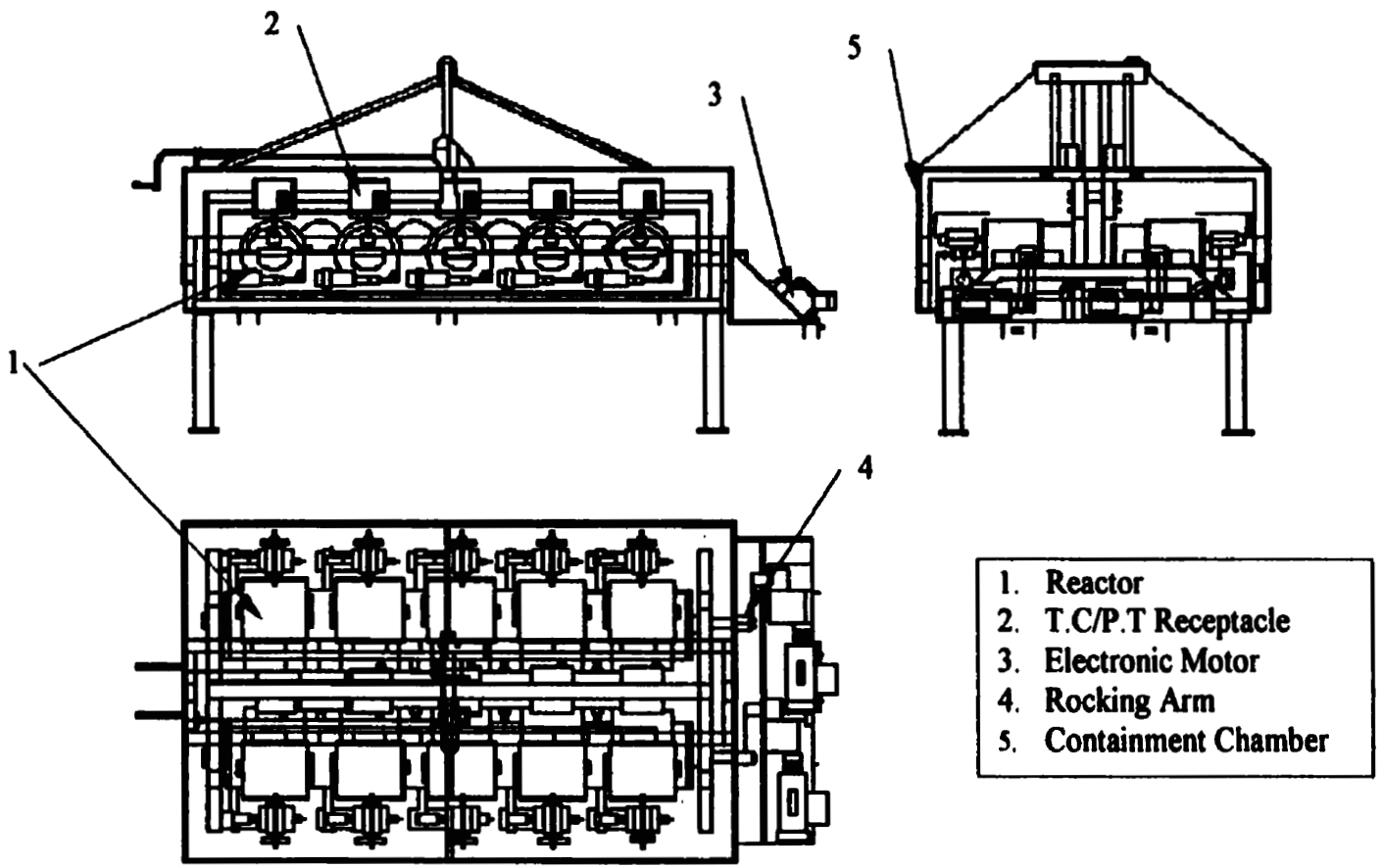

Figure 3.6 Schematic Diagram of the Containment Chamber (Wichert, 1996)

Figure 3.7: Pressure Cell Mounted in Rocker Arm

Figure 3.8: Mounted Pressure Cell – Final Assembly

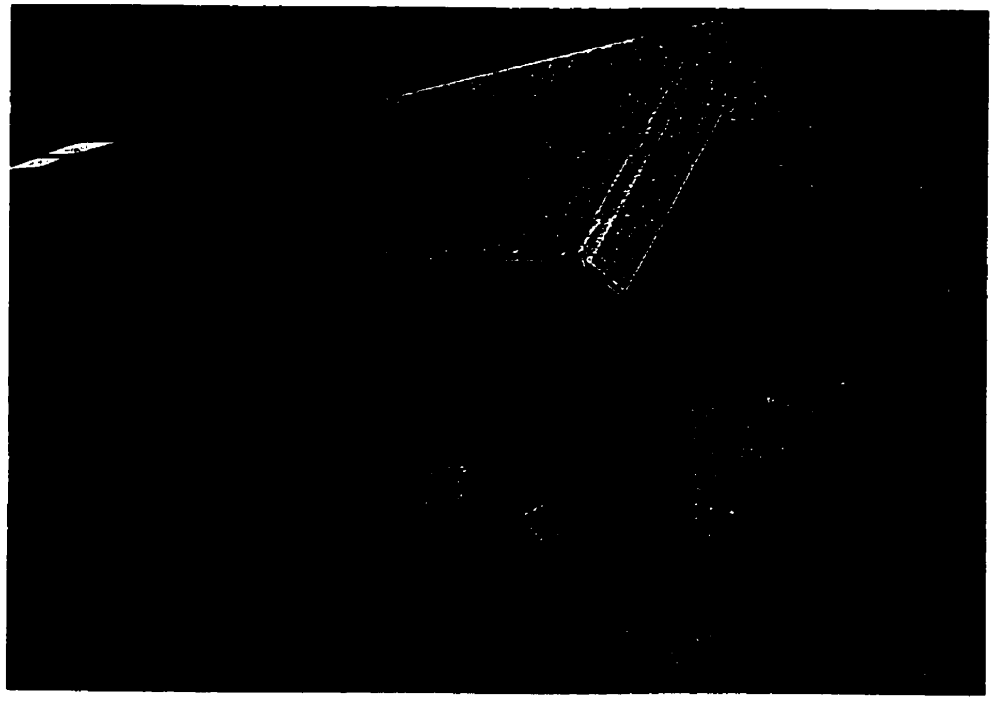

Figure 3.9: Containment Chamber

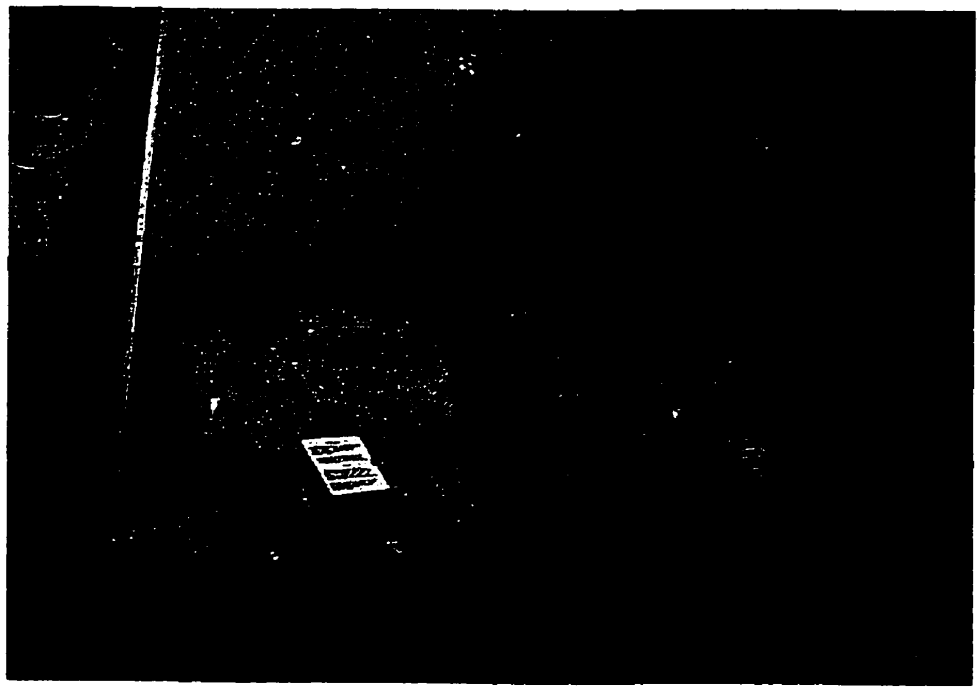

Figure 3.10: Motor and Transmission Assemblies

Table 3.1: Properties of Steam-Produced Athabasca Bitumen

Specific Gravity	25 / 25 °C	1.0138
Viscosity (mPa•s)	25 °C 40 °C 70 °C	218700 32250 1950
Composition	Asphaltenes Maltenes *Heavy Oils (C>40)** *Light Oils (C<40)***	(wt % of total oil) 17.85 82.15 *38.23* *43.92*

**Proportion of maltenes with C > 40*
***Proportion of maltenes with C < 40*

Table 3.2: Composition of Athabasca Brine

element	mg/l
Na^+	5623
Ca^{2+}	72
Mg^{2+}	134
K^+	45
Fe^{2+}, Fe^{3+}	1.5
CO_3^{2-}	27
HCO_3^-	3150
SO_4^{2-}	10
Cl^-	7615
SiO_2	~
OH^-	~
pH	8.55
Total Dissolved Solids	16686

Sand: The solids matrix was Athabasca sand; it was prepared by extracting core samples with toluene, followed by heating of the extracted sand to 316 °C for a period of 16 hours. The properties of the sand matrix are listed on Table 3.3.

Table 3.3: Properties of Athabasca Core

Tyler Sieve Analysis	
mesh size	in mass %
< 60	4.10
60 ~ 80	25.37
80 ~ 120	36.72
120 ~ 170	31.92
170 ~ 270	1.29
> 270	0.60
X-Ray Diffraction Analysis	
Quartz	93%
Potassium Feldspar	5%
Kaolinite (possibly Chlorite)	2%
Illite (possibly Mica)	Traces
EDX Analysis (Net counts)	
Al	1186 cts
Si	13500 cts
K	307 cts
Ti	60 cts
Fe	134 cts

The synthetic core was prepared by weighing the components according to the designed percentage of 20.4 % Athabasca bitumen, 8.6% Athabasca brine and 71.0 % clean core (all in mass percentage), and then using a Hobart mixer to blend them homogeneously.

Air and Nitrogen: The feed gases, air with a purity of 99.6% and nitrogen with a purity of 99.7%, were PRAXAIR products. They were analyzed using a Hewlett-Packard 5830 Gas Chromatograph, which had been calibrated for nitrogen, oxygen, carbon

monoxide, carbon dioxide and light hydrocarbons (methane up to hexane). Table 3.4 lists the composition of the feed gases obtained from the gas chromatograph (GC). Not even trace quantities of hydrocarbons were found in the feed gases.

Table 3.4: GC Analysis Results for the Feed Gases

	N_2 mole fraction	O_2 mole fraction
Air	0.7928	0.2072
Nitrogen	0.9974	0.0026

3.3 Experimental Procedure

A measured amount of bitumen and water (or brine), or bitumen with sand matrix and brine, was introduced into the quartz glass tube, which was then placed in the specially designed stainless steel reaction vessel. In core-free experiments, the mass of oil and aqueous phase were each approximately equal to 50 g. In experiments in which a core matrix was present, approximately 190 g of synthetic core was used to ensure enough oil sample for future analysis. In these core-containing experiments, the mineral matrix or sand comprised 71.0 % (by mass), the oil made up 20.4 %, and the remainder or 8.6 % was brine.

All cells were assembled immediately after being filled to minimize any water loss and the flexible strip heaters, valves and rupture discs were attached. Then the cells were each leak tested using nitrogen and mounted on the rocker arms inside the explosion-

proof chamber. Once mounted, they were attached to the heater control and data acquisition system, and the cells were charged with a known composition of oxidizing gas mixture to a pre-determined initial pressure. The heater temperature controls were then set to the desired run temperature and adjusted as required to insure that the inner cell temperature was within 1°C of the run temperature. The lid of the containment chamber was closed and the apparatus was left in this condition for the duration of the run. The recorded run data were backed up at least once daily.

Upon termination of the run, the final cell pressures and temperatures were recorded, the heaters shut down, and the cells allowed to cool to room temperature.

The gas phase in each cell was then sampled and stored in a gas tight super-syringe made by Hamilton Co. for the GC analysis. Then the cells were removed from the rocker apparatus, disassembled, emptied of residual hydrocarbon, and cleaned in preparation for the next run.

Immediately after each reactor was opened, the quartz liner was removed from the vessel. Most of the liquid and/or solid were observed to remain on the bottom of the liner. Only a small amount of free water and/or oil could be observed in the space between the liner and the stainless steel reactor walls. The free water present was collected. The hydrocarbon emulsion was removed from the liner and was rinsed with toluene into a 1000-mL round-bottomed flask. A Dean-Stark distillation procedure was conducted to remove any remaining water from the emulsion. For samples consisting of bitumen and core, the heavy oil was extracted with toluene in a Soxhlet apparatus for 24

hours in order to separate the oil from the solids. The emulsion water was removed at the same time and the cleaned core was then left in the ambient air so that the toluene would evaporate. Next, the de-watered oil/toluene mixture was filtered to separate any toluene insoluble material (i.e. coke and salts). The solvent was then removed by rotary evaporation followed by a mild vacuum at a temperature between 30 and 40 °C until no change in mass could be observed.

Gas samples were analyzed using a Hewlett-Packard 5890 Gas Chromatograph that had been calibrated for nitrogen, oxygen, carbon monoxide, carbon dioxide and light hydrocarbons (methane up to hexane). Any water removed underwent analysis to determine pH. The reacted oil was subjected to a variety of tests. Viscosity measurements were made using a "RVDV-1+ Viscometer" manufactured by Brookfield, while density was analysed using a "DMA 48 Density Meter" manufactured by Paar. Asphaltenes contents were measured on a 5-gram sample base, using approximately 200 mL of n-pentane for the precipitation, followed by around 500 mL of n-pentane for rising. Finally, coke content was determined, in the sand-free experiments, by weighing the particulate material remaining behind in the oil / toluene mixture after water distillation. For the synthetic core runs, the coke contents were determined from the mass difference between before and after burning the dried-core at 600 °C on a core sample of 30 ~ 40 g. A correction blank was applied to the measured mass loss to account for mass loss of the sand matrix as water of hydration was released from the solids.

A schematic of this procedure is given in Figure 3.11. The Dean-Stark distillation, rotary evaporation equipment, viscometer and density meter are shown in the photographs of Figures 3.12 – 3.15.

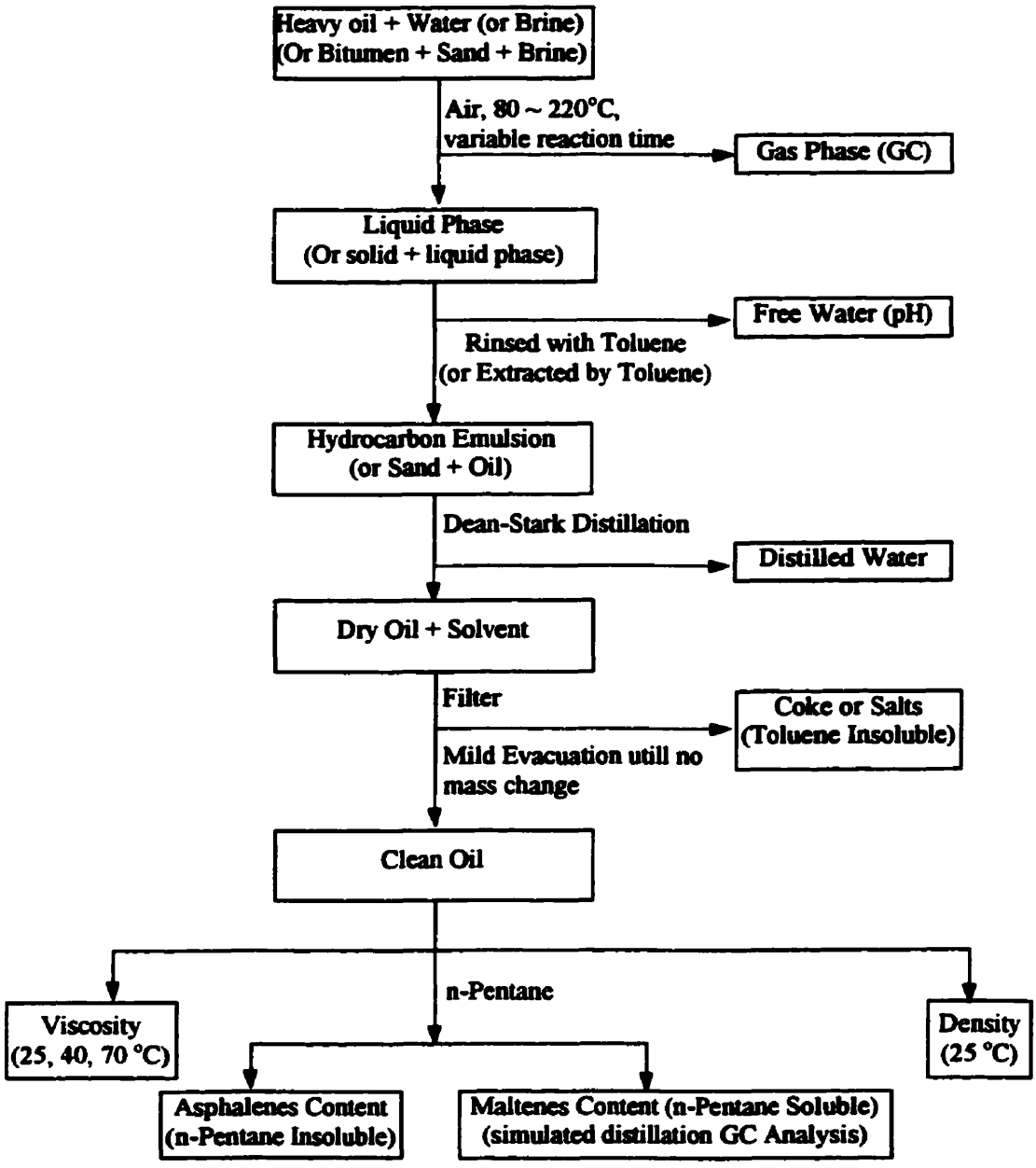

Figure 3.11: Analysis Scheme

Figure 3.12: Dean –Stark Distillation

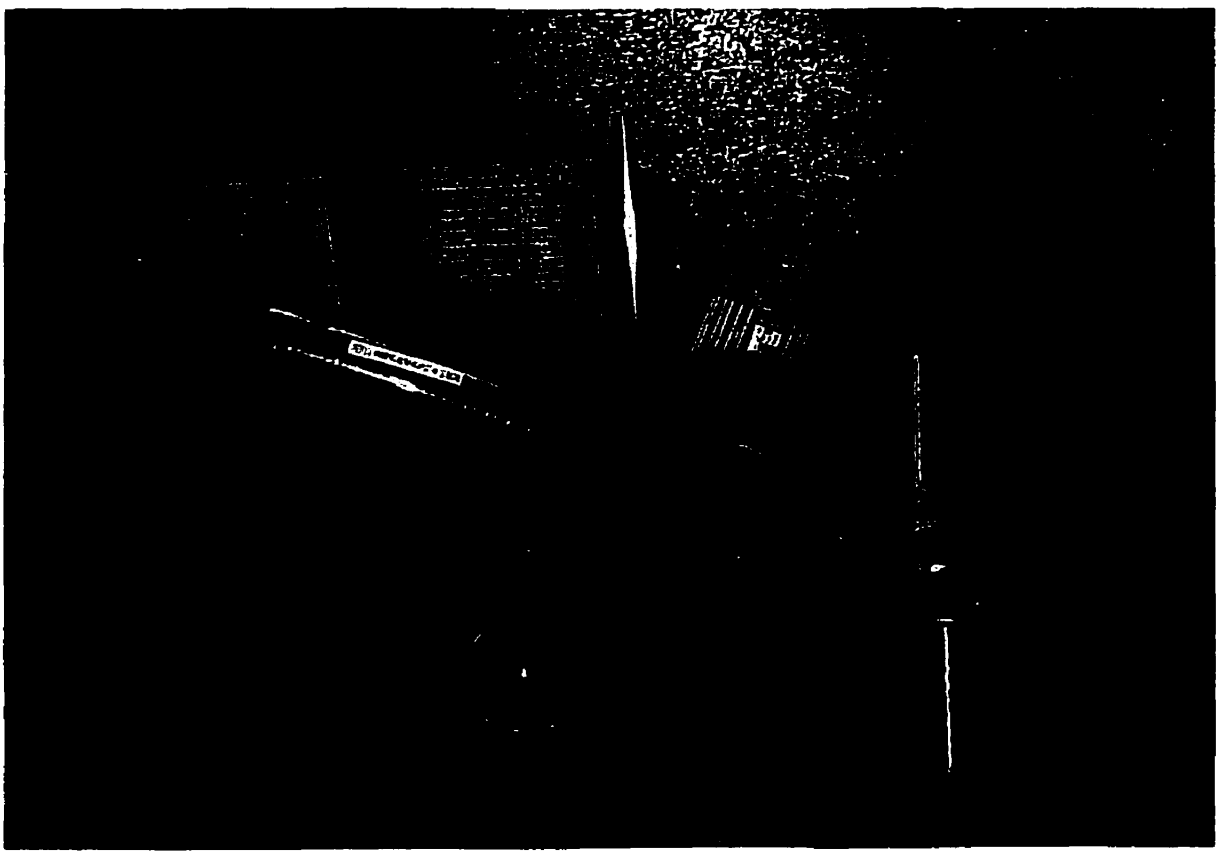

Figure 3.13: Rotary Evaporator

Figure 3.14: RVDV-1+ Viscometer

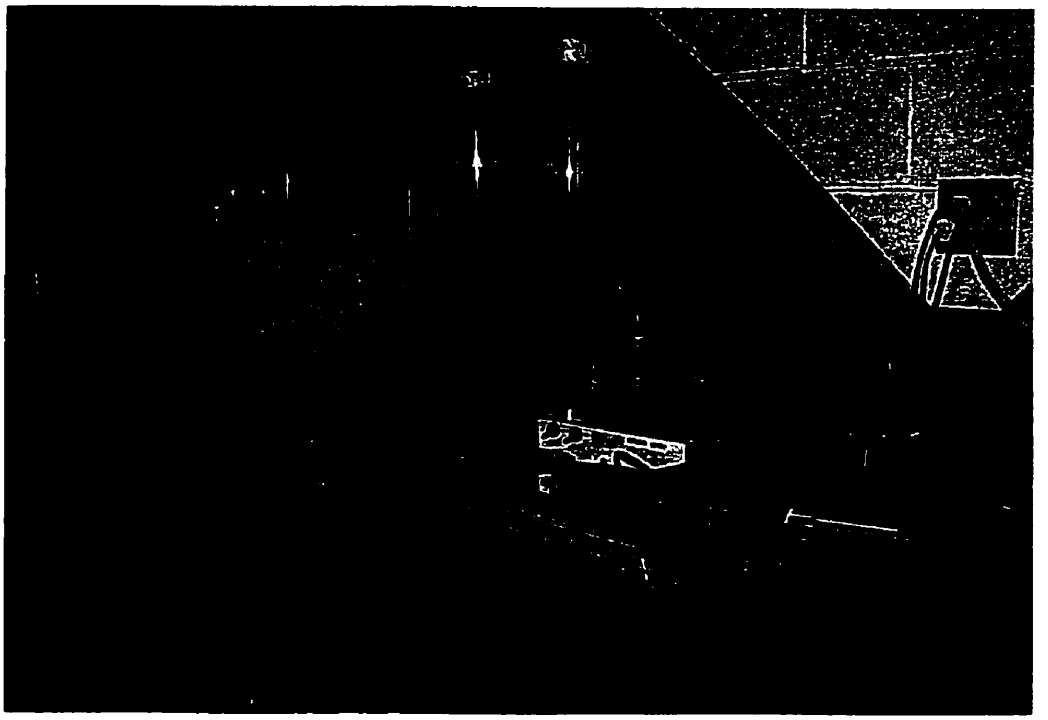

Figure 3.15: DMA48 Density Meter

CHAPTER FOUR RESULTS AND DISCUSSIONS

4.1 DESCRIPTION OF EXPERIMENTAL PROGRAM

A total of 6 runs, consisting of 52 sets of test conditions, have been completed. A summary of the conditions investigated can be found in Table 4.1.

The first run with 10 reaction conditions was performed at initial pressures in the range of 170 ~ 1541 kPa (measured at room temperature), at temperatures in the range of 80 ~ 120 °C, and times between 4 and 18 days. This run was designed to test the LTO effect on the heavy oil properties.

It was thought that at lower temperatures, the controlled oxygen uptake allowed for the free radical chain reactions to start without being dominated by the asphaltenes and coke forming reactions. There was not enough energy available, however, to produce a meaningful amount of cracking. At elevated temperatures, while there was more energy available to promote the thermal cracking reactions, the higher rate of oxygen uptake promoted the oxidation reactions over cracking reactions.

Based on the results of Run #1, and Wichert's (1996) Run #23, a different approach to the experimental program was conceived. In the remaining 5 runs, the experimental process was split into two steps. Initially each experiment was operated for a certain time at 80 ~ 120 °C, allowing the available oxygen to react in a more controlled

Table 4.1 Summary of Experimental Run Conditions

Run No.	React. Temp. °C	Initial Pressure kPa (abs)	React. Time (days)	Agitation Speed (rpm)	Reactants (oil plus)	Comments
1-1	80	338	6	0	dist. Water	
1-2	80	557	6	0	dist. Water	
1-3	80	934	6	0	dist. Water	
1-4	80	1822	6	0	dist. Water	
1-5	80	966	6	0	dist. Water	
1-6	100	951	6	0	dist. Water	
1-7	120	954	6	0	dist. Water	
1-8	80	949	5	0	dist. Water	
1-9	80	959	12	0	dist. Water	
1-10	80	979	18	0	dist. Water	
2-1	80, 200	953	6, 4	0	dist. Water	
2-2	80, 200	965	6, 6	0	dist. Water	
2-3	80, 200	974	6, 12	0	dist. Water	15 d lost pressure
2-4	80, 200	971	6, 18	0	dist. Water	
2-5	80, 200	968	6, 9	0	dist. Water	
2-6	80, 200	989	0, 6	0	dist. Water	
2-7	80, 200	951	12, 6	0	dist. Water	
2-8	80, 200	974	18, 6	0	dist. Water	
2-9	80, 150	955	6, 6	0	dist. Water	
2-10	80, 175	980	6, 6	0	dist. Water	
3-1	80, 200	959	6, 6	1/3	dist. Water	
3-2	80, 200	962	6, 9	1/3	dist. Water	
3-3	80, 200	886	18, 6	1/3	dist. Water	
3-6	80, 200	950	6, 6	0	dist. Water	N_2
3-7	80, 200	942	6, 9	0	dist. Water	N_2
3-8	80, 200	946	18, 6	0	dist. Water	N_2
4-1	80, 200	7045	6, 6	1/3	dist. Water	
4-2	80, 200	3604	6, 6	1/3	dist. Water	
4-3	80, 200	1939	6, 6	1/3	dist. Water	Gas blow out
4-6	80, 200	966	18, 6	1/3	dist. Water	N_2
4-7	80, 220	955	6, 6	1/3	dist. Water	
4-8	80, 220	1806	6, 6	1/3	dist. Water	
5-1	80, 200	981	6, 6	1/3	sand+brine	
5-2	80, 200	966	6, 9	1/3	sand+brine	
5-3	80, 200	969	6, 12	1/3	sand+brine	
5-4	80, 220	980	6, 6	1/3	sand+brine	
5-5	80, 200	997	6, 0	1/3	sand+brine	
5-6	80, 200	969	1, 6	1/3	sand+brine	
5-7	80, 200	948	12, 6	1/3	sand+brine	
5-8	80, 200	924	18, 6	1/3	sand+brine	
5-9	80, 220	1621	6, 6	1/3	sand+brine	
5-10	80, 200	953	6, 6	1/3	sand+brine	N_2
6-1	80, 200	977	6, 6	1/3	brine	
6-2	80, 200	955	6, 9	1/3	brine	
6-3	80, 200	991	6, 12	1/3	brine	Heater malf.
6-4	80, 200	1032	6, 0	1/3	brine	
6-5	80, 200	1066	0, 6	1/3	brine	
6-6	80, 200	980	12, 6	1/3	brine	
6-7	80, 200	972	18, 6	1/3	brine	
6-8	80, 220	572	6, 6	1/3	dist. Water	
6-9	80, 220	1656	6, 6	1/3	dist. Water	Heater malf.
6-10	80, 220	3535	6, 6	1/3	dist. Water	

fashion. This was intended to allow the free radical cracking reactions to start, and was termed as the Low Temperature Soak (LTS). Following the LTS, the temperature of the individual reactors was raised to a pre-defined level in the range of 150 to 220 °C, and maintained at this point for a pre-determined number of days. This stage was defined as the Elevated Temperature Soak (ETS). In a field situation, this process was likened to first injecting air into a formation at low temperatures and rates, and then starting high temperature steam injection (cyclic or flooding).

Each experiment was conducted in a batch reactor that was pressurized with air prior to the low temperature soak. The elevated temperature soak followed without depressurizing the reactor; hence, residual oxygen that remained in the gas phase following the low temperature soak was available for reaction during the elevated temperature soak.

4.2 Calculation Procedures

The raw data for each run has been compiled and can be found in Appendix 1. Calculated parameters for each set of reaction conditions investigated include mass balances, total oxygen uptake, rate of oxygen uptake, and produced gas phase molar concentrations.

4.2.1 Mass Balance, Oxygen Uptake and Effluent Gas Composition Calculations

The raw data in Appendix 1 were used in the calculation of mass balances for each individual test via a Microsoft Excel spreadsheet. Table 4.2 shows an example of the raw data spreadsheet for Run 2. These tabulated results can be found in Appendix 2. An example spreadsheet for Run 2 can be found in Table 4.3. The input data for the spreadsheet calculations include:

1. the measured mass of initial and final Athabasca oil;
2. the measured mass of initial and final water or brine;
3. the measured initial and final cell pressures and temperatures;
4. the run time;
5. the measured mass of produced coke;
6. the measured initial and final Athabasca oil densities at 25 °C;
7. the measured initial and final Athabasca oil viscosities at 25, 40 and 70 °C;
8. pH of the aqueous phase;
9. the measured mass of Asphaltenes for the modified and original Athabasca oil;
10. composition of the initial and post test gas phase obtained by GC;
11. the water / brine solution densities (assumed to be 1.0 g/cm^3 in all calculations);

12. the inner gas volume (using the average value of 120 mL in all the oil-gas-water reaction cases, and 100 mL in the case of oil-gas-brine-core reactions).

It is assumed that the difference between the initial and final number of moles of oxygen present in the cell was reacted and did not simply dissolve in the oil. Thus, the total oxygen uptake is based on the calculated total moles of oxygen consumed and the initial mass of Athabasca oil input into the cell. The moles of oxygen in the gas mixture were calculated using the real gas equation of state:

$$n_{O_2} = \frac{y_{O_2} PV}{z_m RT} \tag{4.1}$$

and the total oxygen uptake was calculated as :

$$O_2 uptake = \frac{n_{O_2} \times 32.0}{m_{oil}} \ (g / g \text{ oil}) \tag{4.2}$$

Where, y_{O2} is the mole fraction of oxygen obtained from the GC, P is the total absolute pressure, T is the corresponding absolute temperature, V is the volume taken up by the gas, R is the universal gas constant, n_{O2} is the number of moles of oxygen, and m_{oil} is the mass of the input oil. The compressibility factor z_m, was calculated using HYSYS software based on the Peng Robinson Equation of State (PR EOS).

Cell #	initial oil input (g)	final oil out (g)	initial water in (g)	final water out (g)	(init@room T) Pressure (psig)	Cell Run Temperature (°C)	Cell Run Time (days)	coke (g)	coke (% oil)	Comment
2~1	51.32	51.49	50.10	49.63	125.5	80,200	6,4	0.0236	0.0460	
2~2	50.50	50.72	50.88	49.71	127.3	80,200	6,6	0.0566	0.1121	
2~3	50.66	49.47	50.25	~	128.6	80,200	6,12	0.1231	0.2430	8th day leak
2~4	50.22	50.18	50.82	49.60	128.1	80,200	6,18	0.1458	0.2903	
2~5	50.34	50.51	50.03	49.26	127.7	80,200	6,9	0.0977	0.1941	
2~6	50.07	50.21	50.22	48.78	130.8	80,200	0,6	0.0748	0.1494	
2~7	50.50	50.89	50.08	49.13	125.3	80,200	12,6	0.0133	0.0263	
2~8	50.90	50.62	51.79	50.37	128.6	80,200	18,6	0.0062	0.0122	
2~9	50.74	50.99	50.66	49.66	125.8	80,150	6,6	0.0079	0.0156	
2~10	51.09	51.26	50.42	49.53	129.5	80,175	6,6	0.0000	0.0000	

Cell #	density (@25°C)	viscosity (@25°C)	viscosity (@40°C)	viscosity (@70°C)	pH	Asphaltenes	GC results N_2	O_2	CO_2	CO	CH_4
	g/cm^3	(mPa·s)	(mPa·s)	(mPa·s)		(% mass)	(% mol)	(% mol)	(% mol)	(% mol)	(% mol)
2~1	1.0071	315000	45410	2615	2.5	21.93	96.32	1.62	2.06	0.00	0.00
2~2	1.0071	228000	33150	2025	2.6	21.23	95.96	1.52	2.51	0.00	0.00
2~3	1.0064	191500	29850	1895	3.2	20.86	-	-	-	-	-
2~4	1.0078	189000	27900	1760	3.4	21.32	95.75	1.75	2.50	0.00	0.00
2~5	1.0058	189200	28650	1860	3.0	20.90	95.35	1.62	3.04	0.00	0.00
2~6	1.0064	210700	31500	2055	2.4	21.34	94.75	1.36	3.89	0.00	0.00
2~7	1.0061	220500	33650	2060	2.6	21.18	96.53	1.71	1.76	0.00	0.00
2~8	1.0084	190500	29500	2058	2.8	21.96	97.79	0.60	1.61	0.00	0.00
2~9	1.0064	253300	36000	2225	2.5	21.40	92.83	3.92	3.26	0.00	0.00
2~10	1.0074	324500	43330	2640	2.5	22.33	97.41	0.90	1.69	0.00	0.00
original	1.0051	218700	32250	1950	6.55	17.85	79.28	20.72	0.00	0.00	0.00

Table 4.2: Raw Data From Run #2

Run2 data

Cell #	initial mass oil (g)	final mass oil (g)	oil mass diff. %	initial mass H_2O (g)	final mass H_2O (g)	GC Analysis Results N_2 mass%	O_2 mass%	CO_2 mass%	CO mass%	CH_4 mass%	C_2H_6 mass%	C_3H_8 mass%	coke contents (g)	coke contents mass%	comment
2-1	51.32	51.49	0.3313	50.1	49.63	96.32	1.62	2.06	0.00	0.00	0.00	0.00	0.0236	0.0460	
2-2	50.5	50.72	0.4356	50.88	49.71	95.96	1.52	2.51	0.00	0.00	0.00	0.00	0.0566	0.1121	
2-3	50.66	49.47	-2.3490	50.25	-	-	-	-	-	-	-	-	0.1231	0.2430	8th day leak, cannot get GC Result
2-4	50.22	50.18	-0.0796	50.82	49.6	95.75	1.75	2.50	0.00	0.00	0.00	0.00	0.1458	0.2903	
2-5	50.34	50.51	0.3377	50.03	49.26	95.35	1.62	3.04	0.00	0.00	0.00	0.00	0.0977	0.1941	
2-6	50.07	50.21	0.2796	50.22	48.78	94.75	1.36	3.89	0.00	0.00	0.00	0.00	0.0748	0.1494	
2-7	50.5	50.89	0.7723	50.08	49.13	96.53	1.71	1.76	0.00	0.00	0.00	0.00	0.0133	0.0263	
2-8	50.9	50.62	-0.5501	51.79	50.37	97.79	0.60	1.61	0.00	0.00	0.00	0.00	0.0062	0.0122	
2-9	50.74	50.99	0.4927	50.66	49.66	92.83	3.92	3.26	0.00	0.00	0.00	0.00	0.0079	0.0156	
2-10	51.09	51.26	0.3327	50.42	49.53	97.41	0.90	1.69	0.00	0.00	0.00	0.00	0.0000	0.0000	
orig.air						79.28	20.72	0.00	0.00	0.00	0.00	0.00			

Cell #	initial temp. °C	initial pressure kPa	initial z factor	initial total gas mol	initial N_2 mol	initial O_2 mol	initial total gas (g)	final temp. °C	final pressure kPa	final z factor	final total gas mol	final N_2 mol	final O_2 mol	final CO_2 mol	O_2 uptake g/g oil	final total gas g	gas mass diff. % oil	total oil mass diff. %
2-1	22.2	865	0.9920	0.0471	0.0373	0.0098	1.3568	34.0	684.1	0.9969	0.0365	0.0351	0.0006	0.0008	0.0059	1.0360	-0.6251	1.0024
2-2	22.2	878	0.9919	0.0477	0.0378	0.0099	1.3745	29.2	684.1	0.9964	0.0371	0.0356	0.0006	0.0009	0.0060	1.0554	-0.6319	1.1796
2-3	22.2	887	0.9918	0.0481	0.0382	0.0100	1.3874								0.0064			-2.1060
2-4	22.2	883	0.9918	0.0480	0.0380	0.0099	1.3824	29.3	691.0	0.9964	0.0374	0.0358	0.0007	0.0009	0.0059	1.0648	-0.6325	0.8432
2-5	22.2	881	0.9918	0.0478	0.0379	0.0099	1.3785	36.6	717.2	0.9967	0.0377	0.0360	0.0006	0.0011	0.0060	1.0772	-0.5984	1.1302
2-6	22.2	902	0.9917	0.0489	0.0388	0.0101	1.4091	33.0	706.2	1.0021	0.0375	0.0355	0.0005	0.0015	0.0062	1.0740	-0.6693	1.0983
2-7	22.2	864	0.9920	0.0470	0.0373	0.0097	1.3548	40.7	663.4	0.9975	0.0347	0.0335	0.0006	0.0006	0.0059	0.9846	-0.7330	1.5316
2-8	22.2	887	0.9918	0.0481	0.0382	0.0100	1.3874	37.7	687.5	0.9631	0.0375	0.0367	0.0002	0.0006	0.0062	1.0601	-0.6430	0.1051
2-9	22.2	868	0.9920	0.0472	0.0374	0.0098	1.3597	37.2	730.3	0.9966	0.0383	0.0355	0.0015	0.0012	0.0053	1.0977	-0.5165	1.0248
2-10	22.2	893	0.9917	0.0484	0.0384	0.0100	1.3963	39.0	693.7	0.9973	0.0363	0.0354	0.0003	0.0006	0.0062	1.0284	-0.7199	1.0527

Table 4.3: Material Balance Spreadsheet for Run # 2

Similarly, the compositions of the other gas products, such as CO_2, CO and C_nH_{2n+2}, were computed by the EOS:

$$n_{CO_2} = \frac{y_{CO_2} PV}{z_m RT} \tag{4.3}$$

$$n_{CO} = \frac{y_{CO} PV}{z_m RT} \tag{4.4}$$

$$n_{C_nH_{2n+2}} = \frac{y_{C_nH_{2n+2}} PV}{z_m RT} \tag{4.5}$$

Where, y_{CO2}, y_{CO} and $y_{CnH2n+2}$ are the mole fractions of the produced gas obtained from GC results. n_{CO2}, n_{CO} and $n_{CnH2n+2}$ are the numbers of moles for the product gas.

The parameters calculated by the spreadsheet include:

1. The initial number of moles for each component making up the injecting gas (N_2 and O_2);
2. The initial and final number of moles for each component making up the effluent gas (N_2, O_2, CO_2, CO and/or C_nH_{2n+2}), the calculation assumes that the final gas volume is the same as the initial gas volume present in the cell;
3. The moles of oxygen consumed in the reaction (assuming that the difference between the initial and final number of moles for oxygen present in the cell were reacted and did not simply dissolve in the oil);
4. The oxygen uptake (based on the calculated total moles of oxygen consumed and the initial mass of Athabasca oil input into the cell, by Equation (4.2)).

5. The masses of initial gas mixture and final gas mixture (based on the calculated number of moles of each component and their individual molecular weights);
6. The percentage differences between the initial and final oil masses.
7. The percentage differences between the initial and final gas masses.
8. The formed coke mass percentage of the initial oil.
9. The percentage differences between the initial and final total oil masses (including the coke and gas changes).

A tabulation of the hydrocarbon mass balance percentage differences for all runs can be found in Table 4.4. A positive value of percentage difference indicates a net gain in mass. Because batch reactors were used (i.e. a closed system), the gain in mass for the hydrocarbon is due to pre and post-run sample handling errors and oxygen uptakes.

Table 4.4: Mass Balance Percentage Differences for Hydrocarbon Liquid Phase (Oil)

Cell #	Run 1 oil mass diff.%	Run 2 oil mass diff.%	Run 3 oil mass diff.%	Run 4 oil mass diff.%	Run 5 oil mass Diff.%	Run 6 oil mass diff.%
1	0.1000	0.3313	0.6960	-1.5458	0.8514	0.2377
2	0.1200	0.4356	0.6550	0.9145	0.7998	0.2978
3	-0.1400	-2.3490	0.2378	1.1355	1.5194	0.8383
4	-0.2597	-0.0796			2.0882	0.4987
5	-0.3000	0.3377			4.3041	0.3986
6	1.3197	0.2796	0.6116	0.6353	2.2188	0.2960
7	-0.3997	0.7723	0.7667	0.5748	0.0516	0.0792
8	-2.6384	-0.5501	-0.2176	0.7346	0.1546	0.4565
9	-0.3399	0.4927			-0.2580	0.1191
10	-0.3399	0.3327			-1.8027	-1.7053

In order to separate the hydrocarbon and aqueous phases at the end of a run, the samples were dissolved in toluene and then subjected to a Dean-Stark distillation and a mild heating-evacuation process. The resultant oil was obtained when all the solvent was removed, as indicated by a stable mass. Determination of this endpoint was one of the most difficult aspects of the analysis. If the solvent removal process was terminated too early, residual toluene would remain in the oil sample and the resultant viscosity would be abnormally low; however, if the process was terminated too late, the lighter hydrocarbon species in the end-product would be removed, and the final viscosity of the sample would be unusually high. Mass balance for the hydrocarbon liquid alone were used to check as to how much residual toluene was left in the oil at the end of the distillation process. For the majority of the experimental conditions that were investigated, the hydrocarbon liquid phases experienced small increases in mass, which were less than ± 1%.

In order to get a more accurate assessment of the amount of residual toluene in the oil at the end of sample processing, a mass balance including the coke precipitation and oxygen uptake was performed. The resulting mass percentages, in effect reflecting the amount of residual toluene in each sample, can be found in Table 4.5. It can be seen that most of the runs had mass percentage difference of less than ± 1.

The net gain in mass due to residual toluene for the majority of samples was on the order of one percent, minimizing any adverse effects on the end-product viscosity measurements.

Table 4.5: Mass Balance Percentage Differences for Hydrocarbon Liquid Phase Taking Coke and Oxygen Masses into Account

	Run 1			Run 2			Run 3		
Cell #	gas mass diff.%	coke mass yields %	total oil mass diff.%	gas mass diff.%	coke mass yields %	total oil mass diff.%	gas mass diff.%	coke mass yields %	total oil mass diff.%
1	-	0.000	0.100	-0.625	0.046	1.002	-0.493	0.366	1.555
2	-	0.000	0.120	-0.632	0.112	1.180	-0.476	0.341	1.473
3	-0.527	0.000	0.387	-	0.243	-2.106	-0.553	0.014	0.805
4	-0.939	0.000	0.679	-0.633	0.290	0.843			
5	-0.625	0.000	0.325	-0.598	0.194	1.130			
6	-0.651	0.000	1.970	-0.669	0.149	1.098	0.102	0.024	0.533
7	-0.648	0.000	0.249	-0.733	0.026	1.532	0.459	0.021	0.329
8	-0.526	0.000	-2.112	-0.643	0.012	0.105	0.409	0.013	-0.614
9	-0.965	0.000	0.625	-0.517	0.016	1.025			
10	-0.633	0.000	0.294	-0.720	0.000	1.053			

	Run 4			Run 5			Run 6		
Cell #	gas mass diff.%	coke mass yields %	total oil mass diff.%	gas mass diff.%	coke mass yields %	total oil mass diff.%	gas mass diff.%	coke mass yields %	total oil mass diff.%
1	-2.958	0.008	2.223	-0.356	0.302	0.797	-0.594	-	0.832
2	-1.943	0.004	3.289	-0.294	0.296	0.802	-0.539	0.339	0.498
3	~	~	1.135	-0.367	0.259	1.411	-0.486	0.134	1.190
4				-0.937	0.639	1.790	-0.847	0.057	1.288
5				-0.481	0.599	4.422	-0.568	2.928	-1.961
6	-0.166	0.000	0.801	-0.405	0.061	1.875	-0.588	0.143	0.741
7	-0.629	0.003	1.504	-0.340	0.327	0.038	-0.569	0.278	0.370
8	-1.010	0.004	2.127	-1.264	0.032	-1.078	-0.283	0.136	0.603
9				-0.337	0.287	-0.309	-0.772	0.269	0.622
10				0.006	0.000	-1.797	-2.113	2.347	-1.940

4.2.2 Low Temperature Soak (LTS) Kinetics and Rate of Oxygen Uptake

As described in Chapter 3, the data acquisition system was capable of monitoring thermocouple and pressure transducer signals simultaneously. The raw data were recorded at 20-minute intervals for the duration of the test. Figure 4.1 is representative of the temperature and pressure profiles of the reaction system for Test 2-3. In this plot, the gas temperature line shows directly under the liquid temperature line. From this figure, it can be seen that the pressure reduction mainly occurred in the LTS stage, while the pressure profile levelled off in the higher temperature stage (ETS stage). Therefore, it could be assumed that the oxygen was mainly consumed in the LTS step, and the oxygen uptake rate calculations were based on the data from the LTS stage.

A method described by Babu and Cormack (1983) was used to estimate the rate of oxygen uptake for each set of reactions. When using this method, it is assumed that the oxidation process is kinetically controlled, and that the solubility of oxygen in bitumen follows Henry's law. The rate of reaction can be described in terms of the oxygen partial pressure of the gas phase by the equation:

$$r = \frac{k}{H^n} P_{O_2}^n \qquad (4.6)$$

Where r is the rate of the reaction, k is the reaction rate constant, H is the Henry's law constant, P_{O2} is the oxygen partial pressure, and n is the order of the reaction. To assist in the analysis of the experimental data, one can carry out a simple mass balance

on oxygen, assuming ideal gas behaviour, for a batch system to obtain the differential equation:

$$\frac{dP_{O_2}}{dt} = -\frac{V_b RT}{V_g}\frac{k}{H^n}P_{O_2}^n \tag{4.7}$$

Where V_b is the volume of the oil in the cell, T is the run temperature, V_g is the volume of gas in the cell and t is the time.

Equation (4.7) can now be integrated to give:

for $n \neq 1$

$$\left(\frac{P_{O_2}^0}{P_{O_2}}\right)^{n-1} - 1 = \frac{V_b RTk}{V_g H^n}(n-1)(P_{O_2}^0)^{n-1}t \tag{4.8}$$

for n = 1

$$\ln\frac{P_{O_2}^0}{P_{O_2}} = \frac{V_b RTk}{V_g H}t \tag{4.9}$$

Where, P_{O2}^0 is the initial oxygen partial pressure.

For a zero-order oxidation kinetics, n = 0, equation (4.8) reduces to:

$$P_{O_2} - P_{O_2}^0 = -\frac{V_b RTk}{V_g}t \tag{4.10}$$

For a second order oxidation kinetics, n = 2, equation (4.8) reduces to:

$$\frac{P_{O_2}^0}{P_{O_2}} - 1 = \frac{V_b RTk}{V_g H^2} P_{O_2}^0 t \qquad (4.11)$$

For non-zero order reactions, the slope of a plot of (P_{O2}^0 / P_{O2}) versus time, t, therefore, can be used to estimate the parameters k/H and k/H^2. For a first order reaction, the plot should be a straight line on semi-log axes; while for a second order reaction, the plot should be linear using Cartesian co-ordinates. On the other hand, the zero-order reaction should be linear using Cartesian co-ordinates by plotting of P_{O2} versus time. For the purpose of the plots, the initial oxygen partial pressure was defined as:

$$P_{O_2}^0 = (P_{max} - P_{H_2O} - P_{HC}) * y_{O_2}^0 \qquad (4.12)$$

The initial oxygen partial pressure, P_{O2}^0, at the given run conditions, was estimated by multiplying the difference between the greatest pressure recorded during the heating phase of the experiment and the vapour pressure of pure water at the given condition of LTS by the initial oxygen mole fraction of the oxidizing gas mixture. The maximum pressure, P_{max}, occurred very near the start of the LTS period. The vapor pressure of water at the given LTS conditions, P_{H2O}, was subtracted from this pressure. The hydrocarbon partial pressure, P_{HC}, was assumed to be zero since it was a heavy oil and the value would be much smaller than that of the other components.

The recorded pressure, after subtracting the nitrogen partial pressure and the vapour pressure of water at the LTS, was assumed to equal the oxygen pressure, P_{O2}, at the given conditions. It was assumed that the nitrogen was an inert gas, so its partial pressure would not change, and was estimated by multiplying the initial partial pressure

of oxygen by the initial nitrogen mole fraction of the injected gas mixture. The equation is as follows:

$$P_{O_2} = P - P_{H_2O} - P_{HC} - P_{O_2}^0 * \frac{y_{N_2}^0}{y_{O_2}^0} \qquad (4.13)$$

P_{H2O} is the vapour pressure under the running condition; y_{N2}^0, y_{O2}^0 express the mole fractions of nitrogen and oxygen in the injected gas (air), obtained from GC results, respectively.

Due to the way the apparatus was designed, it was not possible to estimate the amount of oxygen consumed during the initial heating phase of the run. Therefore, the errors in estimating the initial oxygen partial pressure had to be accepted. In addition, in order to simplify the calculations further, the production of gases such as carbon monoxide / dioxide and light hydrocarbons was neglected and any changes in pressure were considered due only to oxygen consumption.

The values of (P_{O2}^0/P_{O2}) obtained from the data acquisition system were plotted for each cell on both log-linear and linear-linear scales. The slopes of the plotted points were calculated using least-squares regression. The least-squares regression coefficients for each fit were then calculated, and used to determine the order of the reaction based on the closest unit coefficient. Figures 4.2 to 4.4 are the examples of first-, second- and zero-order, plots for Run 2-1, respectively. From these kinetic plots, the zero order regression coefficients were equal to 0.9514 and second order coefficient was 0.9869,

while the first order coefficient was 0.9955. Therefore, this run was deemed first order. Next, the kinetic parameter, k, k/H, or k/H^2, were obtained from the slopes of the curves on the semi-log (or Cartesian) co-ordinate plots. These rate constants for the three orders were similarly determined at each set of reaction conditions and appear, along with the calculated equations and corresponding regression coefficients, in Tables 4.6 to 4.8. From those calculations, it can be seen that most of the runs, (approximately 60.4%) of the identified 48 runs are first order reactions, and 37.5% of them are deemed as second order reactions, while 2.1% are zero order reactions.

For runs at LTS temperatures greater than 80 °C, the peculiar feature of the data is that each run displays two distinct straight lines. For instance, $\ln (P_{O2}^0/P_{O2})$ of Run 1-7 is plotted as a function of time in Figure 4.5 to demonstrate the salient features of the results. During the initial period of the reaction, the rate of oxygen uptake is high, but after approximately 3 days, the rate of reaction abruptly drops to a much lower rate. However, the reaction still retains its first order character. This transition is similar to that reported by Dornte, Ferguson and Haskins (1936) and Babu & Cormack (1983). This transition might occur because the more reactive bonds and molecules oxidize first, and once these reactions are completed, the reaction rate declines. The same trend was found in Run 2-6.

Calculated rate constants for the runs with similar reaction conditions but different temperatures (including data from Run #1, cell 5 to 7) were used to produce an Arrhenius plot, which appears in Figures 4.6. From these plots, the trend lines were used

to estimate the pre-exponential factors and activation energies according to the Arrhenius equation:

$$k/H(T) = Ae^{-E_a/RT} \tag{4.14}$$

Where A is the pre-exponential factor, E_a is the activation energy, R is the universal gas constant, and T is temperature in Kelvin.

The least-squares models that fit these data are:

$$k/H = 25.321\times10^{-10}e^{-\frac{2410}{T}}\ \frac{kmol}{m^3\cdot Pa\cdot s};\qquad R^2 = 0.9586 \tag{4.15}$$

These results should be compared with those of Babu and Cormack (1983, eq.4.16), and Wichert (1996, eq.4.17):

$$k/H = 0.0129e^{-\frac{8136}{T}}\ \frac{kmol}{m^3\cdot Pa\cdot s}\ (\text{at } \textit{low rate regime}) \tag{4.16}$$

$$k/H = 0.9309e^{-\frac{3796.0}{T}} \tag{4.17}$$

It can be seen that values for the pre-exponential factor and activation energy are significantly different from the previously published results. It is not surprising that this discrepancy between the present and previous work exists due to the manner in which the previous work was carried out; specifically, mass transfer resistance likely affected the results. Babu and Cormack obtained an approximate temperature range of 406 K ~ 414 K and Wichert performed the oxidation tests at temperatures in the range of 353 K ~ 393 K. While the experiments performed in the current study were conducted at

temperatures similar to those of Wichert (1996), different agitation / rocking conditions were used.

By substituting the calculated rate parameters into the appropriate form of equation (4.6), it is possible to plot the rate of oxygen uptake at any given time, for any of the reaction conditions investigated in the experimental program. Figure 4.7 shows a typical oxygen uptake rate profile for Test 2-2.

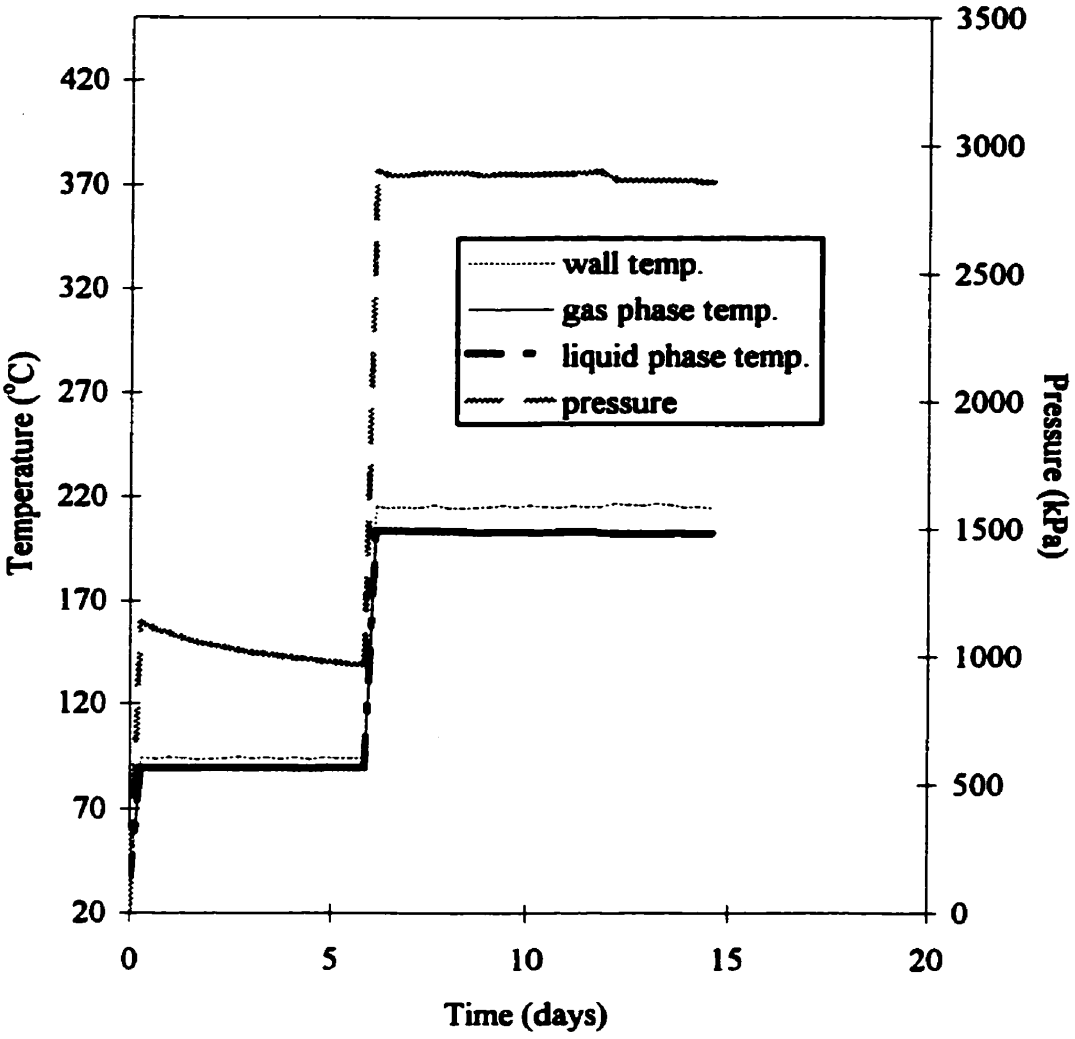

Figure 4.1: Run 2-3 Typical Pressure and Temperature Profiles

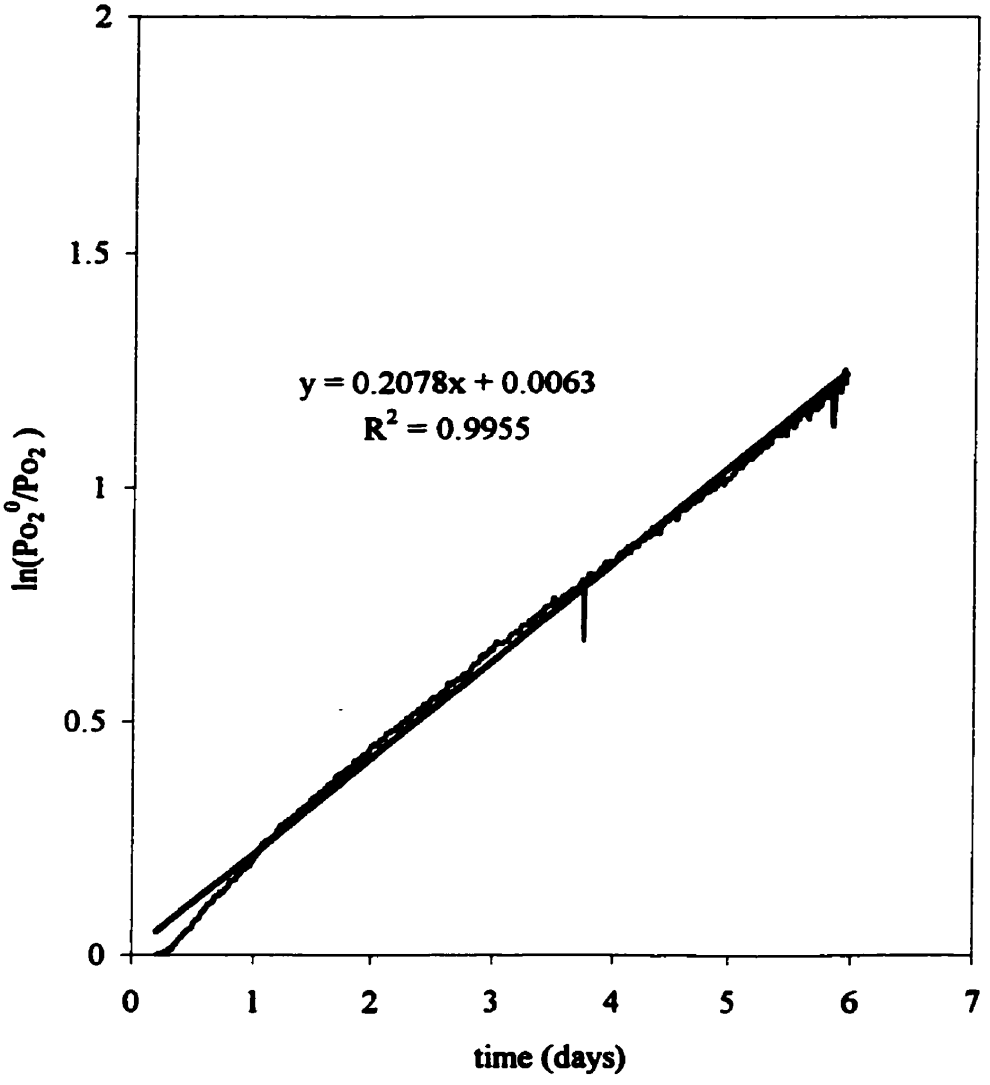

Figure 4.2.: First Order Plot of Po_2^0 / Po_2 For Run 2-1 (at 80 °C LTS stage)

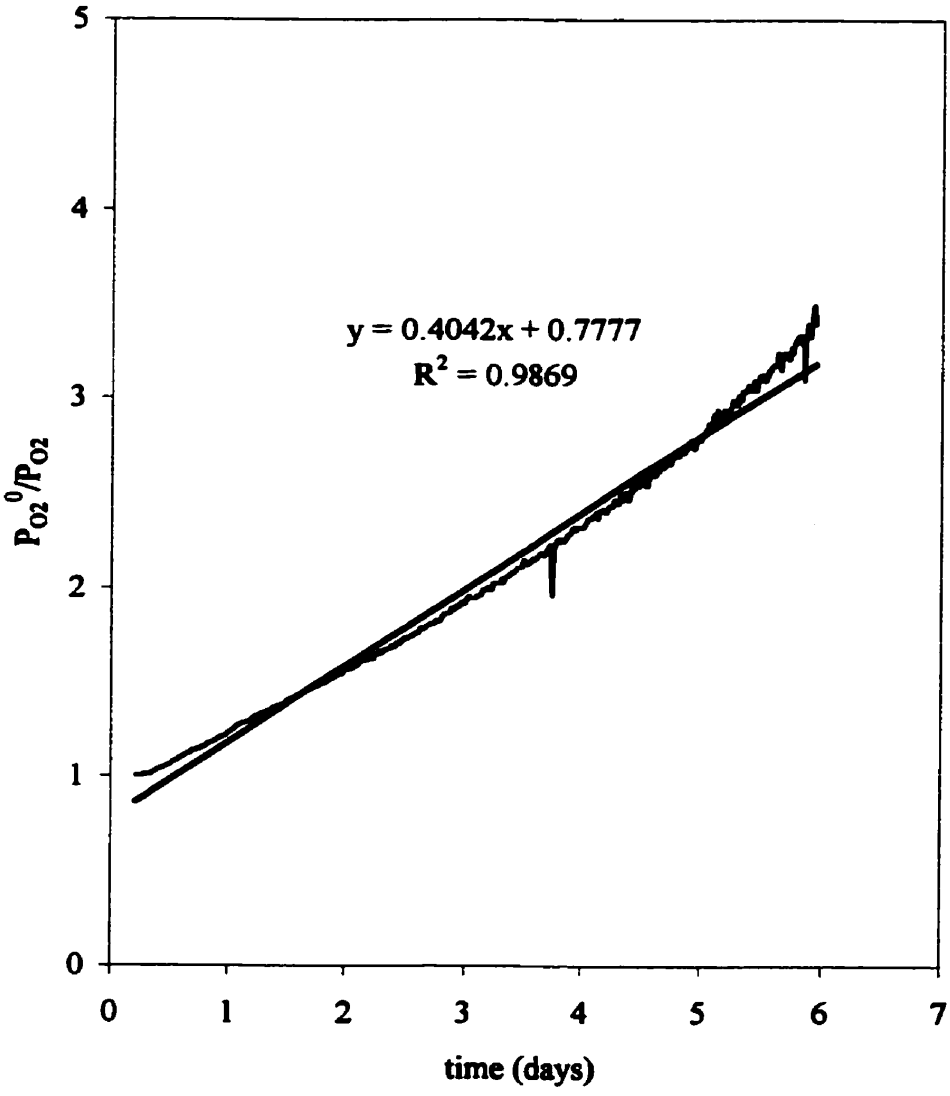

Figure 4.3: Second Order Plot of P_{O2}^{0}/P_{O2} For Run 2-1
(at 80 °C LTS stage)

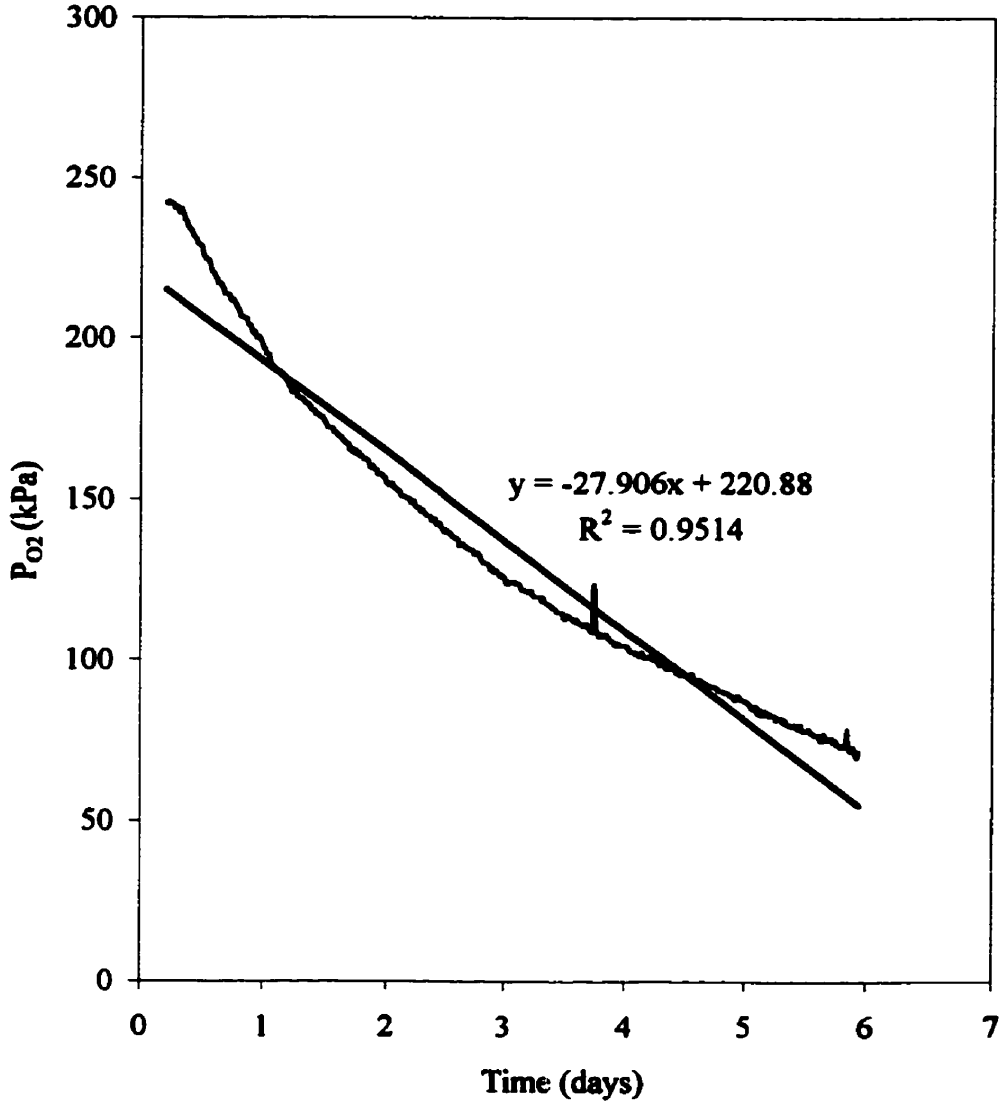

Figure 4.4: Zero-order plot of P_{O2} For Run 2-1
(at 80 °C LTS stage)

Table 4.6: Equations Regression and k/H Parameters for the First Order Reactions

cell #	Run 1 1st order equations	R^2	k/H mol/(m^3.Pa.s)	Run2 1st order equations	R^2	k/H mol/(m^3.Pa.s)	Run 3 1st order equations	R^2	k/H mol/(m^3.Pa.s)
1	y=0.4578x-0.0871	0.9954	4.370E-09	y=0.2078x+0.0063	0.9955	1.927E-09	y=0.1036x+0.0556	0.9943	9.833E-10
2	y=0.5136x-0.0072	0.9982	4.887E-09	y=0.1831x-0.0044	0.9937	1.733E-09	y=0.0933x-0.0018	0.9941	8.777E-10
3	y=0.2694x-0.055	0.9970	2.579E-09	y=0.2185x+0.0655	0.9952	2.056E-09	y=0.337x+0.0269	0.9974	3.201E-09
4	y=0.2021x+0.0668	0.9940	1.930E-09	y=0.255x+0.0808	0.9972	2.413E-09			
5	y=0.2783x+0.0427	0.9961	2.660E-09	y=0.2249x+0.0155	0.9930	2.114E-09			
6	y=0.3681x+0.1231	0.9757	3.341E-09	-	-	-	-	-	-
7	-	-	-	y=0.3447x-0.0413	0.9942	3.244E-09	-	-	-
8	y=0.3026x+0.014	0.9948	2.887E-09	y=0.2995x-0.0426	0.9977	2.793E-09	-	-	-
9	y=0.8384x-0.3369	0.9861	8.002E-09	-	-	-			
10	y=0.2693x-0.0937	0.9985	2.581E-09	y=0.2778x+0.0157	0.9952	2.581E-09			

cell #	Run 4 1st order equations	R^2	k/H mol/(m^3.Pa.s)	Run5 1st order equations	R^2	k/H mol/(m^3.Pa.s)	Run 6 1st order equations	R^2	k/H mol/(m^3.Pa.s)
1	-	-	-	-	-	-	y=0.31x-0.0288	0.9954	2.906E-09
2	-	-	-	-	-	-	y=0.2987x-0.0418	0.9931	2.802E-09
3	y=0.3255x+0.1758	0.9759	3.073E-09	-	-	-	y=0.3649x+0.0419	0.9968	3.432E-09
4				-	-	-	y=0.5227x+0.0185	0.9607	4.927E-09
5				-	-	-	-	-	-
6	-	-	-	-	-	-	y=0.3659x+0.0878	0.9976	3.414E-09
7	-	-	-	-	-	-	y=0.2095x+0.1976	0.9755	1.964E-09
8	-	-	-	-	-	-	y=0.0788x+0.0803	0.9909	7.413E-10
9				y=0.079x+0.0489	0.8777	8.038E-10	-	-	-
10				-	-	-	-	-	-

Table 4.7: Equations Regression and k/H^2 Parameters for the Second Order Reactions

	Run 1			Run2			Run 3		
cell #	2nd order equations	R^2	k/H^2 mol/(m^3.Pa^2.s)	2nd order equations	R^2	k/H^2 mol/(m^3.Pa^2.s)	2nd order equations	R^2	k/H^2 mol/(m^3.Pa^2.s)
1	-	-	-	-	-	-	-	-	-
2	-	-	-	-	-	-	-	-	-
3	-	-	-	-	-	-	-	-	-
4	-	-	-	-	-	-			
5	-	-	-	-	-	-			
6	-	-	-	-	-	-	y=0.3187x+1.0617	0.9862	1.223E-14
7	y=1.7422x0.2915	0.9937	6.377E-14	-	-	-	y=0.0383x+1.1156	0.9123	1.468E-15
8	-	-	-	-	-	-	y=0.0164x+1.0864	0.8857	6.382E-16
9	-	-	-	y=0.1223x+1.1886	0.9912	4.631E-15			
10	-	-	-	-	-	-			

	Run 4			Run5			Run 6		
cell #	2nd order equations	R^2	k/H^2 mol/(m^3.Pa^2.s)	2nd order equations	R^2	k/H^2 mol/(m^3.Pa^2.s)	2nd order equations	R^2	k/H^2 mol/(m^3.Pa^2.s)
1	y=0.1614x+1.1235	0.9616	8.242E-16	y=0.128x+1.0336	0.9899	5.545E-15	-	-	-
2	y=0.1882x+1.0878	0.9898	1.959E-15	y=0.2011x+0.611	0.9923	8.700E-15	-	-	-
3	-	-	-	y=0.2458x+0.9803	0.9968	1.063E-14	-	-	-
4				y=0.1902x+1.1042	0.9148	8.244E-15	-	-	-
5				y=0.1543x+0.9886	0.9291	6.518E-15	-	-	-
6	-	-	-	y=0.2896x+0.9455	0.9951	1.226E-14	-	-	-
7	y=0.3784x+0.9178	0.9842	1.474E-14	y=0.2966x+0.9893	0.9955	1.294E-14	-	-	-
8	y=0.1447x+1.0367	0.9630	2.983E-15	y=0.3175x+0.984	0.9959	1.376E-14	-	-	-
9				-	-	-	-	-	-
10				-	-	-	y=0.2585x+1.0964	0.9701	2.744E-15

Table 4.8: Equations Regression and k Parameters for the Zero Order Reactions

	Run 1			Run2			Run 3		
cell #	0 order equations	R^2	k $(mol/m^3).s^{-1}$	0 order equations	R^2	k $(mol/m^3).s^{-1}$	0 order equations	R^2	k $(mol/m^3).s^{-1}$
1	-	-	-	-	-	-	-	-	-
2	-	-	-	-	-	-	-	-	-
3	-	-	-	-	-	-	-	-	-
4	-	-	-	-	-	-			
5	-	-	-	-	-	-			
6	-	-	-	-	-	-	-	-	-
7	-	-	-	-	-	-	-	-	-
8	-	-	-	-	-	-	-	-	-
9	y=-87.041x+240.15	0.9760	8.307E-04	-	-	-			
10	-	-	-	-	-	-			

	Run 4			Run5			Run 6		
cell #	0 order equations	R^2	k $(mol/m^3).s^{-1}$	0 order equations	R^2	k $(mol/m^3).s^{-1}$	0 order equations	R^2	k $(mol/m^3).s^{-1}$
1	-	-	-	-	-	-	-	-	-
2	-	-	-	-	-	-	-	-	-
3	-	-	-	-	-	-	-	-	-
4				-	-	-	-	-	-
5				-	-	-	-	-	-
6	-	-	-	-	-	-	-	-	-
7	-	-	-	-	-	-	-	-	-
8	-	-	-	-	-	-	-	-	-
9				-	-	-	-	-	-
10				-	-	-	-	-	-

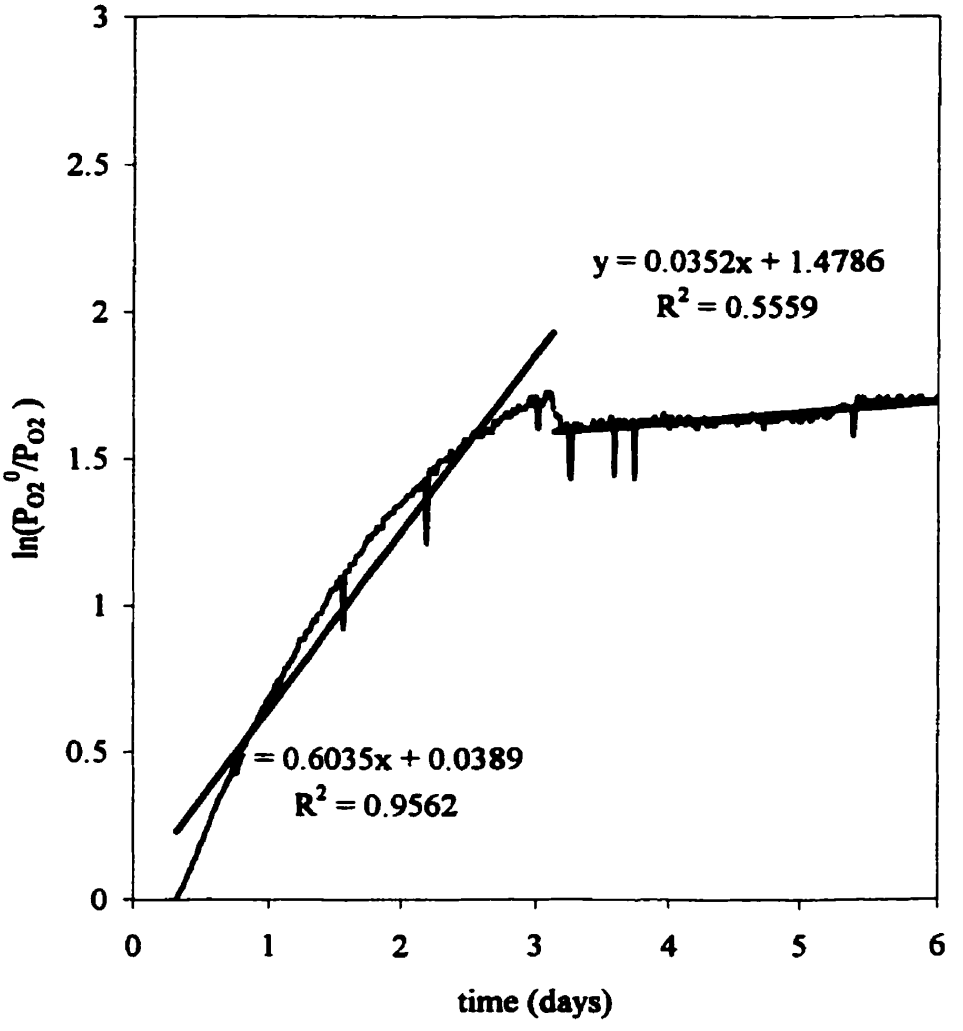

Figure 4.5: First order plot of P_{O2}^{0}/P_{O2} For Run 1-7

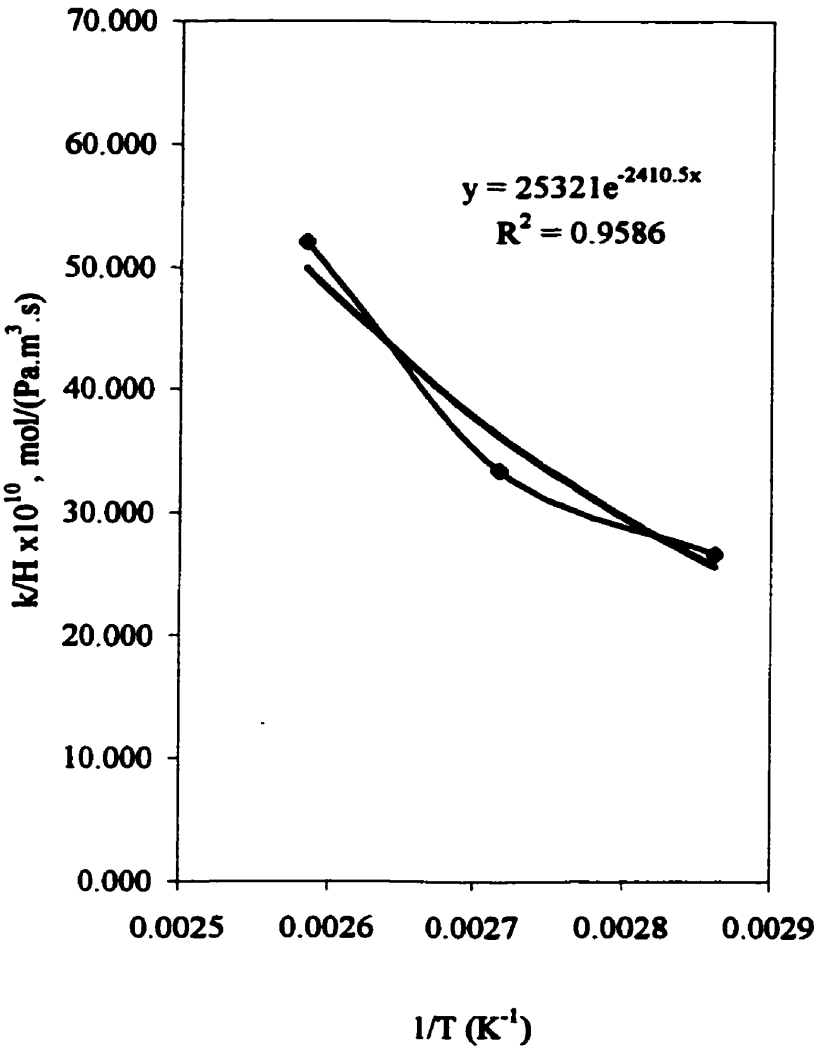

Figure 4.6: First order Arrhenius Plot (from Tests 1-5, 1-6 and 1-7)

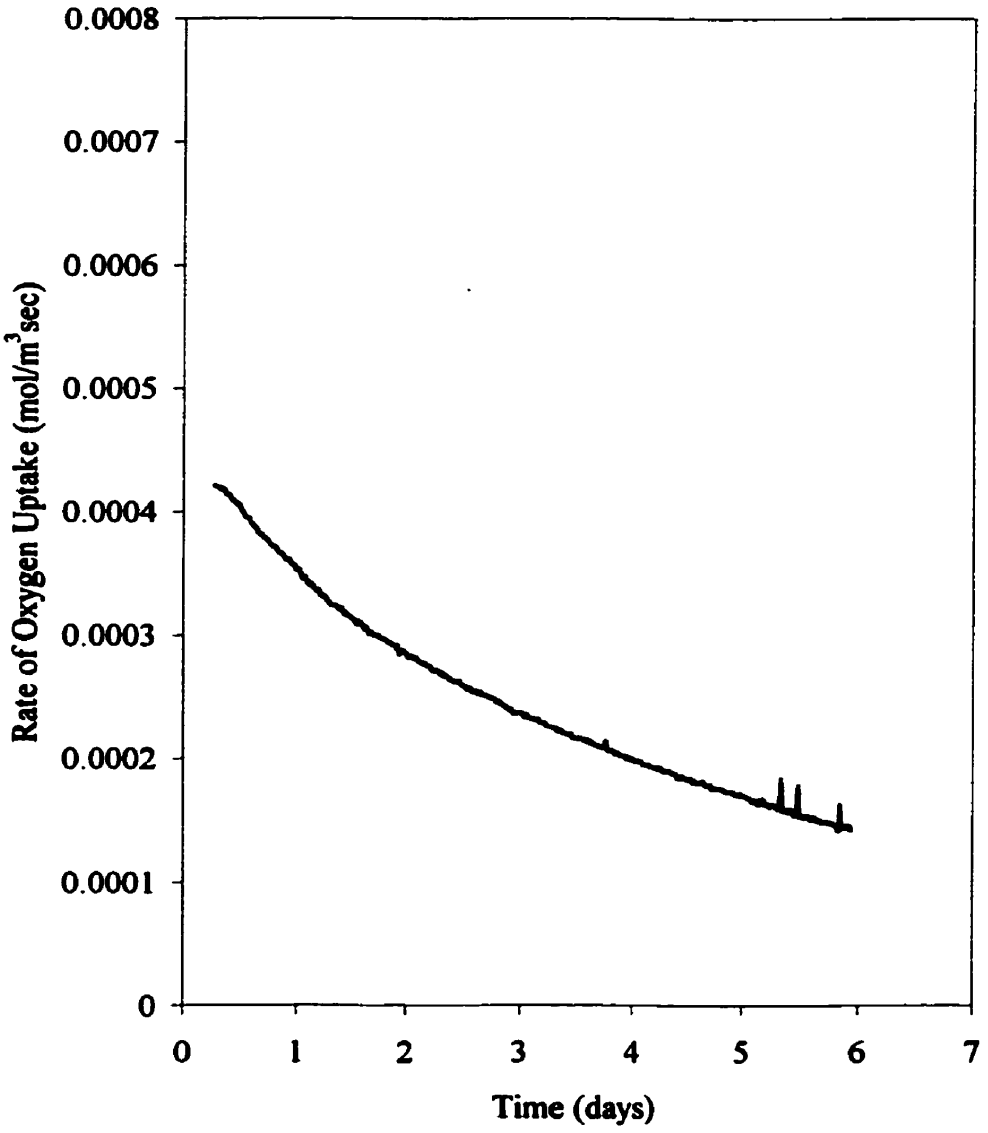

Figure 4.7: Rate of Oxygen Uptake Profile for Test 2-2

4.3 Observed Compositional Results

At the end of each run, the different fluid phase compositions were determined. A large volume of compositional data was collected. All of the data have been tabulated for each individual run and included in the raw data tabulations found in Appendix 1. The observed compositional results include viscosity ratio, asphaltenes content, coke content, as well as effluent aqueous and gas phase analyses.

4.3.1 Viscosity Ratio

Viscosity is the main parameter utilized in this study for evaluating the upgrading process. The end-product viscosities, as well as the original viscosity, have been tabulated and can be found in Table 4.9. The most important crude oil property for thermal flooding is the viscosity dependence on temperature. For most liquids, the Andrade (1930) equation captures this dependence:

$$\mu_o = A_1 e^{B/T} \tag{4.19}$$

Where T is absolute temperature, A_1 and B are empirical parameters whose values are determined from two viscosity measurements at different temperatures. For extrapolation or interpolation, Equation (4.19) indicates that a semilog plot of viscosity versus T^{-1} should be a straight line. In this experimental work, viscosities of the original and reacted samples were measured at 25 °C, 40 °C and 70 °C, hence it should be possible to correlate the temperature behaviour using the Andrade equation. The

regression coefficients are between 0.9998 to 1. Figures 4.8 and 4.9 are representative of the viscosity-temperature relation, its linear form and the regression coefficients. The equations and coefficients are listed in Table 4.10.

In order to more easily compare the results, the viscosity ratio was used, which is defined as the reacted sample viscosity over the initial sample viscosity at the corresponding temperature. If the viscosity ratio is less than 1, then upgrading is deemed to have been achieved. The calculated viscosity ratios were tabulated and can be found in Table 4.11. To keep the data compatible, the viscosity ratio for all figures uses the values measured at 70 °C, if not otherwise indicated.

A plot of the viscosity ratios for all samples regardless of reaction conditions versus initial oxygen partial pressure, and versus asphaltenes contents are shown in Figures 4.10 and 4.11. The points identified with open diamonds indicate experiments in which the contents of the reactor vessel were exposed to Low Temperature Soak (LTS) at temperatures between 80 and 120 °C. As a result of LTS alone, the majority of these samples saw a rise in viscosity ratio. This indicates that during LTS, oxygen was incorporated into the bond structure of the hydrocarbon components (as evident by the pressure decline), but that negligible thermal chain breaking occurred. The observed behaviour confirmed earlier published results of Adegbesan (1987).

Table 4.9: Measured Oil Viscosity

Cell #	Run 1 viscosity 25°C (mPa·s)	Run 1 viscosity 40°C (mPa·s)	Run 1 viscosity 70°C (mPa·s)	Run 2 viscosity 25°C (mPa·s)	Run 2 viscosity 40°C (mPa·s)	Run 2 viscosity 70°C (mPa·s)	Run 3 viscosity 25°C (mPa·s)	Run 3 viscosity 40°C (mPa·s)	Run 3 viscosity 70°C (mPa·s)
1	208200	32200	2085	315000	45410	2615	106300	18670	1380
2	252000	37800	2275	228000	33150	2025	100300	16700	1305
3	487000	63500	3050	191500	29850	1895	175500	30000	1840
4	1338000	137100	5708	189000	27900	1760			
5	560800	70910	3300	189200	28650	1860			
6	528000	69830	3380	210700	31500	2055	104200	18050	1250
7	549100	70830	3470	220500	33650	2060	96620	16300	1150
10	608000	75120	3572	190500	29500	2197	174500	26600	1705
9	621000	78900	3700	253300	36000	2225			
10	575000	73400	3455	324500	43330	2640			
original	218700	32250	1950	218700	32250	1950	218700	32250	1950

Cell #	Run 4 viscosity 25°C (mPa·s)	Run 4 viscosity 40°C (mPa·s)	Run 4 viscosity 70°C (mPa·s)	Run 5 viscosity 25°C (mPa·s)	Run 5 viscosity 40°C (mPa·s)	Run 5 viscosity 70°C (mPa·s)	Run 6 viscosity 25°C (mPa·s)	Run 6 viscosity 40°C (mPa·s)	Run 6 viscosity 70°C (mPa·s)
1	745000	92500	4220	208000	33200	2015	187700	31450	1970
2	217500	34000	2075	135000	24900	1620	223000	36800	2140
3	180500	29850	1935	109200	19700	1415	56200	11270	935
4				78370	15600	1190	358500	49870	2540
5				130700	26550	1635	143500	23500	1540
6	105100	18900	1355	184200	30200	1840	188800	31456	1980
7	137800	23300	1575	172700	30900	1900	189000	31450	1978
8	93500	16820	1235	141700	25250	1595	106500	20500	1425
9				69750	13750	1095	280500	44300	5035
10				140000	23750	1535	195000	32350	1975
original	218700	32250	1950	218700	32250	1950	218700	32250	1950

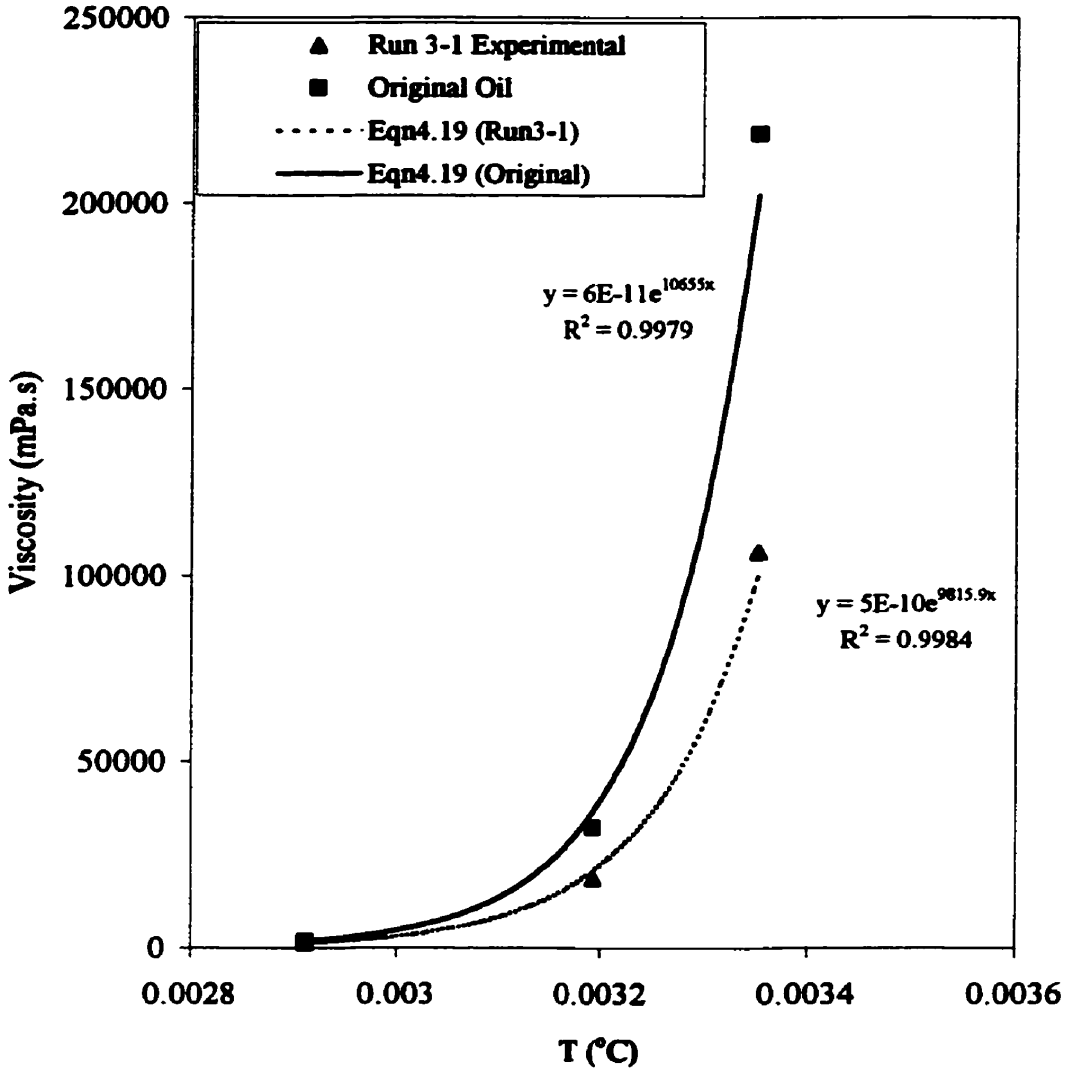

Figure 4.8: Andrade Equation and Measured Data For Run 3-1

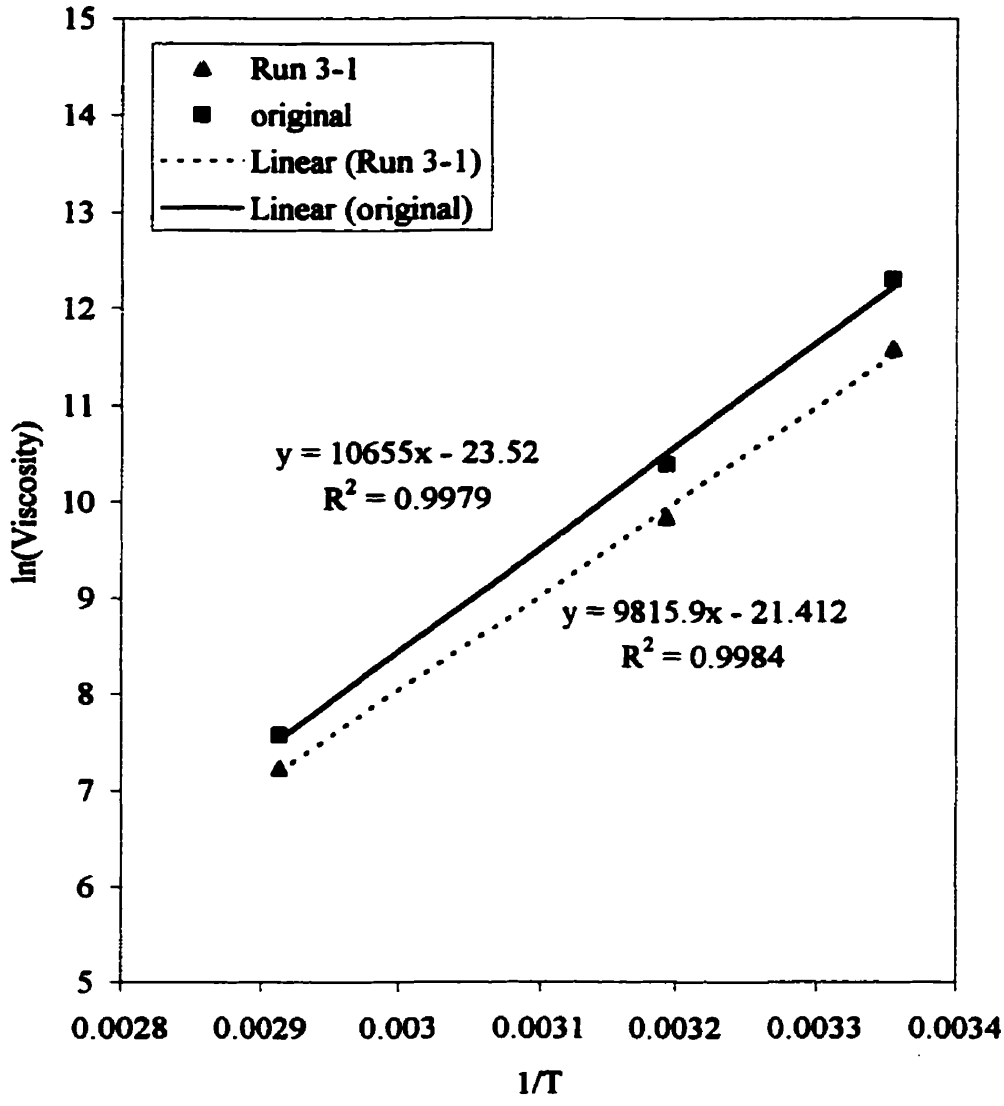

Figure 4.9: Andrade Equation Linear Form For Run 3-1

Table 4.10: Andrade Equation to Describe Reacted Oil Viscosity and The Regression Coefficients

	Run 1		Run 2		Run 3	
Cell #	Andrade Equation	R^2	Andrade Equation	R^2	Andrade Equation	R^2
1	u_o = 1.4e-10Exp(10393/T)	0.9979	u_o = 5.1e-11Exp(10819/T)	0.9980	u_o = 5.0e-10Exp(9815.9/T)	0.9984
2	u_o = 7.6e-11Exp(10632/T)	0.9982	u_o = 6.2e-11Exp(10659/T)	0.9976	u_o = 5.1e-10Exp(9789.2/T)	0.9971
3	u_o = 9.1e-12Exp(11461/T)	0.9983	u_o = 1.2e-10Exp(10425/T)	0.9982	u_o = 1.6e-10Exp(10322/T)	0.9994
4	u_o = 1.5e-12Exp(12293/T)	0.9965	u_o = 7.4e-11Exp(10550/T)	0.9975		
5	u_o = 6.6e-12Exp(11599/T)	0.9982	u_o = 1.1e-10Exp(10429/T)	0.9976		
6	u_o = 1.2e-11Exp(11413/T)	0.9984	u_o = 1.2e-10Exp(10444/T)	0.9974	u_o = 2.7e-10Exp(10001/T)	0.9988
7	u_o = 1.1e-11Exp(11435/T)	0.9980	u_o = 8.6e-11Exp(10556/T)	0.9982	u_o = 2.4e-10Exp(10010/T)	0.9983
8	u_o = 7.2e-12Exp(11594/T)	0.9978	u_o = 3.9e-10Exp(10052/T)	0.9964	u_o = 9.8e-11Exp(10447/T)	0.9978
9	u_o = 8.0e-12Exp(11571/T)	0.9982	u_o = 6.5e-11Exp(10677/T)	0.9972		
10	u_o = 7.9e-12Exp(11552/T)	0.9982	u_o = 4.9e-11Exp(10837/T)	0.9963		
original	u_o = 6.1e-11Exp(10655/T)	0.9979	u_o = 6.1e-11Exp(10655/T)	0.9979	u_o = 6.1e-11Exp(10655/T)	0.9979

	Run 4		Run 5		Run 6	
Cell #	Andrade Equation	R^2	Andrade Equation	R^2	Andrade Equation	R^2
1	u_o = 6.6e-12Exp(11684/T)	0.9981	u_o = 1.0e-10Exp(10486/T)	0.9988	u_o = 1.7e-10Exp(10312/T)	0.9991
2	u_o = 9.8e-11Exp(10515/T)	0.9985	u_o = 3.3e-10Exp(10026/T)	0.9996	u_o = 1.0e-10Exp(10522/T)	0.9994
3	u_o = 2.0e-10Exp(10255/T)	0.9987	u_o = 5.0e-10Exp(9831.1/T)	0.9989	u_o = 1.7e-09Exp(9268.7/T)	0.9991
4			u_o = 1.1e-09Exp(9486.8/T)	0.9995	u_o = 1.7e-11Exp(11188/T)	0.9986
5			u_o = 4.0e-10Exp(9963.6/T)	1.0000	u_o = 1.6e-10Exp(10249/T)	0.9985
6	u_o = 4.6e-10Exp(9842.1/T)	0.9989	u_o = 1.2e-10Exp(10422/T)	0.9990	u_o = 1.7e-10Exp(10311/T)	0.9990
7	u_o = 2.4e-10Exp(10109/T)	0.9987	u_o = 2.1e-10Exp(10224/T)	0.9997	u_o = 1.7e-10Exp(10316/T)	0.9990
8	u_o = 5.0e-10Exp(9783.6/T)	0.9988	u_o = 2.1e-10Exp(10167/T)	0.9995	u_o = 5.9e-10Exp(9779.4/T)	0.9996
9			u_o = 1.3e-09Exp(9402.3/T)	0.9992	u_o = 1.9e-08Exp(8989.7/T)	0.9886
10			u_o = 1.8e-10Exp(10211/T)	0.9990	u_o = 1.3e-10Exp(10394/T)	0.9991
original	u_o = 6.1e-11Exp(10655/T)	0.9979	u_o = 6.1e-11Exp(10655/T)	0.9979	u_o = 6.1e-11Exp(10655/T)	0.9979

Table 4.11: Calculated Reacted Oil Viscosity Ratio (Compared to the Original)

Cell #	Run 1 viscosity ratio @25°C	Run 1 viscosity ratio @40°C	Run 1 viscosity ratio @70°C	Run 2 viscosity ratio @25°C	Run 2 viscosity ratio @40°C	Run 2 viscosity ratio @70°C	Run 3 viscosity ratio @25°C	Run 3 viscosity ratio @40°C	Run 3 viscosity ratio @70°C
1	0.952	0.998	1.069	1.440	1.408	1.341	0.486	0.579	0.708
2	1.152	1.172	1.167	1.043	1.028	1.038	0.459	0.518	0.669
3	2.227	1.969	1.564	0.876	0.926	0.972	0.802	0.930	0.944
4	6.118	4.251	2.927	0.864	0.865	0.903			
5	2.564	2.199	1.692	0.865	0.888	0.954			
6	2.414	2.165	1.733	0.963	0.977	1.054	0.476	0.560	0.641
7	2.511	2.196	1.779	1.008	1.043	1.056	0.442	0.505	0.590
8	2.780	2.329	1.832	0.871	0.915	1.055	0.798	0.825	0.874
9	2.840	2.447	1.897	1.158	1.116	1.141			
10	2.629	2.276	1.772	1.484	1.344	1.354			

Cell #	Run 4 viscosity ratio @25°C	Run 4 viscosity ratio @40°C	Run 4 viscosity ratio @70°C	Run 5 viscosity ratio @25°C	Run 5 viscosity ratio @40°C	Run 5 viscosity ratio @70°C	Run 6 viscosity ratio @25°C	Run 6 viscosity ratio @40°C	Run 6 viscosity ratio @70°C
1	3.406	2.868	2.164	0.951	1.029	1.033	0.858	0.975	1.010
2	0.995	1.054	1.064	0.617	0.772	0.831	1.020	1.141	1.097
3	0.825	0.926	0.992	0.499	0.611	0.726	0.257	0.349	0.479
4				0.358	0.484	0.610	1.639	1.546	1.303
5				0.598	0.823	0.838	0.656	0.729	0.790
6	0.481	0.586	0.695	0.842	0.936	0.944	1.316	1.339	1.286
7	0.630	0.722	0.808	0.790	0.958	0.974	1.317	1.338	1.284
8	0.428	0.522	0.633	0.648	0.783	0.818	0.487	0.636	0.731
9				0.319	0.426	0.562	1.283	1.374	2.582
10				0.640	0.736	0.787	0.892	1.003	1.013

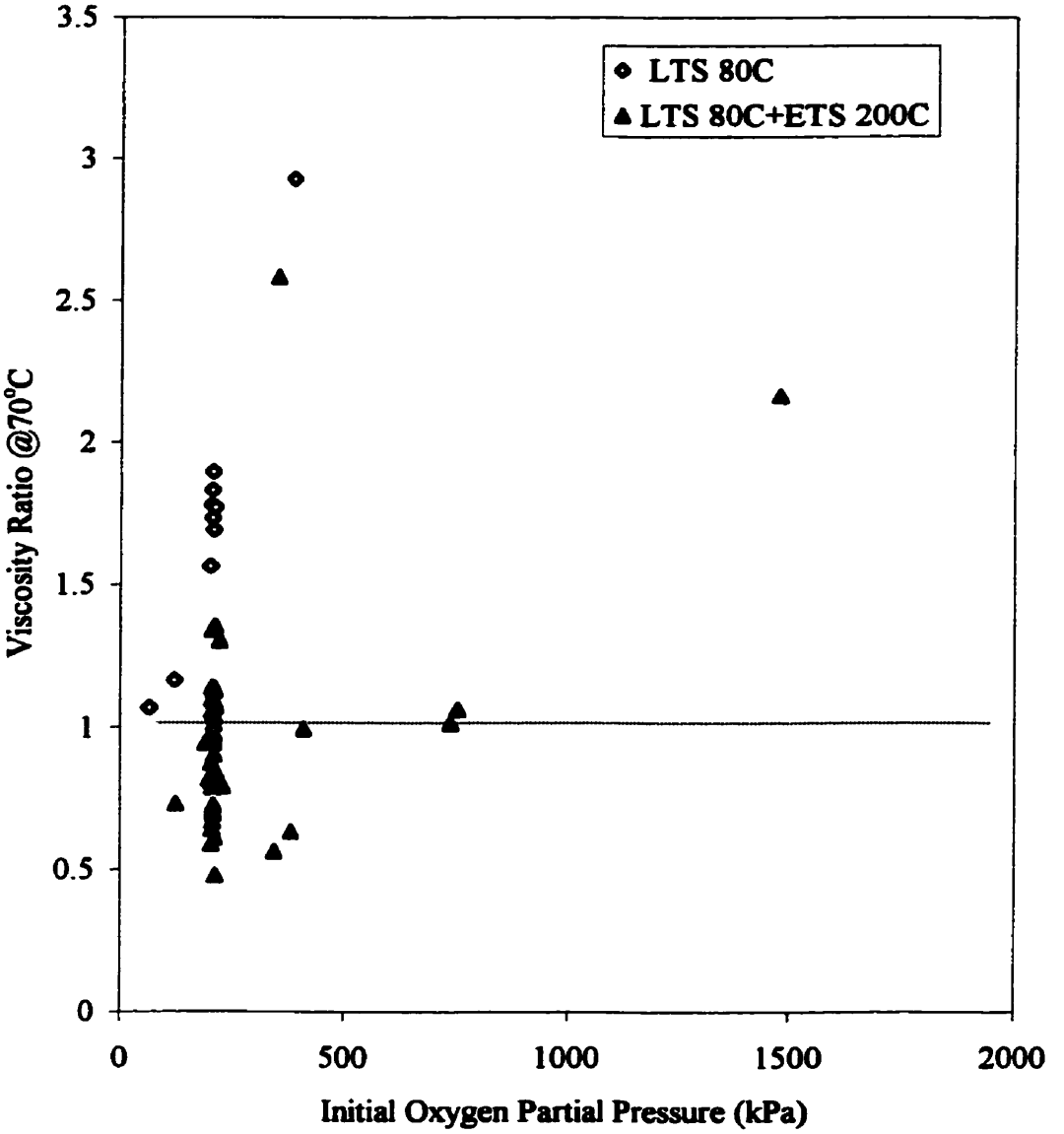

Figure 4.10: Effect of Oxygen Partial Pressure on Viscosity Ratio

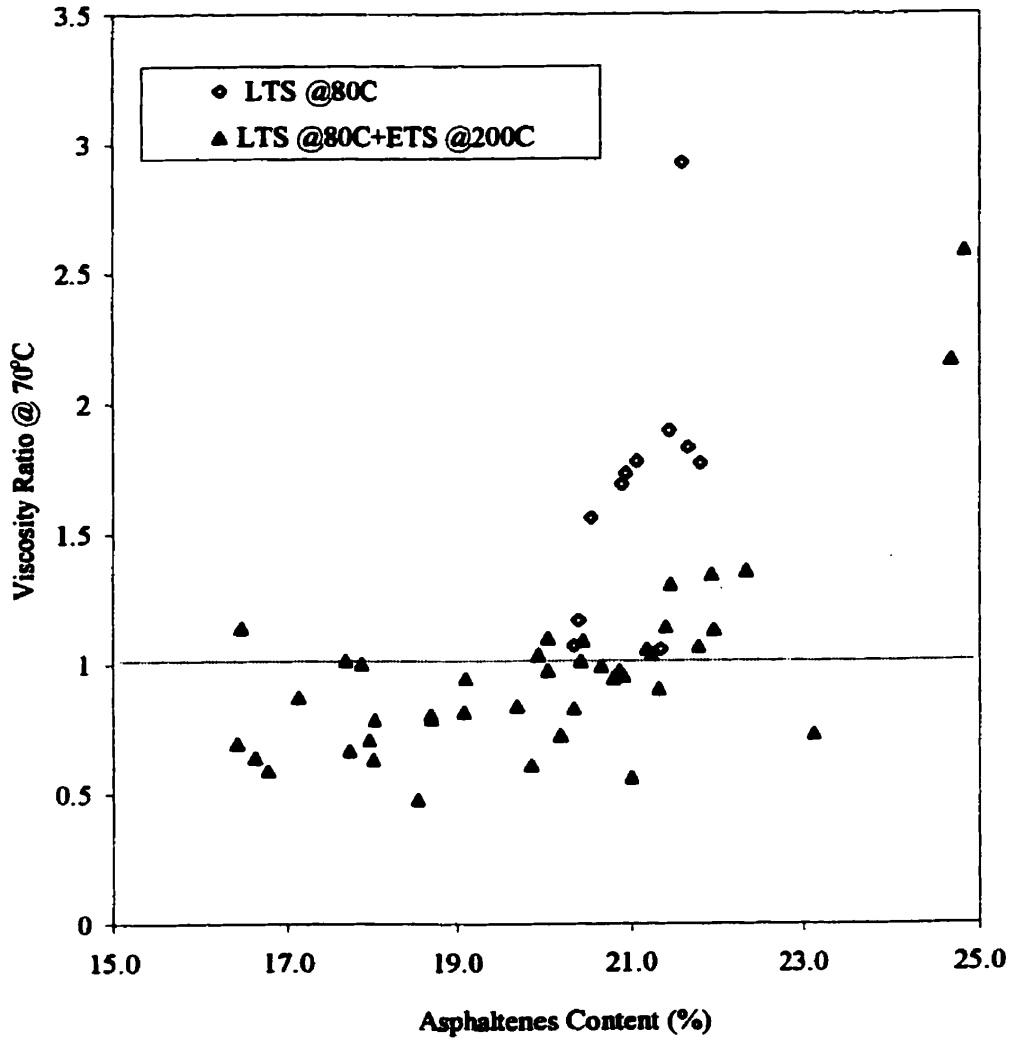

Figure 4.11: Effect of Asphaltenes Content on Viscosity

The solid triangle points represent experiments where oil was exposed to Low Temperature Soak (LTS) at a temperature of 80 °C, followed by extended periods of oxidative soaking at higher temperature, herein referred to as Elevated Temperature Soak (ETS). As a result of the ETS periods, a large number of samples were observed to achieve reduced viscosities; the range of viscosity ratios observed for the upgraded oils fell between 0.4 and 1.0. It is believed that the LTS step incorporates oxygen into some of the hydrocarbons, resulting in labile bonds that should break at lower temperatures than those normally utilized in upgrading processes. Once initiating free radicals are formed, they can then proceed to promote thermal chain-breaking reactions during the higher temperature step.

4.3.2 Density

The end-product densities, measured at 25 °C, are tabulated in Table 4.12. As was done for viscosity, a density ratio (defined as the ratio of the end-product density to the original oil density at 25 °C) was calculated in order to more easily compare the results. These ratios can also be found in Table 4.12. For the majority of the runs, small changes (less than 1%) were observed. The final densities increased in the majority of the experiments, which is consistent with Wichert's (1996) results.

Table 4.11: Calculated Reacted Oil Viscosity Ratio (Compared to the Original)

Cell #	Run 1 viscosity ratio @25°C	Run 1 viscosity ratio @40°C	Run 1 viscosity ratio @70°C	Run 2 viscosity ratio @25°C	Run 2 viscosity ratio @40°C	Run 2 viscosity ratio @70°C	Run 3 viscosity ratio @25°C	Run 3 viscosity ratio @40°C	Run 3 viscosity ratio @70°C
1	0.952	0.998	1.069	1.440	1.408	1.341	0.486	0.579	0.708
2	1.152	1.172	1.167	1.043	1.028	1.038	0.459	0.518	0.669
3	2.227	1.969	1.564	0.876	0.926	0.972	0.802	0.930	0.944
4	6.118	4.251	2.927	0.864	0.865	0.903			
5	2.564	2.199	1.692	0.865	0.888	0.954			
6	2.414	2.165	1.733	0.963	0.977	1.054	0.476	0.560	0.641
7	2.511	2.196	1.779	1.008	1.043	1.056	0.442	0.505	0.590
8	2.780	2.329	1.832	0.871	0.915	1.055	0.798	0.825	0.874
9	2.840	2.447	1.897	1.158	1.116	1.141			
10	2.629	2.276	1.772	1.484	1.344	1.354			

Cell #	Run 4 viscosity ratio @25°C	Run 4 viscosity ratio @40°C	Run 4 viscosity ratio @70°C	Run 5 viscosity ratio @25°C	Run 5 viscosity ratio @40°C	Run 5 viscosity ratio @70°C	Run 6 viscosity ratio @25°C	Run 6 viscosity ratio @40°C	Run 6 viscosity ratio @70°C
1	3.406	2.868	2.164	0.951	1.029	1.033	0.858	0.975	1.010
2	0.995	1.054	1.064	0.617	0.772	0.831	1.020	1.141	1.097
3	0.825	0.926	0.992	0.499	0.611	0.726	0.257	0.349	0.479
4				0.358	0.484	0.610	1.639	1.546	1.303
5				0.598	0.823	0.838	0.656	0.729	0.790
6	0.481	0.586	0.695	0.842	0.936	0.944	1.316	1.339	1.286
7	0.630	0.722	0.808	0.790	0.958	0.974	1.317	1.338	1.284
8	0.428	0.522	0.633	0.648	0.783	0.818	0.487	0.636	0.731
9				0.319	0.426	0.562	1.283	1.374	2.582
10				0.640	0.736	0.787	0.892	1.003	1.013

4.3.3. Asphaltenes plus Coke Contents

It is usually the high-boiling constituents of petroleum that exert considerable influence on the physical properties of the crude oils, such as the specific gravity (or API gravity). The asphaltic constituents of petroleum usually appear as a dark brown to black, semisolid fraction, but what constitutes the asphaltic fraction of petroleum is a matter of conjecture. Separation of the asphaltic portion of the petroleum into asphaltenes, resins, and oils can be achieved by a variety of methods. As mentioned in Chapter 3, the asphaltenes were precipitated by the addition of a low-boiling paraffinic solvent, n-pentane, to the crude oil. The mass fraction of asphaltenes in the end product is presented in Table 4.13. The asphaltenes content increased in almost all cases.

The coke content determination is also method-dependent. In this thesis, the coke matrix was defined as toluene and n-pentane insoluble, except in experiments involving core where the coke was determined by the loss on ignition (at 600°C). The coke amount and mass fraction for all runs are summarized in Table 4.14. It was found that the amount of coke in the reactions (Run 2 to Run 5) was less than 1% for all cases. For Run #1 of the LTS only reaction, coke was not formed. For Run #6 with brine, the coke contents for Run 6-2 to Run 6-7 were coke plus salts as it was hard to separate them.

A plot of the asphaltenes (in mass percentage) versus the initial oxygen partial pressure for all samples is shown in Figure 4.12. It can be seen from this plot that, even though upgrading in terms of viscosity occurred in some cases, the asphaltenes content

increased in most of the cases (the original asphaltenes content was approximately 17.8%). This would suggest that the thermal cracking of the oil occurred mainly in the lighter maltenes fractions.

4.3.4 Maltenes Composition Analyses

The carbon distribution of the maltenes fraction for the last ten samples and the original bitumen was determined with simulated distillation gas chromatography. The results can be lumped into light and heavy components according to the carbon number of 40 and these lumped data are showed in Table 4.15.

From Table 4.15, it can be seen that an increase of the lighter carbon components (C<40) from 53.46 in the original sample to 55.94 (% maltenes) occurs for the Run 6, Cell 5. The increase of the lighter ends suggests that the chain-breaking reactions occurred in the maltenes components. As a result of the combined LTS/ETS treatment, the asphaltenes content of the oil for Test 6-5 increased from 17.8% to 18.9 %, while the viscosity ratio of this sample was reduced to 0.79. This provides evidence that the viscosity reduction which occurred even though the asphaltenes contents increased was a result of the maltenes fractions cracking. Figure 4.13 shows a comparison of the carbon distribution of the oxidized sample of Test 6-5 with the original oil. It shows that the oxidized sample lost some lighter ends (up to approximately C_{10}) due to the post treatment, but the total amount of light components (C<40) increased. The recovery rate increase (from 74.16 to 77.07 %) also indicated the enhancement of the distillable

portion of the maltenes phase. The carbon distribution comparisons curves for the rest of the runs are similar to Figure 4.13.

The component changes after the LTS/ETS process could be obtained by incorporating the asphaltenes and coke contents analyses. It is seen that although the asphaltenes contents increase, the lighter carbon composition increases simultaneously, which explains the viscosity reduction cases.

Table 4.13: Reacted Oil Asphaltenes Contents

Cell #	Run 1 Asphaltenes %	Run 2 Asphaltenes %	Run 3 Asphaltenes %	Run 4 Asphaltenes %	Run 5 Asphaltenes %	Run 6 Asphaltenes %
1	20.33	21.93	17.95	24.68	19.93	20.42
2	20.39	21.23	17.71	21.78	20.33	20.04
3	20.54	20.86	19.10	20.65	20.18	18.54
4	21.59	21.32			19.86	21.45
5	20.88	20.90			19.70	18.69
6	20.93	21.34	16.62	16.41	20.79	20.44
7	21.06	21.18	16.77	18.69	20.04	16.46
8	21.66	21.96	17.12	17.99	19.08	23.13
9	21.44	21.40			21.00	24.82
10	21.80	22.33			18.02	17.66
original	17.85	17.85	17.85	17.85	17.85	17.85

Table 4.14: Reacted Oil Coke Contents

Cell #	Run 1 Coke %	Run 2 Coke %	Run 3 Coke %	Run 4 Coke %	Run 5 Coke %	Run 6 Coke %
1	0.0000	0.0460	0.3659	0.8109	0.3017	-
2	0.0000	0.1121	0.3414	0.4324	0.2958	0.3387
3	0.0000	0.2430	0.0141	0.3594	0.2586	0.1342
4	0.0000	0.2903			0.6390	0.0572
5	0.0000	0.1941			0.5992	2.9279
6	0.0000	0.1494	0.0243	0.0000	0.0607	0.1430
7	0.0000	0.0263	0.0214	0.3003	0.3267	0.2784
8	0.0000	0.0122	0.0127	0.3826	0.0317	0.1363
9	0.0000	0.0156			0.2865	0.2686
10	0.0000	0.0000			0.0000	2.3468

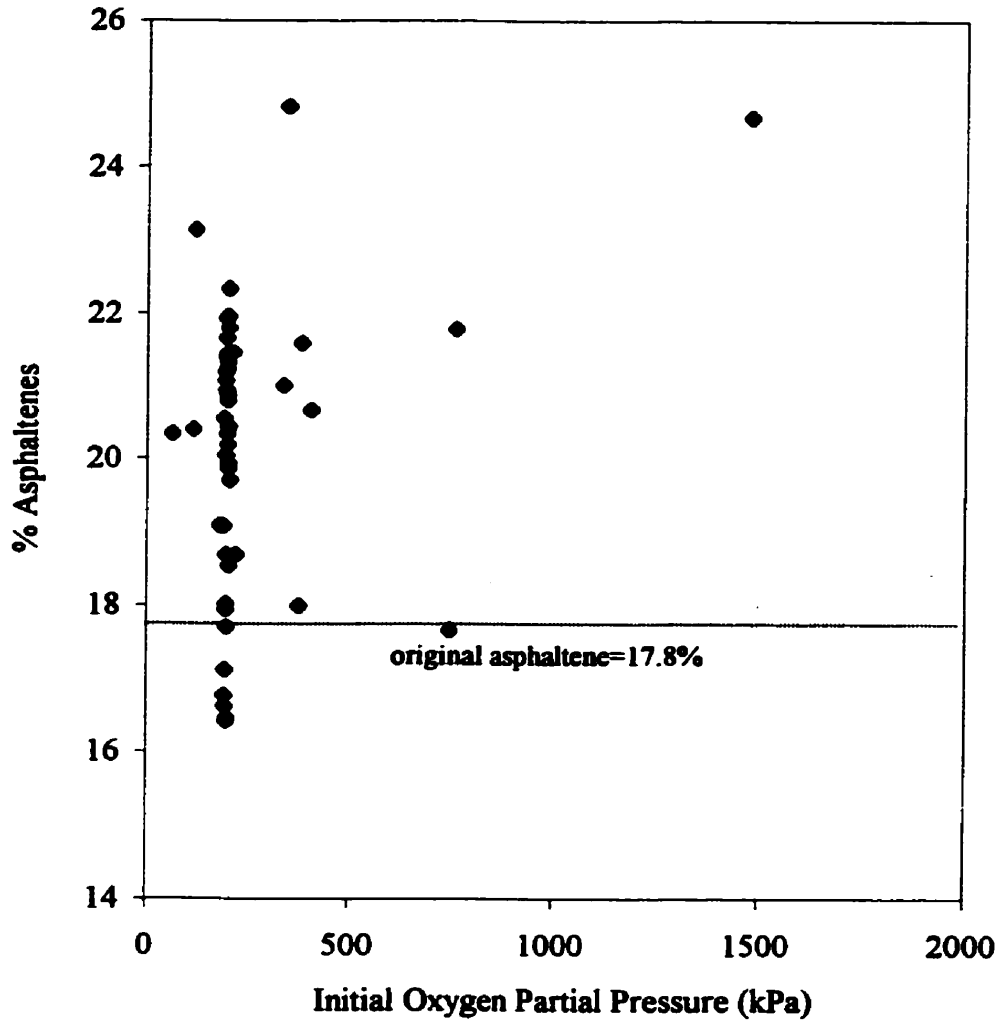

Figure 4.12: Effect of Oxygen Partial Pressure on Asphaltenes Content

Table 4.15: Lumped Compositions Comparison of Reacted and Original Oils

cell #	Asphaltenes	Maltenes	Light Part in Maltenes	Light Part in Total	Heavy Part in Maltenes	Heavy Part in Total	Recovery	Viscosity ratio
	%	%	(C < 40) % maltenes	(C < 40) % total	(Asph.>C>40) % maltenes	(Asph.>C>40) % total	(%from GC)	70°C
6-1	20.416	79.584	53.730	42.761	46.270	36.824	76.17	1.010
6-2	20.038	79.962	52.470	41.956	47.530	38.006	75.22	1.097
6-3	18.542	81.458	55.130	44.908	44.870	36.550	78.44	0.479
6-4	21.453	78.547	55.070	43.256	44.930	35.291	77.51	1.303
6-5	18.693	81.307	55.940	45.483	44.060	35.824	77.07	0.790
6-6	20.439	79.561	53.150	42.287	46.850	37.275	77.03	1.286
6-7	16.462	83.538	54.070	45.169	45.930	38.369	77.06	1.284
6-8	17.664	82.336	52.550	43.267	47.450	39.068	76.06	0.731
6-9	24.823	75.177	53.950	40.558	46.050	34.619	78.24	2.582
6-10	23.134	76.866	55.440	42.615	44.560	34.252	79.29	1.013
Original	17.850	82.150	53.460	43.917	46.540	38.233	74.16	1.000

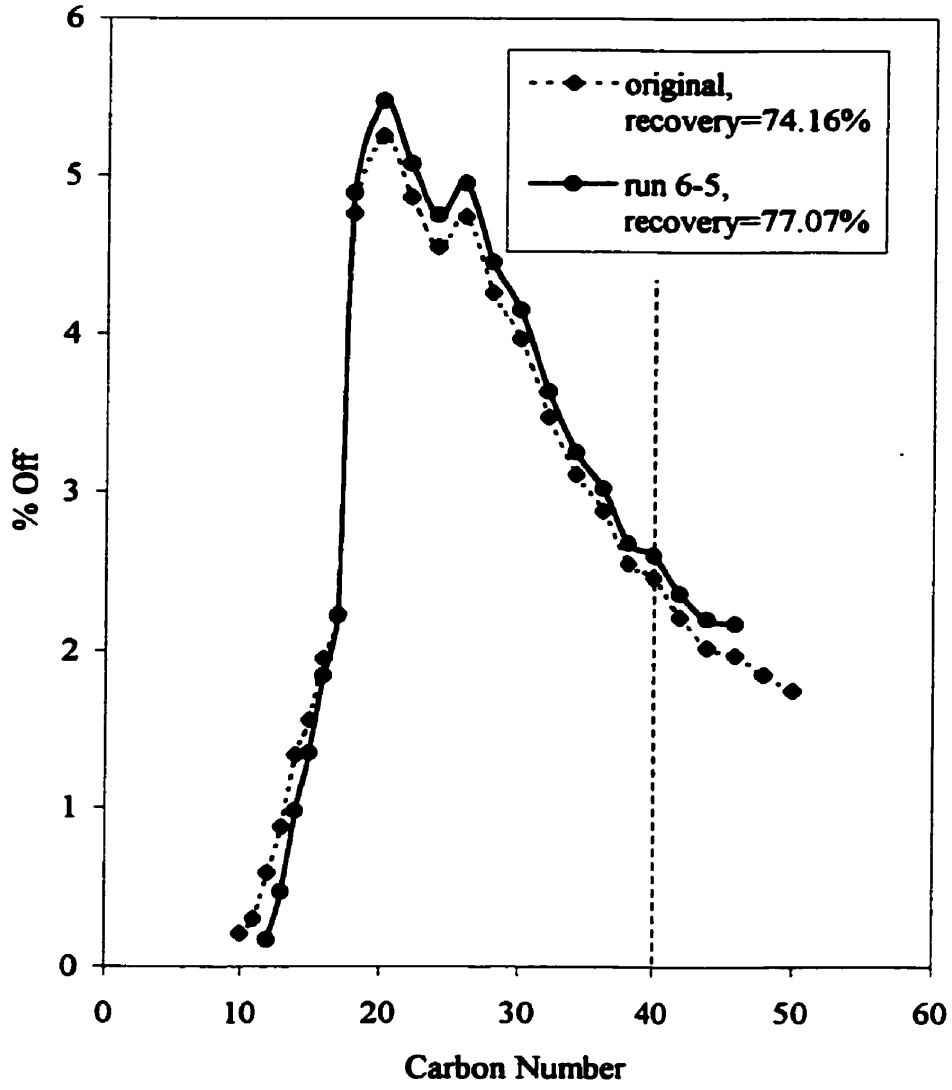

Figure 4.13: Carbon Distribution Comparison of Run 6-5

4.3.5. Effluent Gas Analyses / Compositions

As was stated earlier in Chapter 3, the effluent product gases were sampled and analyzed via gas chromatography. Tables 4.16 to 4.22 give the molar percentages of oxygen, nitrogen, carbon dioxide, carbon monoxide and some light hydrocarbons for each run.

The vapor phase oxygen content of each run was found to decrease, as expected. In most cases, where the reaction was allowed to continue until the oxygen was used up, the final oxygen concentration was consistently very small (generally around 0.1 to 1% in the produced gas as compared to the original air containing 21% oxygen). This happened because most of the oxygen was consumed as a result of the LTS and ETS reactions.

The relative amount of nitrogen was seen to increase proportionally to the decrease in oxygen. This is because the inert property of nitrogen and the total amount of the gas decreases after the oxidation reaction process.

Bond-scission reactions are usually evidenced by a rapid increase in the generation of carbon oxides and light hydrocarbon gases such as methane and ethane. From Table 4.18, it can be seen that the main gas phase cracking product is CO_2, and that it appears in almost all of the runs. CO was the second most abundant generated gas. The light hydrocarbon gases, such as CH_4, C_2H_6 and C_3H_8, only appeared in experiments involving sand and brine or high temperatures. For example, during Run 6-3, a thermocouple malfunction occurred and the control system drove the reactor from its

setpoint of 200 °C to 300 °C for approximately one hour during the ETS stage. This resulted in the production of CH_3, C_2H_6 and C_3H_8, and their combined amount is around 9 % of the CO amount. This will be discussed later.

Figure 4.14 shows the effluent CO_2 content versus oxygen uptake for each run. Figure 4.15 shows the total cracked gas (CO_2 plus CO, CH_4, C_2H_6 and C_3H_8) versus the oxygen uptake. Since CO_2 was the main product (composing almost 90% of the effluent product gas), the two figures appear very similar. Evidence of thermal cracking (i.e. the presence of carbon-oxides, and light hydrocarbon gases such as methane and ethane) was found in most of the two-stage tests, with the mass percentages of these gases in the effluent gases between 2 and 10 %. Experiments conducted with core were observed to produce enhanced levels of CO_2. This may have been due to surface area and catalytic effects as the sand matrix contained no appreciable carbonates. In the LTS only reaction (Run #1), the CO_2 content in the effluent gas analysis was always less than 1%, implying that less thermal cracking occurred. Moreover, the effluent gas for the nitrogen runs contained less than 1% CO_2, except test 5-10 that involved sand matrix.

Table 4.16: Nitrogen Contents

Cell #	Run 1 N_2 %	Run 2 N_2 %	Run 3 N_2 %	Run 4 N_2 %	Run 5 N_2 %	Run 6 N_2 %
1	-	96.32	93.56	92.87	89.70	95.63
2	-	95.96	93.44	94.62	89.76	95.46
3	94.28	-	97.54	93.71	89.78	90.60
4	92.09	95.75			89.41	96.36
5	94.40	95.35			91.63	90.47
6	98.21	94.75	98.84	99.88	89.78	95.51
7	98.61	96.53	99.39	96.57	89.27	95.53
8	93.26	97.79	99.52	93.71	87.18	93.69
9	98.07	92.83			90.89	96.22
10	98.57	97.41			93.71	94.85
orig.air	79.28	79.28	79.28	79.28	79.28	79.28
orig.N_2	99.74	99.74	99.74	99.74	99.74	99.74

Table 4.17: Oxygen Contents

Cell #	Run 1 O_2 %	Run 2 O_2 %	Run 3 O_2 %	Run 4 O_2 %	Run 5 O_2 %	Run 6 O_2 %
1	-	1.62	1.75	0.44	0.37	0.38
2	-	1.52	1.44	0.42	0.50	0.12
3	5.09	-	1.13	0.51	0.85	0.30
4	7.47	1.75			0.32	2.65
5	5.15	1.62			5.88	0.72
6	0.97	1.36	0.61	0.12	0.78	0.23
7	0.43	1.71	0.28	0.64	0.59	0.26
8	6.35	0.60	0.26	0.51	2.97	0.67
9	1.25	3.92			0.43	0.40
10	0.69	0.90			0.19	0.47
orig.air	20.72	20.72	20.72	20.72	20.72	20.72
orig.N_2	0.003	0.003	0.003	0.003	0.003	0.003

Table 4.18: Carbon Dioxide Contents

Cell #	Run 1 CO_2 %	Run 2 CO_2 %	Run 3 CO_2 %	Run 4 CO_2 %	Run 5 CO_2 %	Run 6 CO_2 %
1	-	2.06	4.69	6.69	9.72	3.99
2	-	2.51	5.13	4.97	9.74	4.19
3	0.63	-	1.32	5.78	9.37	5.13
4	0.44	2.50			9.91	1.00
5	0.45	3.04			2.48	8.81
6	0.82	3.89	**0.55**	**0.00**	9.27	3.95
7	0.96	1.76	**0.33**	2.79	10.14	4.00
8	0.39	1.61	**0.22**	5.78	9.85	5.13
9	0.68	3.26			8.28	3.17
10	0.74	1.69			**6.10**	4.43
orginal	0.00	0.00	0.00	0.00	0.00	0.00

*N2 runs shown in bold

Table 4.19: Carbon Monoxide Contents

Cell #	Run 1 CO %	Run 2 CO %	Run 3 CO %	Run 4 CO %	Run 5 CO %	Run 6 CO %
1	-	0.00	0.65	0.59	0.21	0.00
2	-	0.00	0.61	0.54	0.00	0.00
3	0.00	-	0.00	0.72	0.00	0.00
4	0.00	0.00			0.00	0.00
5	0.00	0.00			0.00	0.00
6	0.00	0.00	0.00	0.00	0.17	0.00
7	0.00	0.00	0.00	0.25	0.00	0.00
8	0.00	0.00	0.00	0.72	0.00	0.51
9	0.00	0.00			0.15	0.21
10	0.00	0.00			0.00	0.25
orginal	0.00	0.00	0.00	0.00	0.00	0.00

Table 4.20: Methane Contents

Cell #	Run 1 CH_4 %	Run 2 CH_4 %	Run 3 CH_4 %	Run 4 CH_4 %	Run 5 CH_4 %	Run 6 CH_4 %
1	-	0.00	0.00	0.00	0.00	0.00
2	-	0.00	0.00	0.00	0.00	0.23
3	0.00	-	0.00	0.00	0.00	1.91
4	0.00	0.00			0.37	0.00
5	0.00	0.00			0.00	0.00
6	0.00	0.00	0.00	0.00	0.00	0.32
7	0.00	0.00	0.00	0.00	0.00	0.21
8	0.00	0.00	0.00	0.00	0.00	0.00
9	0.00	0.00			0.25	0.00
10	0.00	0.00			0.00	0.00
orginal	0.00	0.00	0.00	0.00	0.00	0.00

Table 4.21: Ethane Contents

Cell #	Run 1 C_2H_6 %	Run 2 C_2H_6 %	Run 3 C_2H_6 %	Run 4 C_2H_6 %	Run 5 C_2H_6 %	Run 6 C_2H_6 %
1	-	0.00	0.00	0.00	0.00	0.00
2	-	0.00	0.00	0.00	0.00	0.00
3	0.00	-	0.00	0.00	0.00	1.82
4	0.00	0.00			0.00	0.00
5	0.00	0.00			0.00	0.00
6	0.00	0.00	0.00	0.00	0.00	0.00
7	0.00	0.00	0.00	0.00	0.00	0.00
8	0.00	0.00	0.00	0.00	0.00	0.00
9	0.00	0.00			0.00	0.00
10	0.00	0.00			0.00	0.00
orginal	0.00	0.00	0.00	0.00	0.00	0.00

Table 4.22: Propane Contents

Cell #	Run 1 C_3H_8 %	Run 2 C_3H_8 %	Run 3 C_3H_8 %	Run 4 C_3H_8 %	Run 5 C_3H_8 %	Run 6 C_3H_8 %
1	-	0.00	0.00	0.00	0.00	0.00
2	-	0.00	0.00	0.00	0.00	0.00
3	0.00	-	0.00	0.00	0.00	0.23
4	0.00	0.00			0.00	0.00
5	0.00	0.00			0.00	0.00
6	0.00	0.00	0.00	0.00	0.00	0.00
7	0.00	0.00	0.00	0.00	0.00	0.00
8	0.00	0.00	0.00	0.00	0.00	0.00
9	0.00	0.00			0.00	0.00
10	0.00	0.00			0.00	0.00
orginal	0.00	0.00	0.00	0.00	0.00	0.00

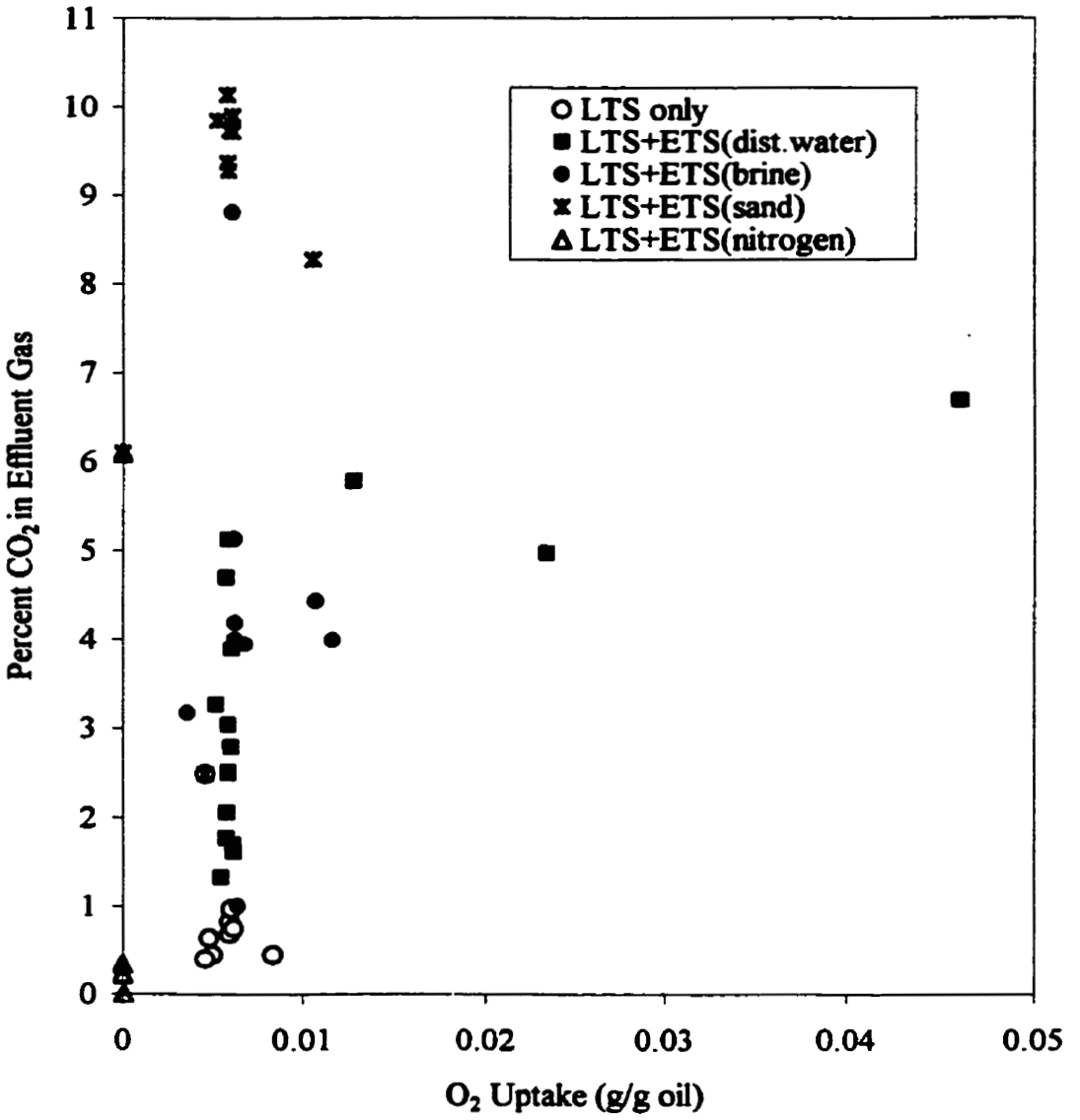

Figure 4.14: CO_2 Contents of Effluent Gas vs. Oxygen Uptake For Overall Runs

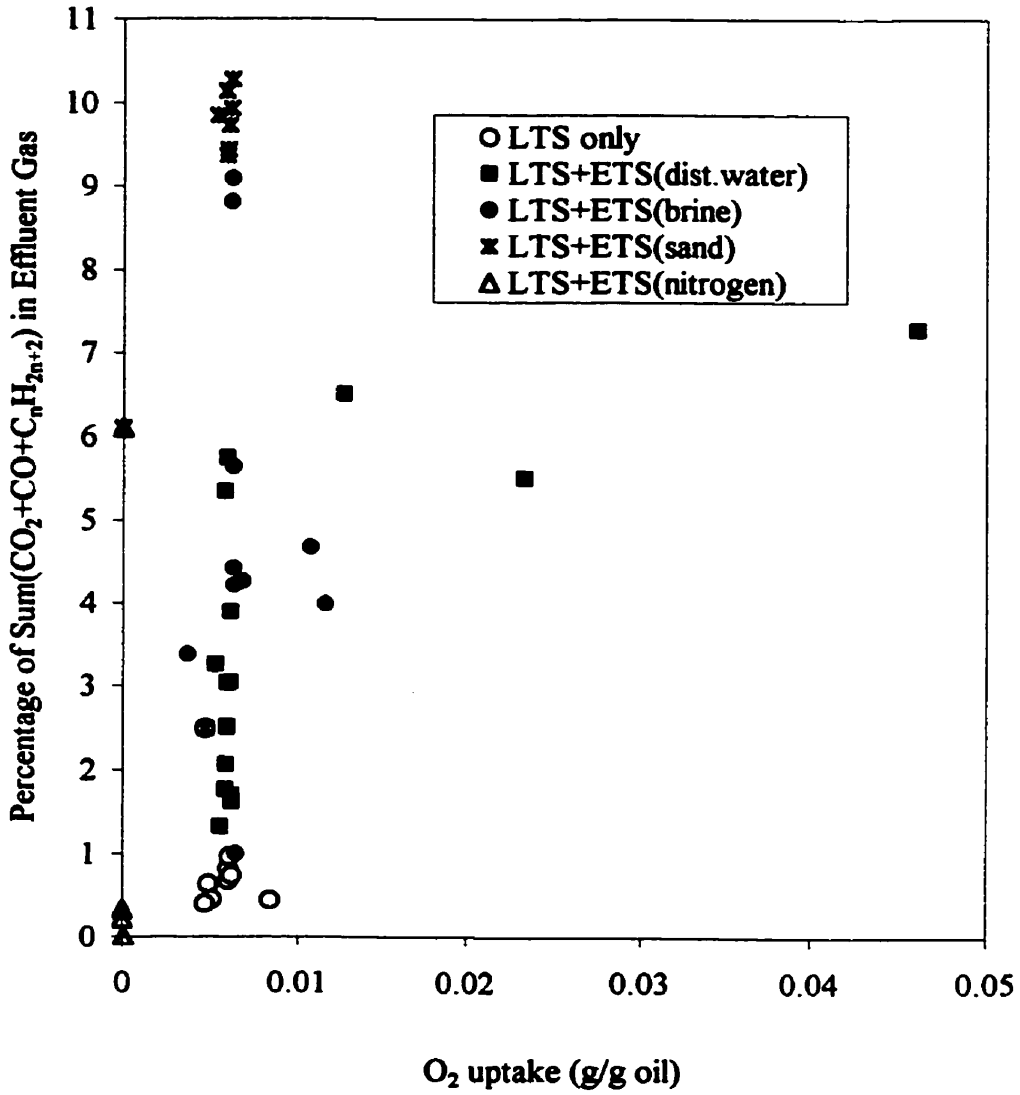

Figure 4.15: Sum of CO_2,CO and Light Hydrocarbon at Effluent Gas vs. Oxygen Uptake

4.3.6. Effluent Aqueous Phase

The measured pHs of the free water phase recovered from all the cells are summarized in Table 4.23 and are plotted in Figure 4.16. The diamond points show the brine runs, while the other points show the distilled water runs. It can be seen that, in most cases, the pHs of the distilled water runs changed from the original value (pH = 6.2) to acidic, and the trend is that the more the oxygen uptake, the sharper the pH changes (for example, in Run 4, cell 1, the final pH is only 1.81). The degree of change implies that acid groups, such as carboxylic acids, are being formed as part of the LTS process. However, the effluent aqueous phase with the brine showed the pH range from 8.25 ~ 9.05. Comparing with the original pH value of 8.55, it illustrates that the brine has a buffering effect on the pH.

Table 4.23: pH of Free Water Phase

Cell #	Run 1 pH	Run 2 pH	Run 3 pH	Run 4 pH	Run 5 pH	Run 6 pH
1	6.25	2.50	2.63	1.81	-	8.49
2	~	2.60	2.72	2.04	-	8.88
3	4.13	3.20	3.06	2.82	-	8.70
4	3.73	3.40			-	9.28
5	4.12	3.00			-	-
6	3.31	2.40	3.73	7.52	-	8.96
7	3.04	2.60	6.95	3.07	-	8.55
8	4.14	2.80	3.53	2.79	-	3.43
9	2.84	2.50			-	2.73
10	3.45	2.50			-	2.27
Distilled H_2O	6.20	6.20	6.20	6.20		6.20
Brine					8.55	8.55

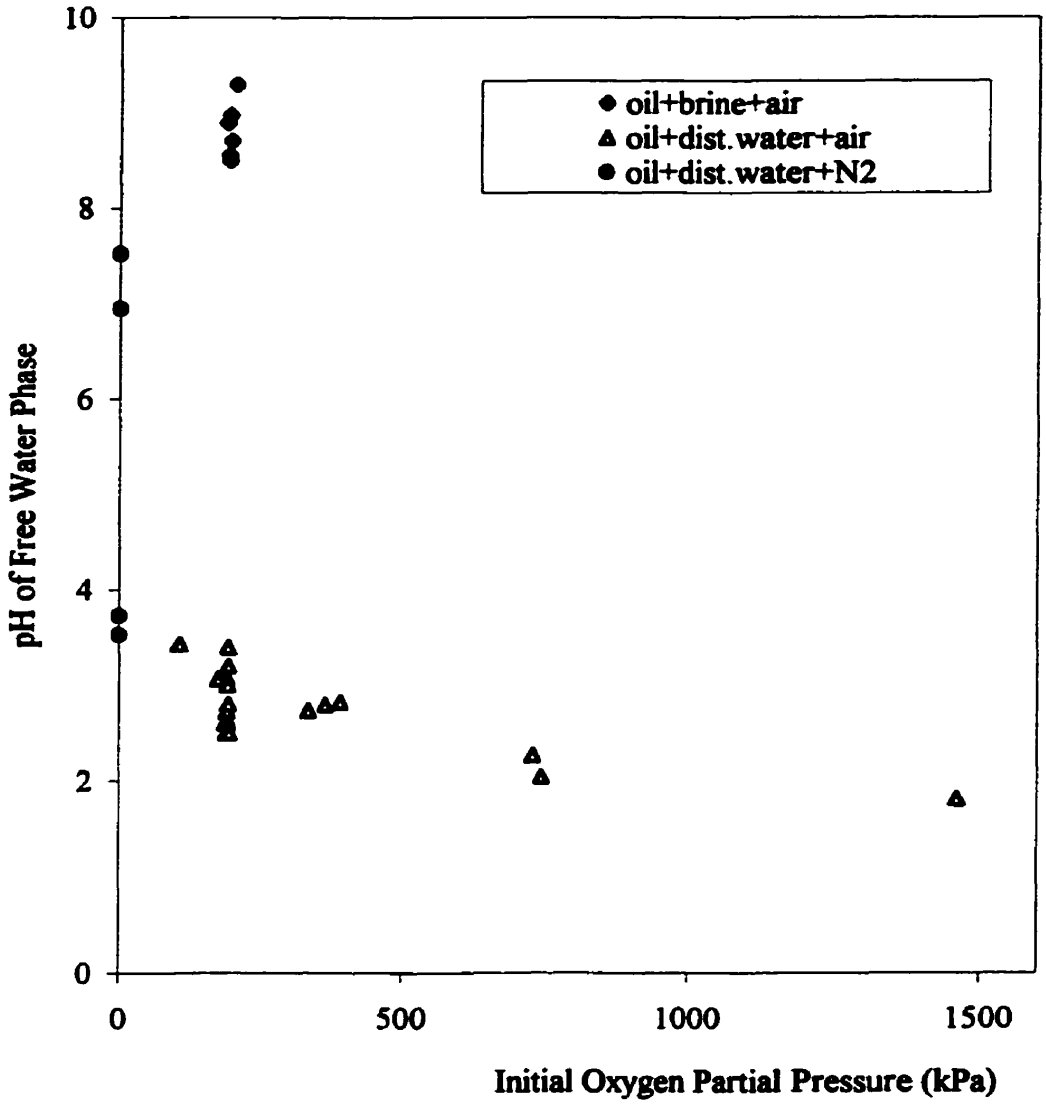

Figure 4.16: Effect of Oxygen Partial Pressure on pH

4.4 Reaction Parameter Effects

The examined effects of reaction parameters included effects of initial pressure, reaction temperature, time, oxygen uptake rate, agitation, core and brine. To keep the data compatible, as mentioned before, the viscosity ratios for all figures were measured at 70 °C.

4.4.1 Pressure

It has been assumed that the total pressure does not profoundly affect the system because of the liquid phase reactions (Wichert et al., 1995). Air was used in all of the experimental runs and each figure compares the effect of initial oxygen partial pressure on various parameters.

4.4.1.1 Oxygen Partial Pressure Effect on the Viscosity

The effect of oxygen partial pressure on the viscosity ratio for various LTS/ETS reaction scenarios is shown in Figure 4.17. Points for three cases of LTS (6 days at 80 °C-only with distilled water), 6 days LTS at 80 °C and 6 days ETS at 200 °C with distilled water and 6 days LTS at 80 °C and 6 days ETS at 200 °C with synthetic core, and at different initial oxygen partial pressures are shown. From this plot it can be seen that the oxygen partial pressure affects the viscosity ratio significantly. With the low oxygen partial pressure, there was not really enough oxygen in the system to promote significant viscosity modifications. High oxygen partial pressures intensified the

oxidation reaction, which increased the viscosity. When the ETS was conducted at 200 °C, adding oxygen does not appear to be advantageous to the thermal treatment of the oil. In these cases, the viscosity ratio was actually the lowest when the oxygen partial pressure was zero (i.e. a nitrogen environment).

An interesting phenomenon shown in Figure 4.17 is that when the process was conducted with 6 days LTS at 80 °C and 6 days ETS at 220 °C (with distilled water), the viscosity ratio decreased at lower initial pressures. A minimum point was observed at 458 kPa of initial oxygen partial pressure.

Beyond this oxygen partial pressure, the viscosity ratio increased with the higher initial oxygen pressures. The temperature applied to the oil during the ETS stage plays an important role in utilizing the oxygen stored within the oil during the LTS stage. In addition, it is worth mentioning that when the reaction cell, in which the minimum viscosity was observed, was opened, the reacted heavy crude was a foamy gas/oil emulsion. This observed phenomenon suggests that the contact area between the oil and oxygen plays an important role in the viscosity reduction. At very low oxygen partial pressures, there was not enough oxygen in the system to promote the free radial initiation reactions at the LTS temperature. However, significantly higher oxygen partial pressures provided too much oxygen and thus intensified the oxidation reactions, thus raising the viscosity. Similar results were observed in the presence of core (6 days LTS at 80 °C and 6 days ETS at 220°C). These results suggest that if the amount and rate of oxygen uptake is controlled, then the temperature necessary to propagate the thermal cracking reactions will be optimized such that overall viscosity reduction will be attained through the

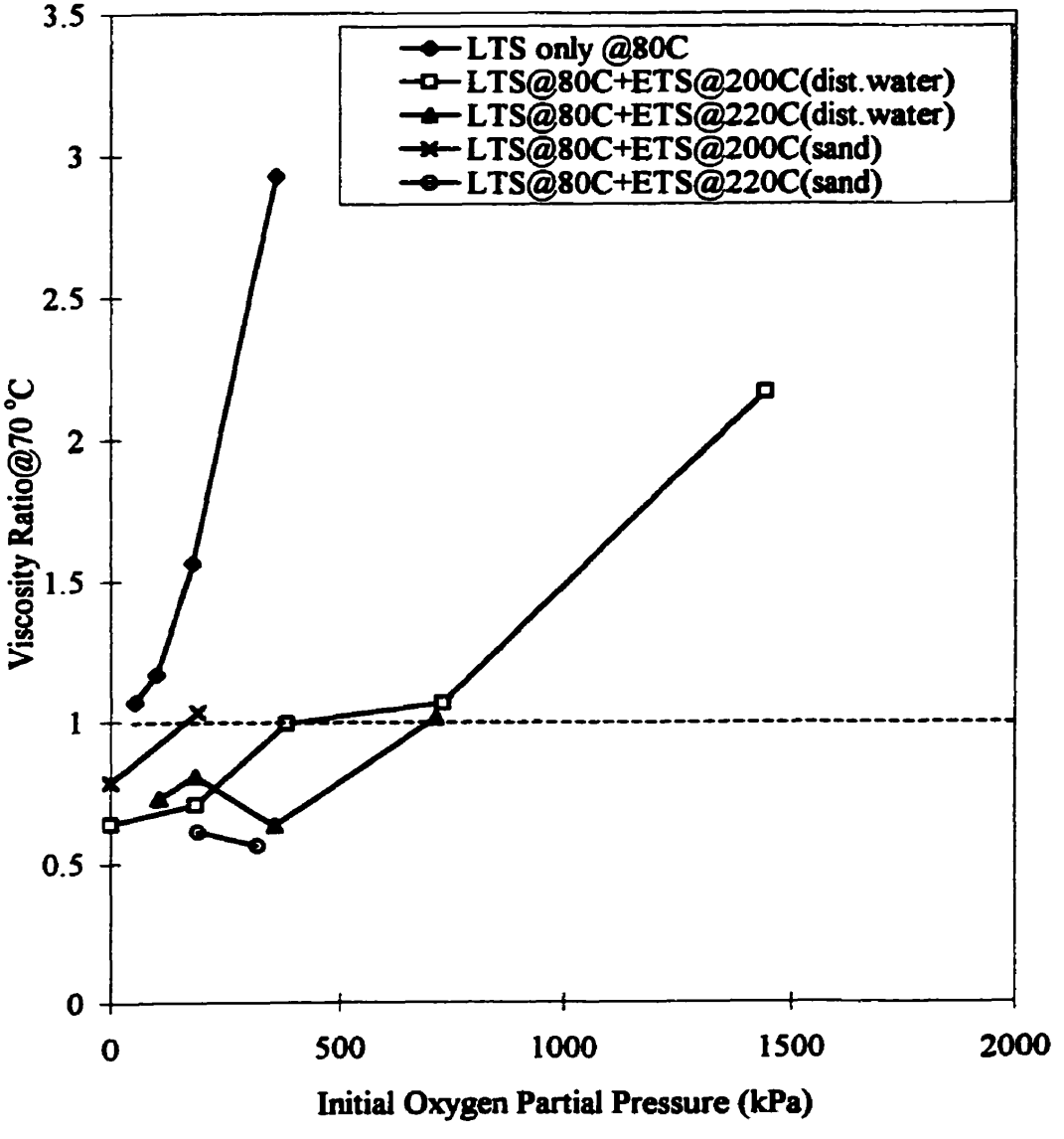

Figure 4.17: Effect of Initial Pressure on Viscosity

cracking of the maltenes fractions.

4.4.1.2 Oxygen Partial Pressure Effect on the Coke, Asphaltenes Content and Oxygen Uptake

Figure 4.18 shows the effect of the initial oxygen partial pressure on the reaction system oxygen uptake. Points from the aforementioned five series (i.e. 6 days LTS at 80 °C-only with distilled water, 6 days LTS at 80 °C + 6 days ETS at 200°C with distilled water, 6 days LTS at 80 °C + 6 days ETS at 200°C with synthetic core, 6 days LTS at 80 °C + 6 days ETS at 220°C with distilled water, 6 days LTS at 80 °C + 6 days ETS at 220°C with synthetic core) with different initial oxygen partial pressures are shown. It can be seen that the oxygen uptake increases with the initial oxygen partial pressure for all cases. This observation confirms that essentially all of the oxygen which was initially in the reactors was consumed over the course of each test.

Figure 4.19 shows the effect of initial oxygen partial pressure on the asphaltenes contents of the produced oil. Three series of experimental points (i.e. 6 days LTS at 80 °C-only with distilled water, 6 days LTS at 80 °C + 6 days ETS at 200°C with distilled water, and 6 days LTS at 80 °C + 6 days ETS at 220°C with distilled water) with different initial oxygen partial pressures are shown. It can be seen that the asphaltenes contents increase with the initial oxygen partial pressure for the first two series, but the amount of asphaltenes decrease with the initial oxygen partial pressure for the case involving the 6-day ETS at 220 °C. The behavior at 220°C suggests a meaningful degree of cracking of the asphaltenes fraction.

Figure 4.20 shows the effect of the initial oxygen partial pressure on the pH of the free water phase for the static reactor tests involving oil and distilled water only. Points from the above three series (i.e. 6 day LTS at 80 °C-only with distilled water, 6 day LTS at 80 °C + 6 day ETS at 200°C with distilled water and 6 day LTS at 80 °C + 6 day ETS at 220°C with distilled water) with different initial oxygen partial pressures are shown. It can be observed that the pH decreases with the initial oxygen partial pressure for all cases. This confirms that acid groups, such as carboxylic acids, are being formed as part of the process and the more oxygen uptake in the system, the more acid groups formed. It appears that the change in the ETS temperature from 200 to 220 °C had little effect on the produced free water pH.

Figure 4.21 shows the effect of the initial oxygen partial pressure on coke formation. Points from the two series (i.e. 6 day LTS at 80 °C + 6 day ETS at 200 °C with distilled water and 6 day LTS at 80 °C + 6 day ETS at 220 °C with distilled water) at different initial oxygen partial pressures are shown. It can be observed that the initial oxygen partial pressure enhances the coke formation. This is consistent with the findings of Millour et al. (1985) that the coke concentration is related to the level of total oxygen uptake. However, in essentially all of the cases the produced amounts of coke are less than 1 % of the initial oil mass. Therefore, for the levels of oxygen uptake associated with the reaction conditions for the core-free tests, coke formation is not significant.

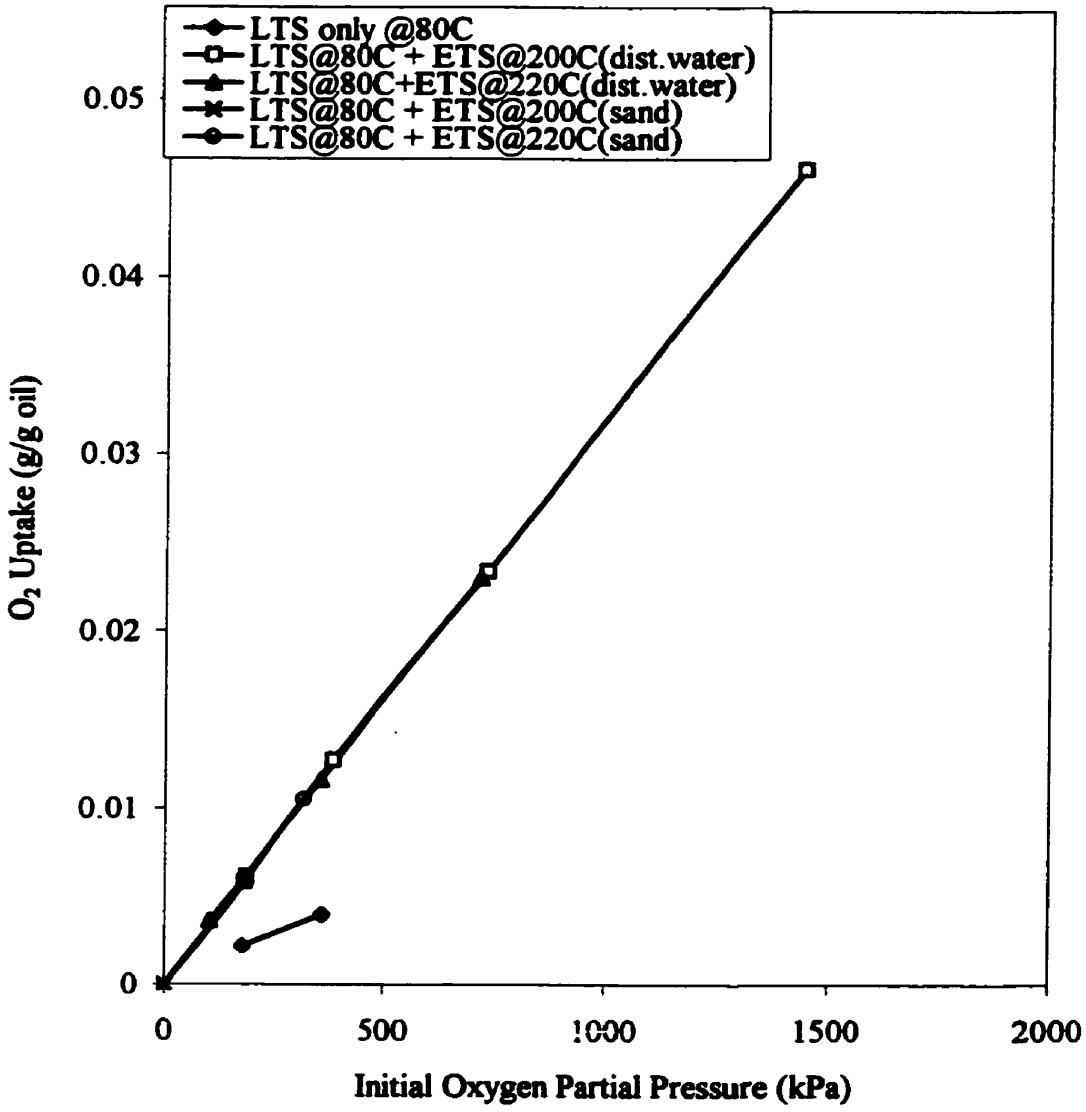

Figure 4.18: Effect of Initial O_2 Partial Pressure on O_2 Uptake

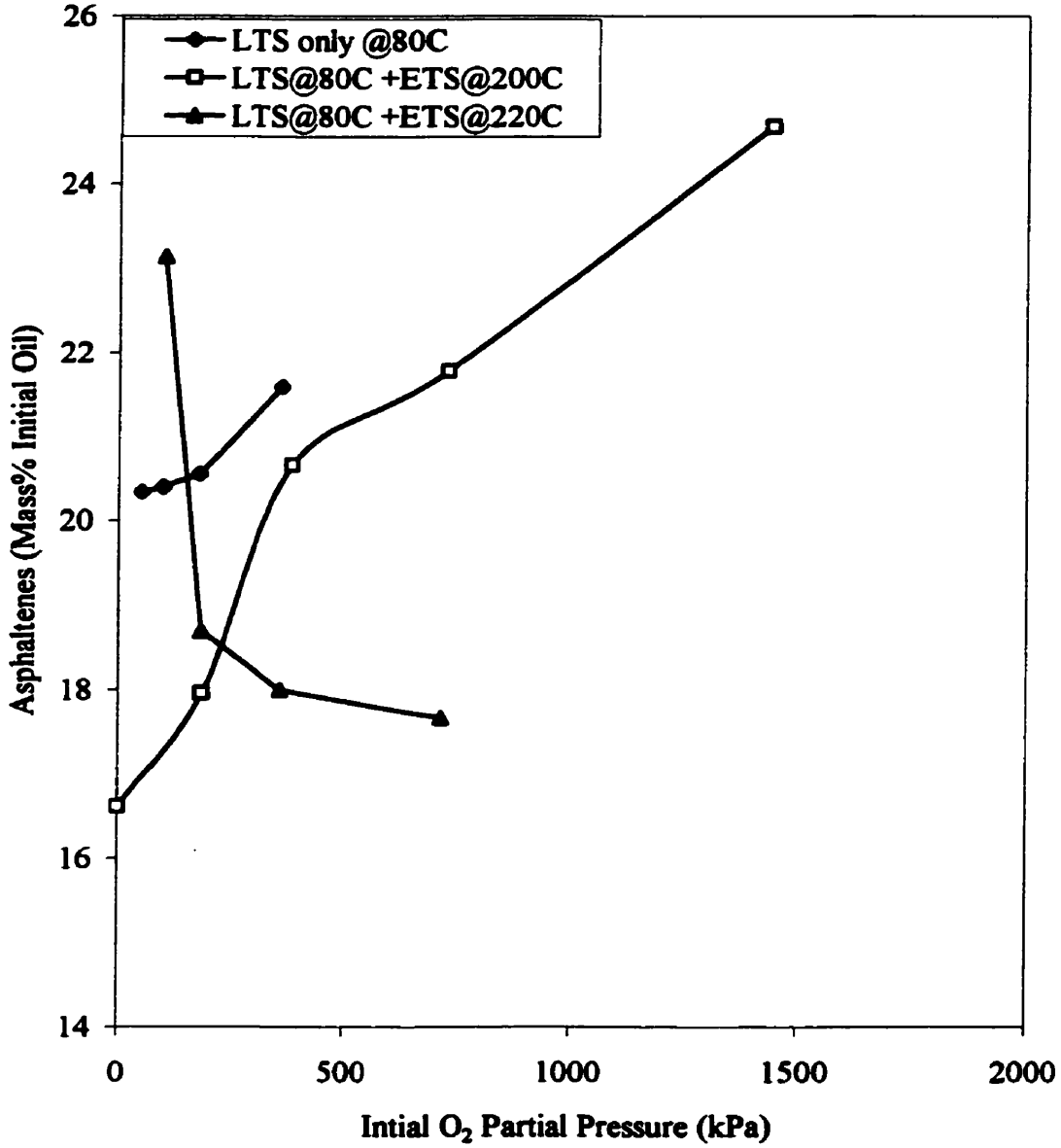

Figure 4.19: Effect of Initial Oxygen Partial Pressure on Asphaltenes Content

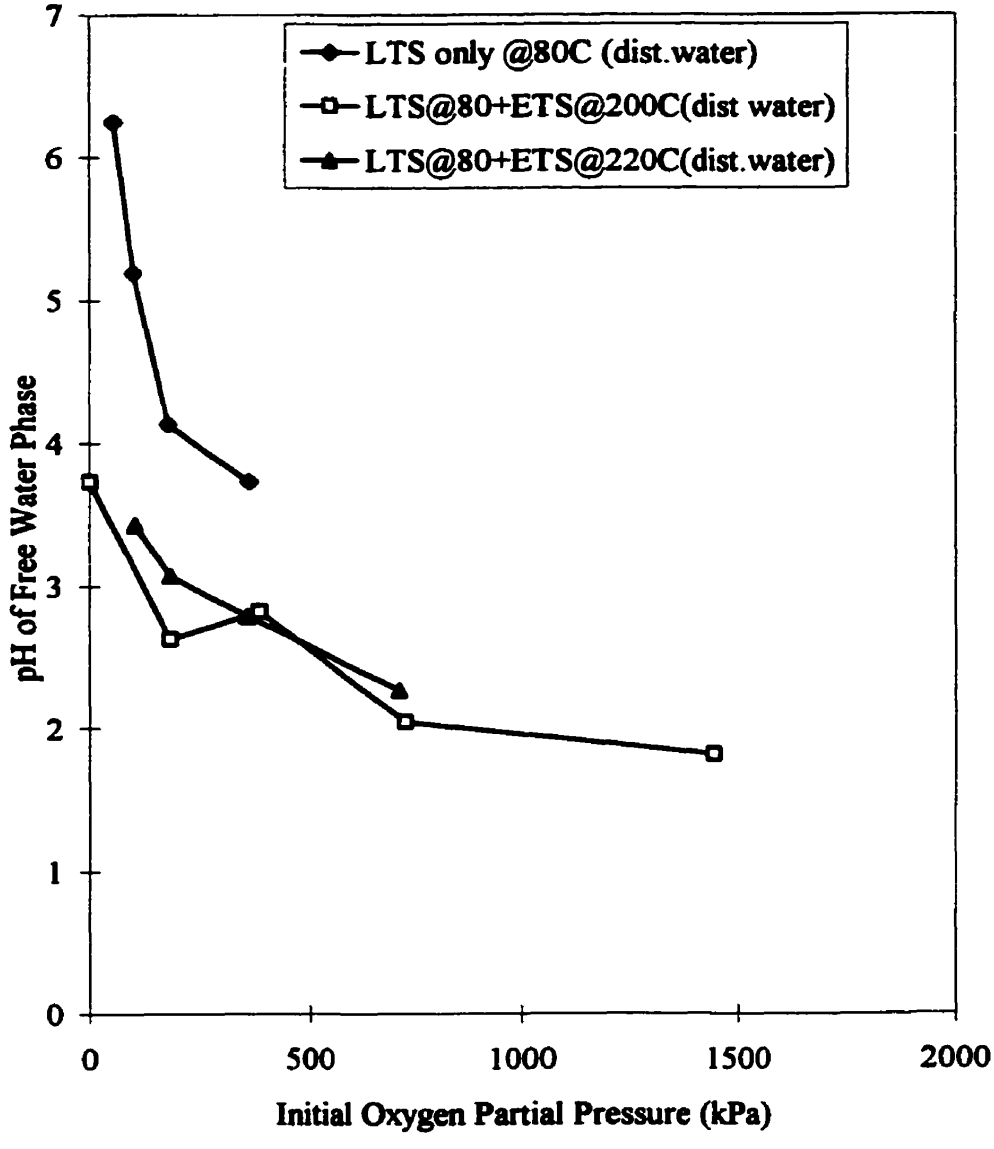

Figure 4.20: Effect of Initial Oxygen Partial Pressure on pH of the Aqueous Phase (oil plus distilled water)

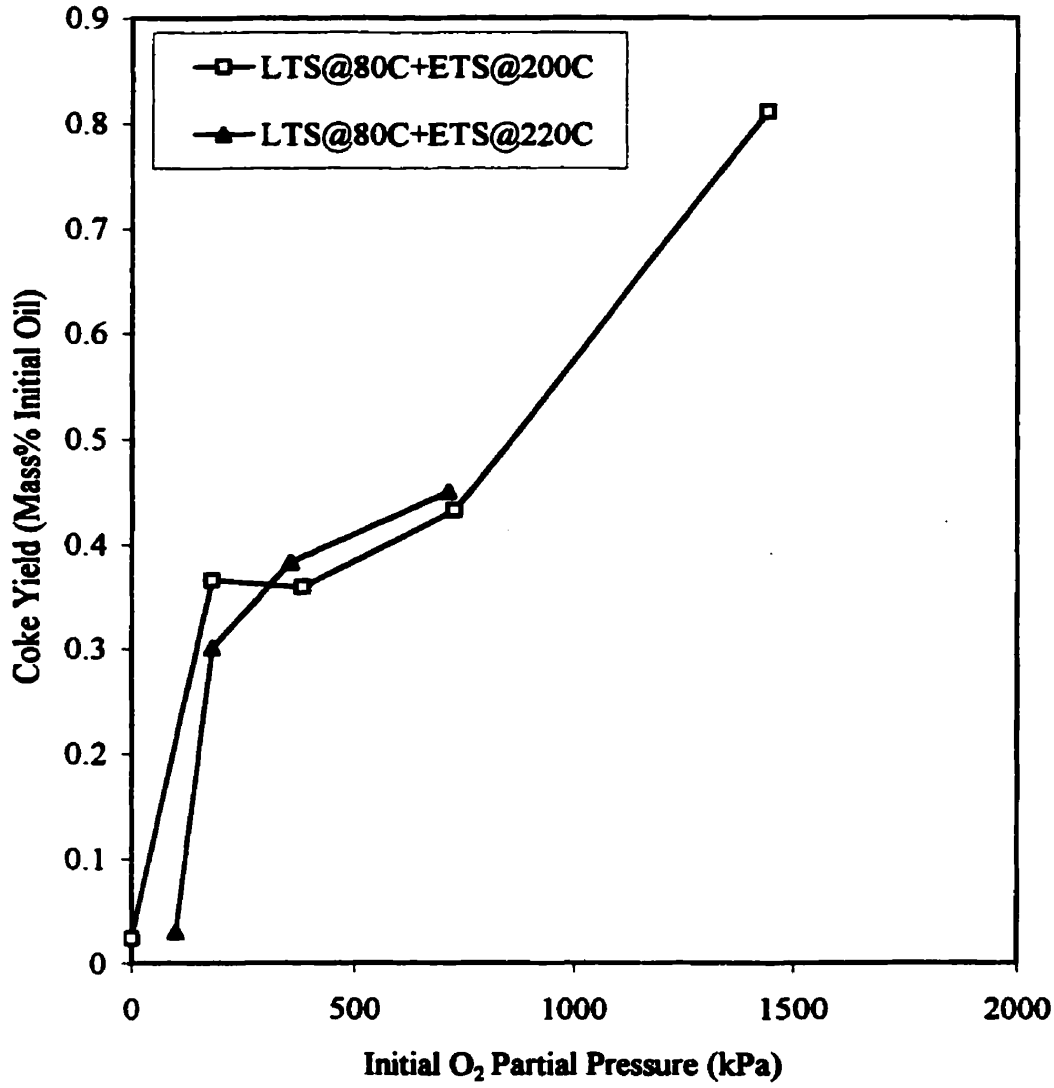

Figure 4.21: Effect of Initial Oxygen Partial Pressure on Coke Formation (oil plus distilled water)

4.4.2 Reaction Temperature Effects

4.4.2.1 Low Temperature Soak (LTS) Reaction Temperature Effects

Figure 4.22 presents viscosity ratios for Runs # 1-5, #1-6 and #1-7 to illustrate the effect of LTS temperature on the viscosity ratio. Experimental points for the case of 6 days LTS at 80 °C and approximately 970 kPa initial pressure and different temperatures are shown. It can be seen that the higher the LTS temperature, the higher the resulting viscosity ratio.

Figure 4.23 shows the effect of LTS temperature on the total oxygen uptake. Points from the above case (i.e. LTS only at 6 days and about 970 kPa initial pressures with different LTS temperatures) are shown. It can be seen that the oxygen uptakes increase with LTS temperature. This is consistent with the viscosity increase. While not shown, it is recognised that as the temperature increases, the total oxygen uptake will approach an asymptote corresponding to complete utilization of the oxygen which was initially charged to reactors.

Figure 4.24 shows, for the same three runs, the LTS temperature effect on the asphaltenes contents of the produced oil. It can be seen that the asphaltenes contents increase with LTS temperature. This behavior is reflected in the viscosity increase with temperature and is related to the effect of LTS temperature on total oxygen uptake.

Figure 4.25 shows the effect of LTS temperature on the resulting pH value of the free water phase. It can be observed that the pH decreases with LTS temperature. This corresponds to an increase in oxygen uptake and results in the production of more acidic species.

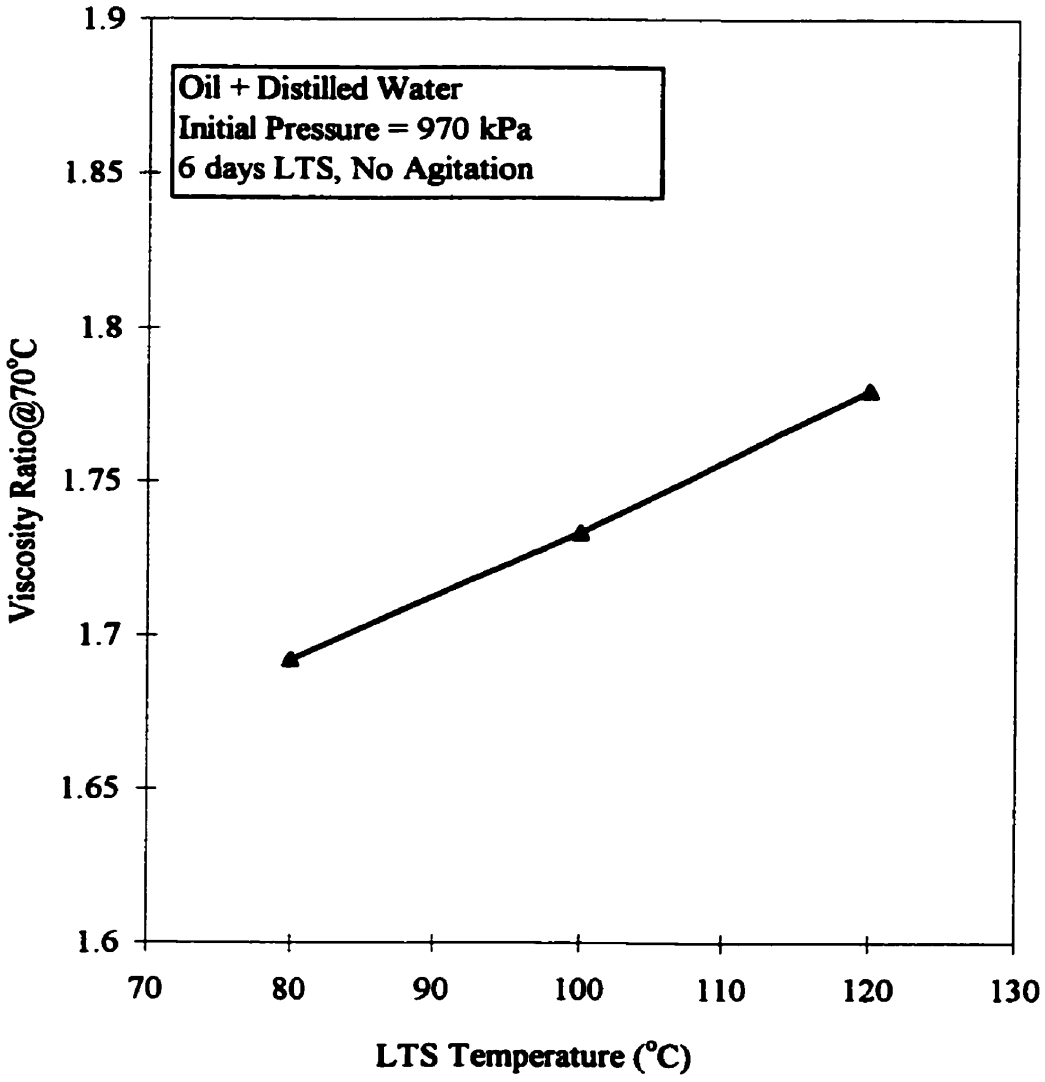

Figure 4.22: Effect of LTS Temperature on Viscosity Ratios

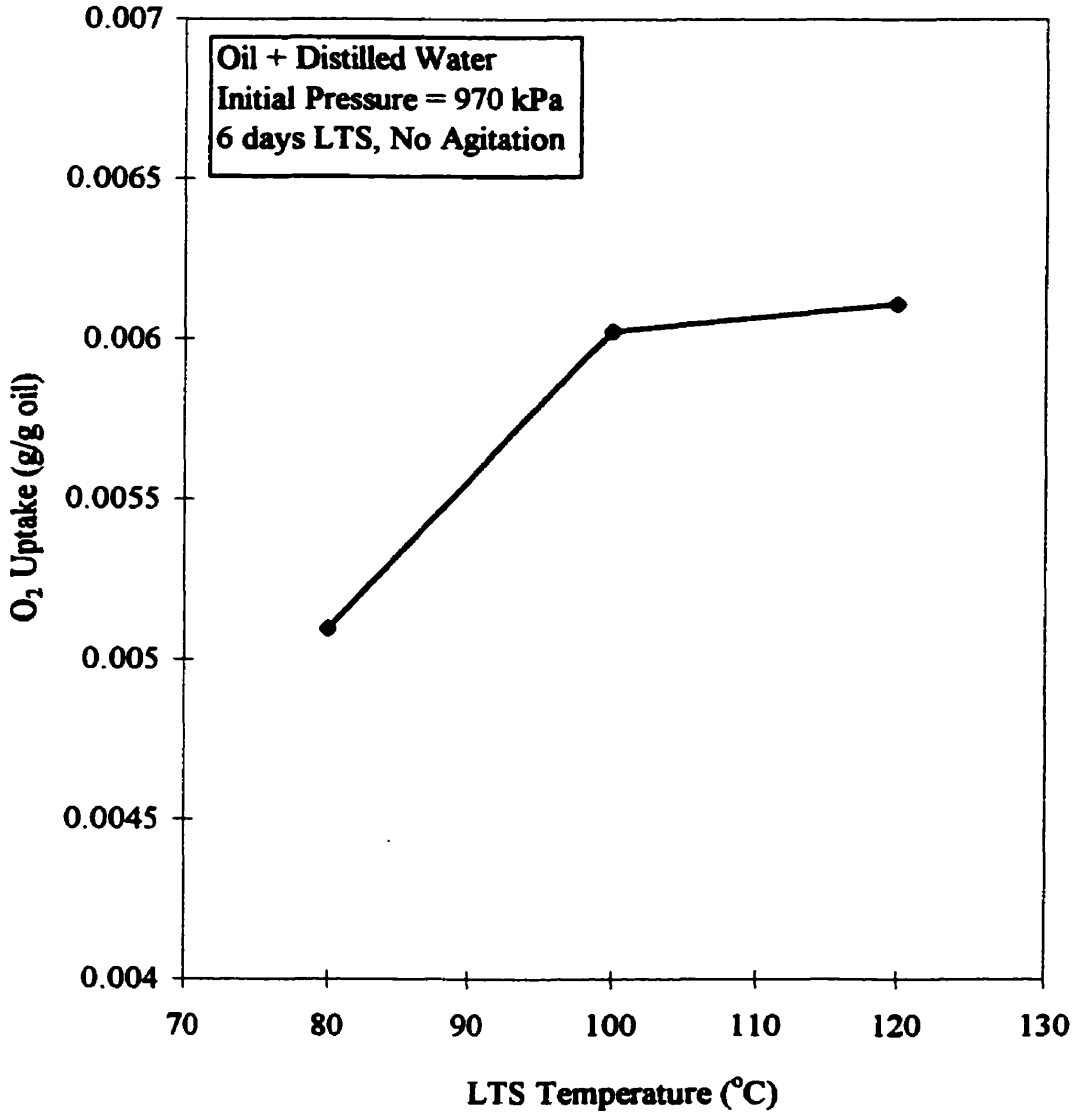

Figure 4.23: Effect of LTS Temperature on Oxygen Uptake

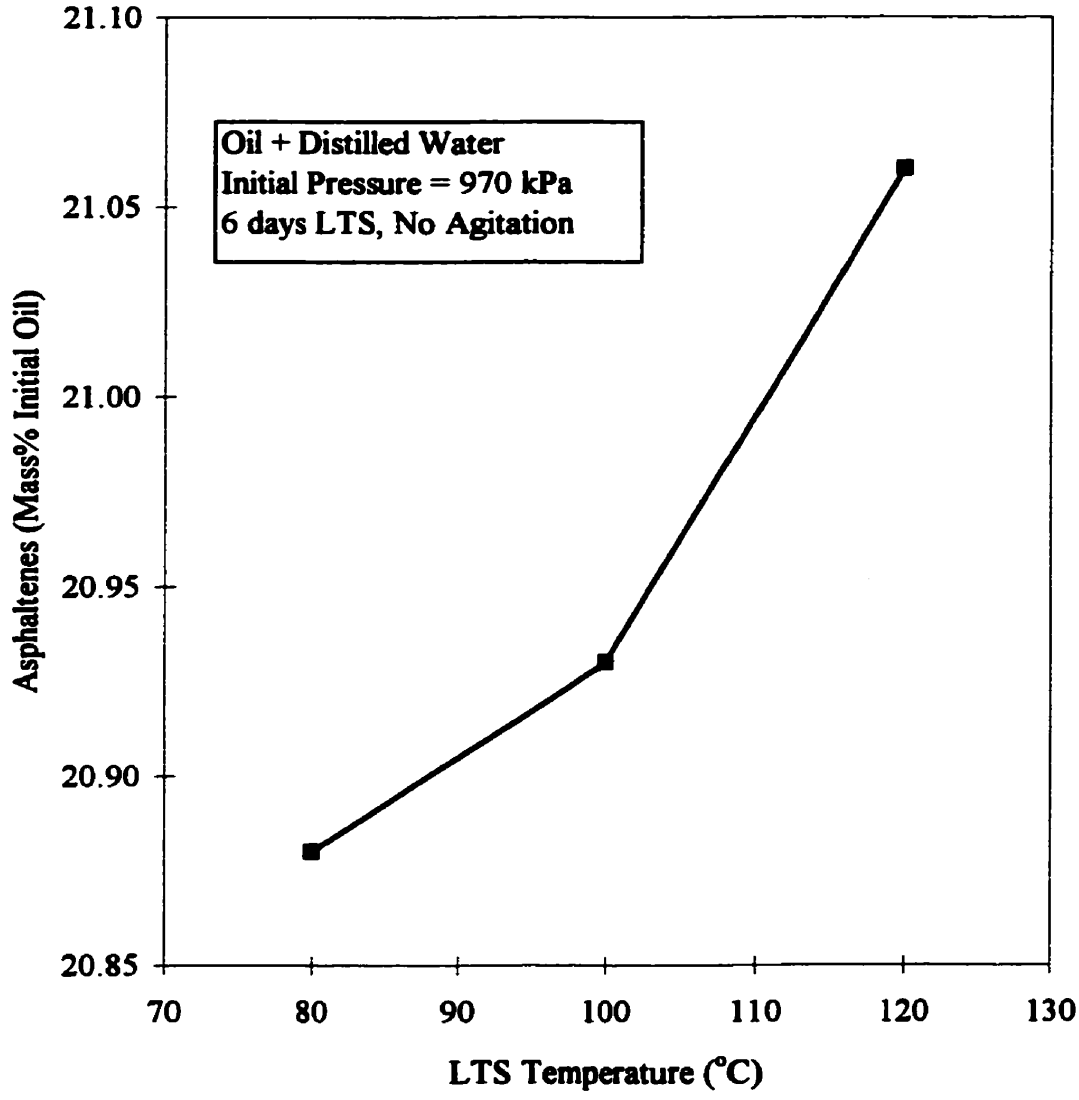

Figure 4.24: Effect of LTS Temperature on Asphaltenes Contents

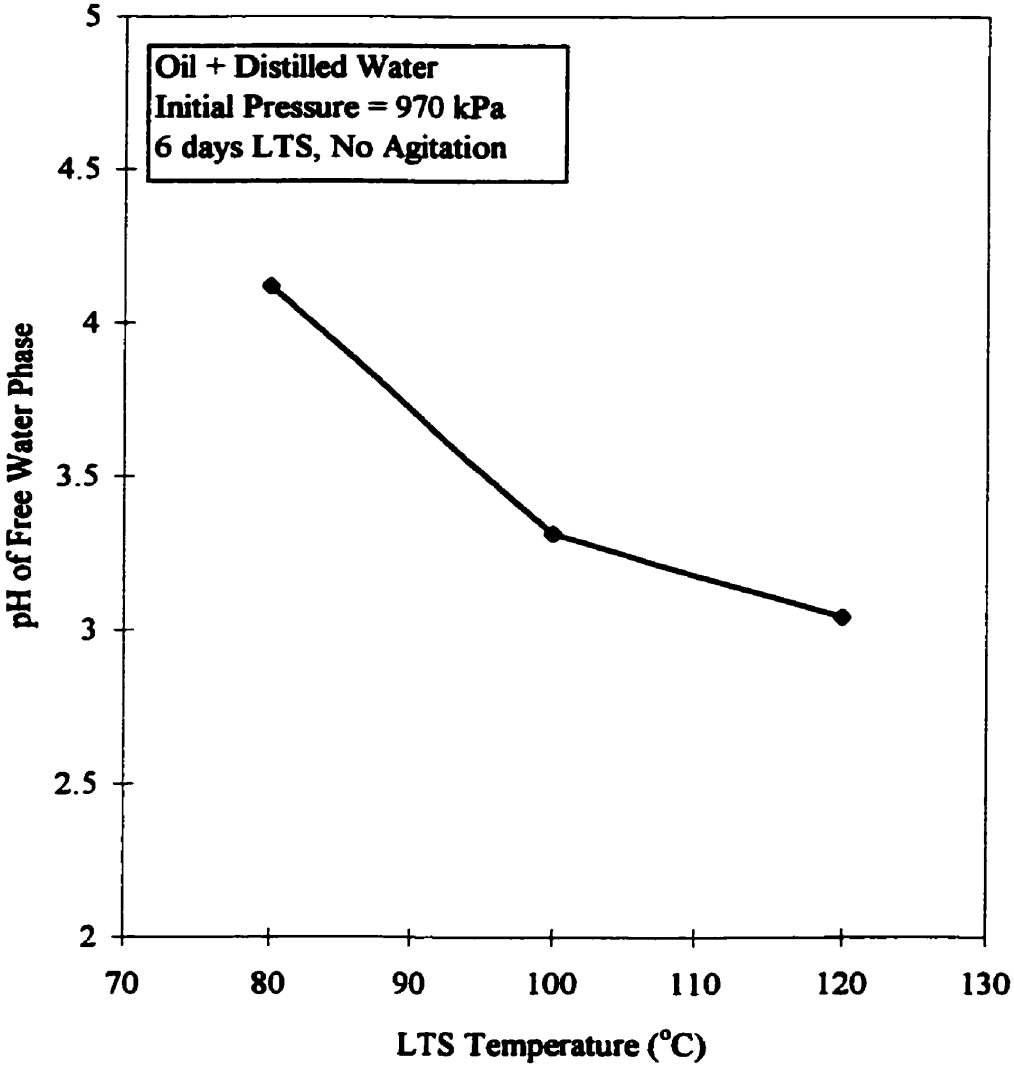

Figure 4.25: Effect of LTS Temperature on pH of Free Water Phase

4.4.2.2 ETS Temperature Effects

Figure 4.26 utilizes data from Tests #1-9, #2-2, #2-9 and #2-10 to show the effect of ETS temperature on the viscosity ratio. These tests involved oil plus distilled water, no agitation, 6 day LTS at 80 °C plus 6 day ETS at various temperatures at an initial pressure of approximately 970 kPa. The general trend with increasing ETS temperature is that of a viscosity ratio reduction.

Figure 4.27 shows the effect of ETS temperature on oxygen uptake for the same tests. Figure 4.28 shows the effect of ETS temperature effect on the asphaltenes and coke contents of the products. Points from the above case (i.e. LTS 6 days at 80 °C + ETS at various temperatures and about 970 kPa initial pressure) are shown. It can be seen that the oxygen uptake and asphaltenes do not show a significant sensitivity to the ETS temperature over the range of run conditions investigated. Coke formation appears to be enhanced by ETS temperature, but it can be seen that the coke amount is approximately 1 % of the asphaltenes content.

Figure 4.29 shows the ETS temperature effect on the pH of the effluent aqueous phase. Points from the above case (i.e. 6 day LTS @80 °C + ETS at various temperatures and 970 kPa initial pressure) are shown. pH levels are relatively consistent but are significantly more acidic than those observed when LTS is not followed by ETS.

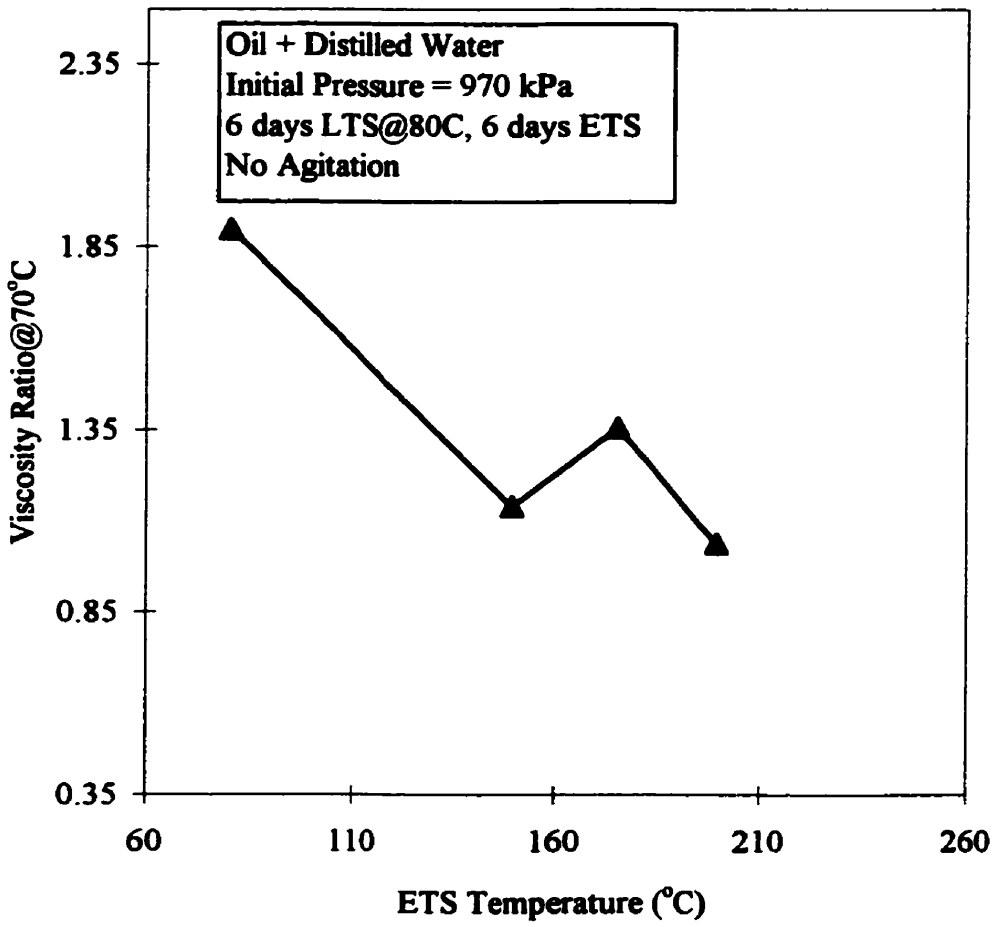

Figure 4.26: Effect of ETS Temperature on The Viscosity Ratio

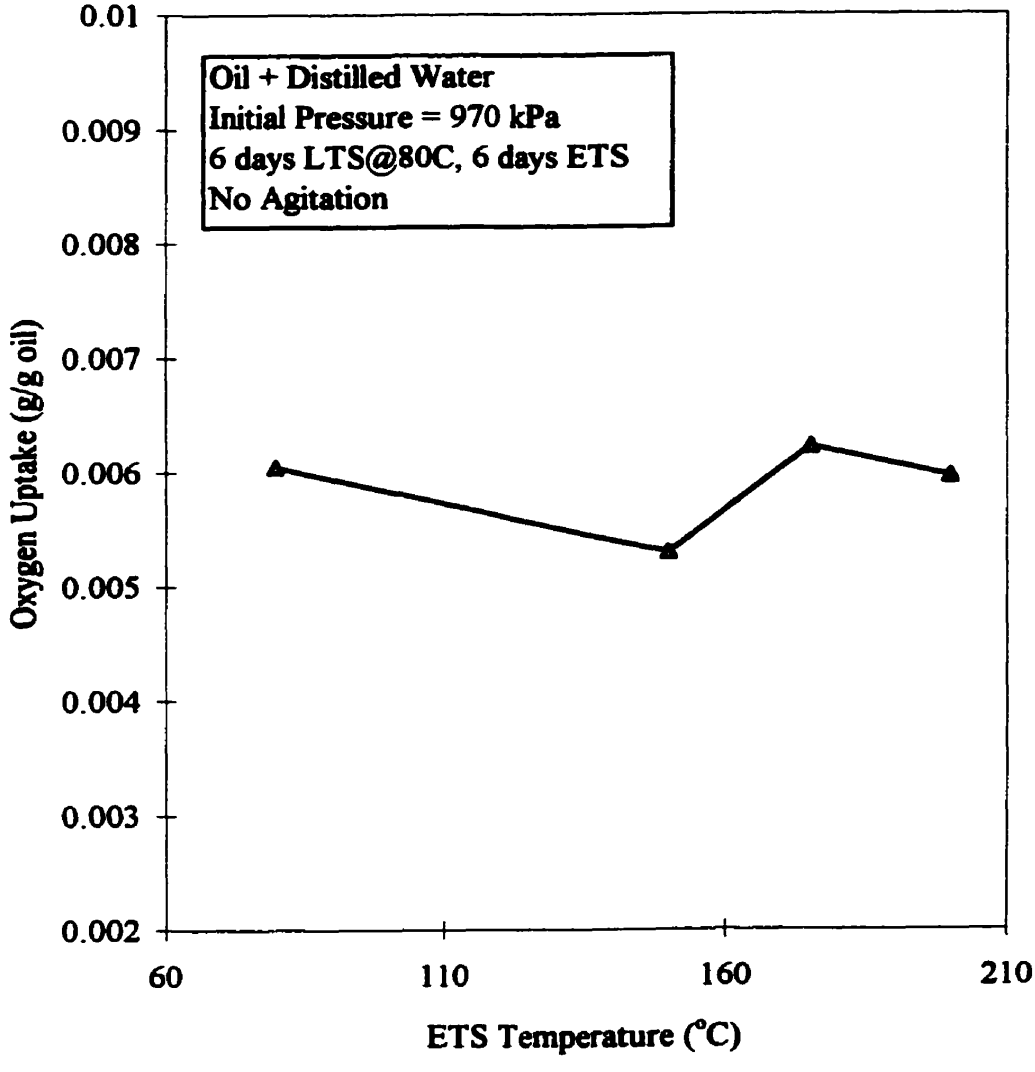

Figure 4.27: Effect of ETS Temperature on Oxygen Uptake

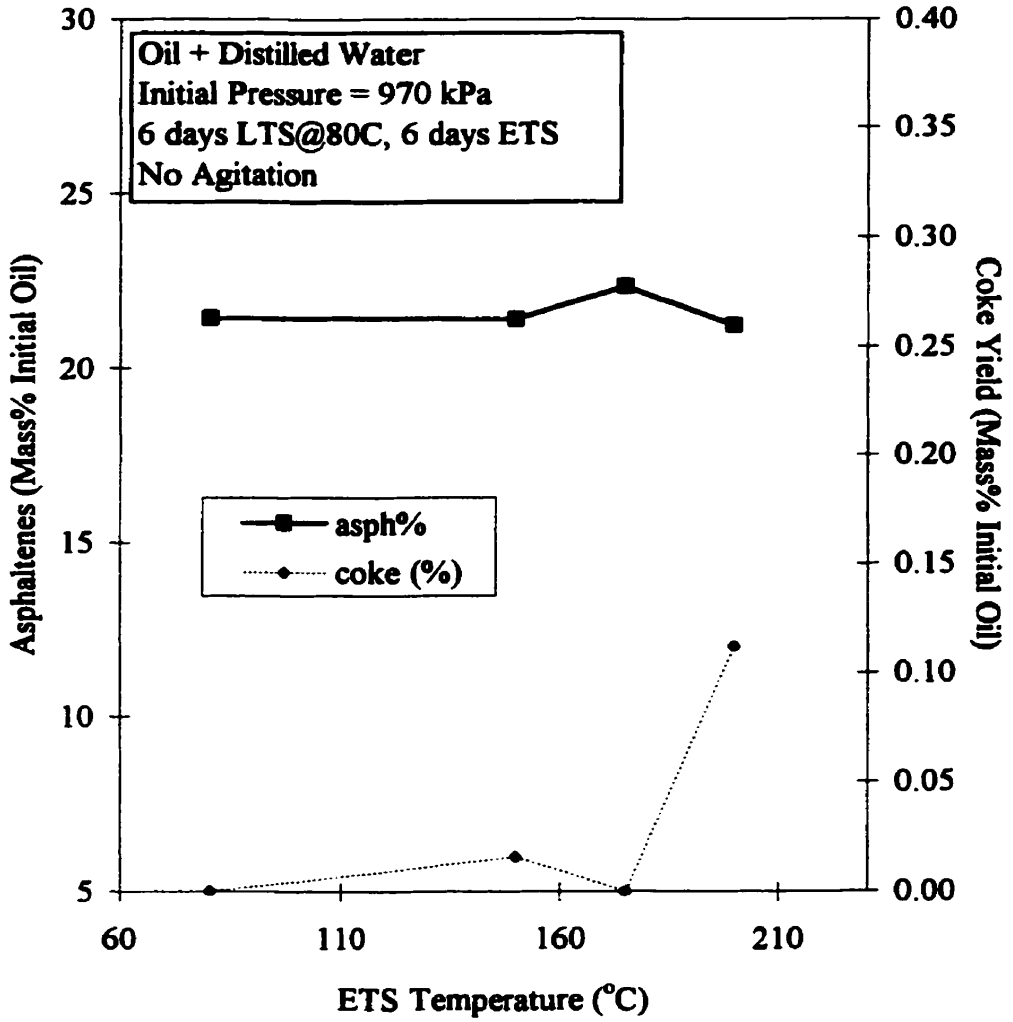

Figure 4.28: Effect of ETS Temperature on Asphaltenes & Coke Contents

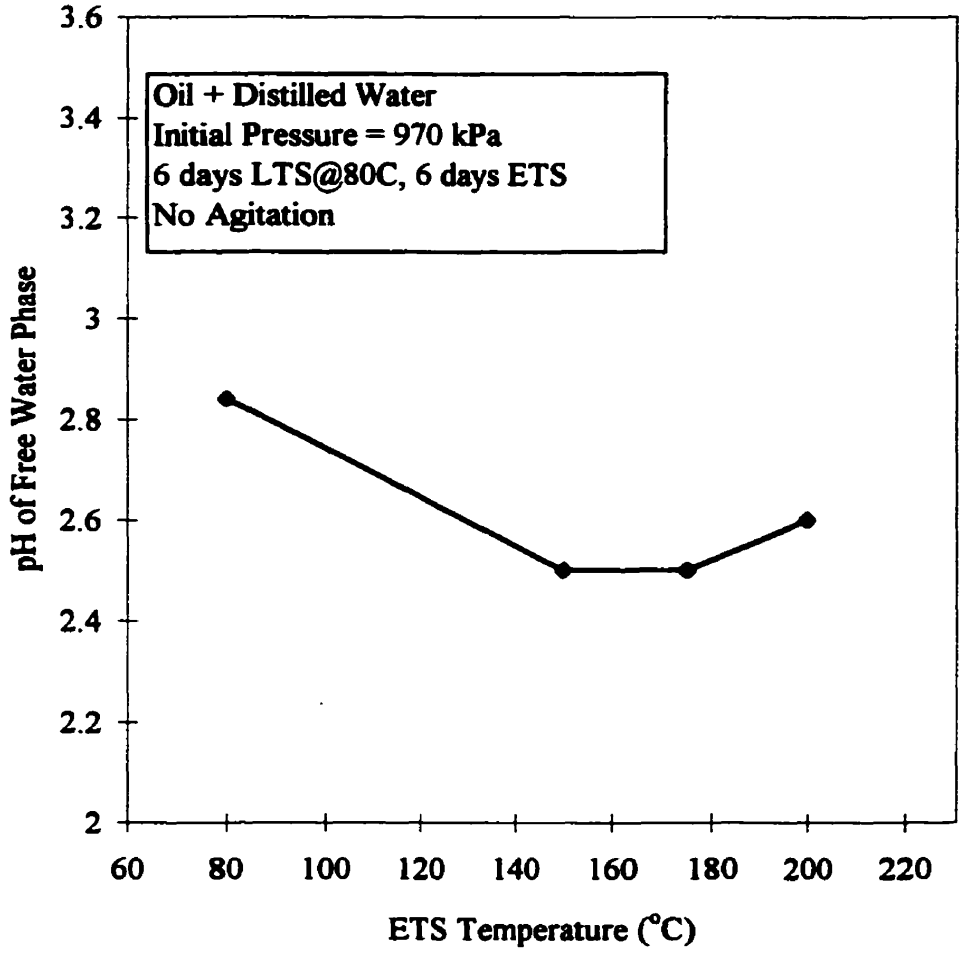

Figure 4.29: Effect of ETS Temperature on pH of Free Water Phase

4.4.3 Reaction Time Effects

Several experimental runs were performed at identical reaction conditions with the exception of run duration in order to evaluate the effect of LTS and ETS times on the properties of the reacted oil. Because the experimental program was conducted in batch reactors with limited initial pressure, only a limited amount of oxygen was available during each test. All experiments in this set were conducted with a LTS temperature of 80°C and ETS temperatures of 200°C, as well as initial pressures of 970 kPa.

4.4.3.1 LTS Reaction Time Effects (Oil plus Distilled Water, No Agitation)

Figure 4.30 shows the LTS time effect on the viscosity ratio for ETS times of 0 days (i.e. the LTS only case) and 6 days. It is apparent from this figure that varying the length of the LTS oxidation time above the 5 day minimum LTS period investigated has a negligible effect on the resultant viscosity ratio. This suggests that the viscosity ratio modification is essentially insensitive to the LTS time for times above 5 days at the 80 °C temperature of the tests considered.

Figure 4.31 and 4.32 are plots showing the LTS time effect on the compositional properties, such as asphaltenes contents and pH of the effluent aqueous phase. Total oxygen uptake is also provided for reference. Figure 4.31 is plotted for the LTS only case (i.e. Tests 1-8, 1-5, 1-9 and 1-10) while Figure 4.32 is for the LTS plus ETS case (i.e. Tests 2-6, 2-2, 2-7 and 2-8). It seems the LTS time has little effect on the asphaltenes and

oxygen uptake. pH levels decrease with LTS time for the no ETS tests, but increase with LTS time for the tests involving the 6 day ETS at 200 °C.

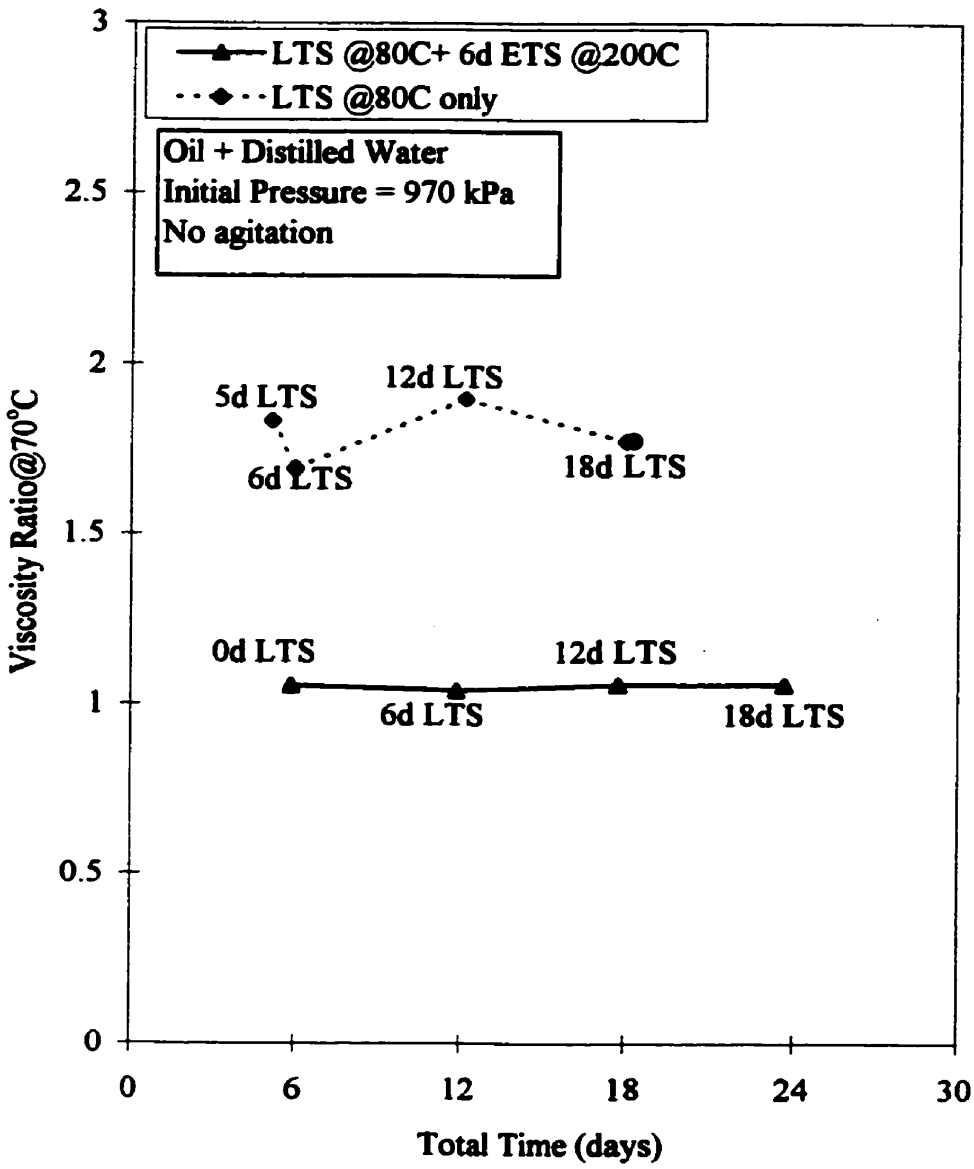

Figure 4.30: Effect of LTS Time on Viscosity Ratio

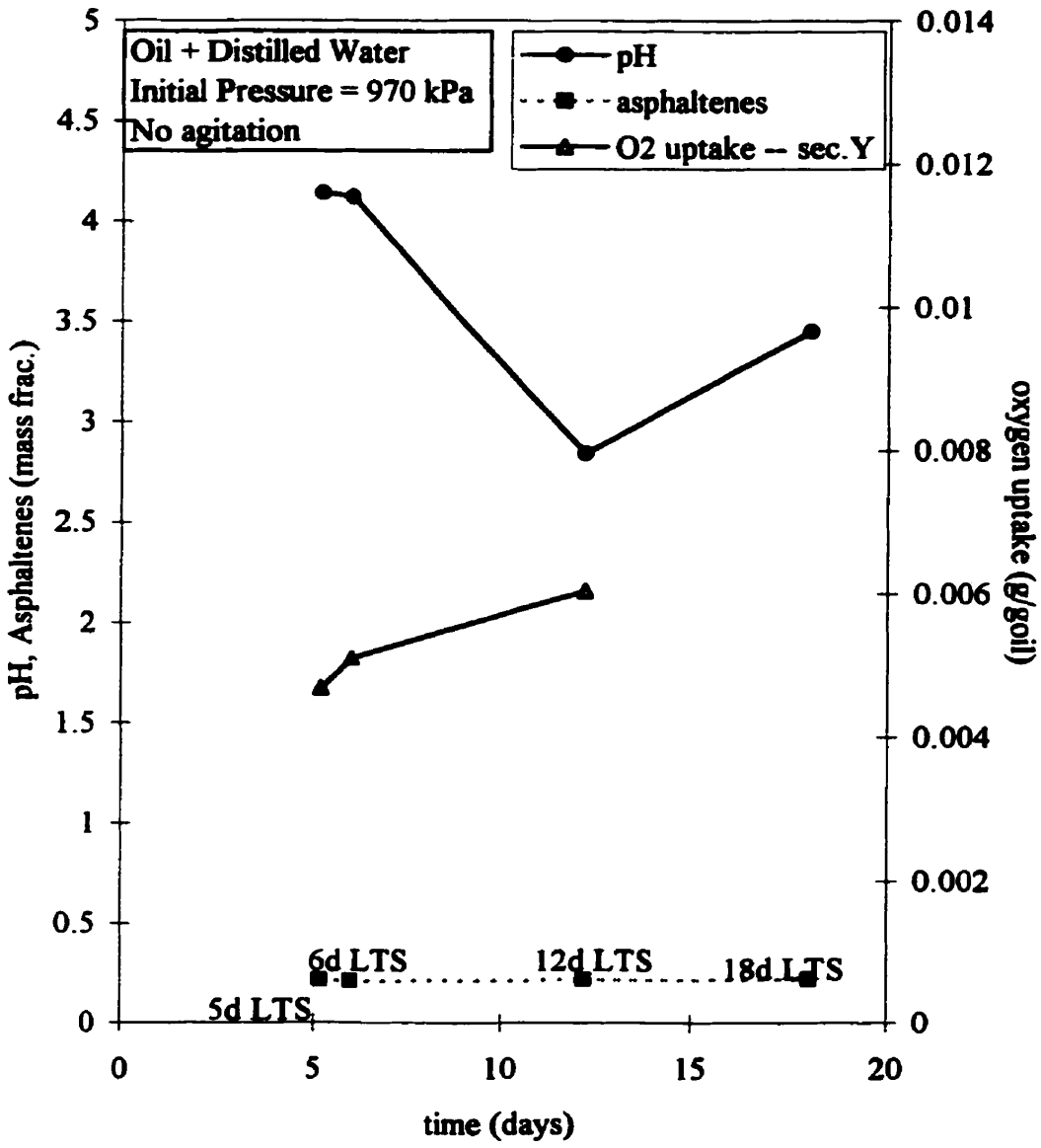

Figure 4.31: LTS Time Effects on pH, Asphaltenes Content and Oxygen Uptake (LTS only Cases)

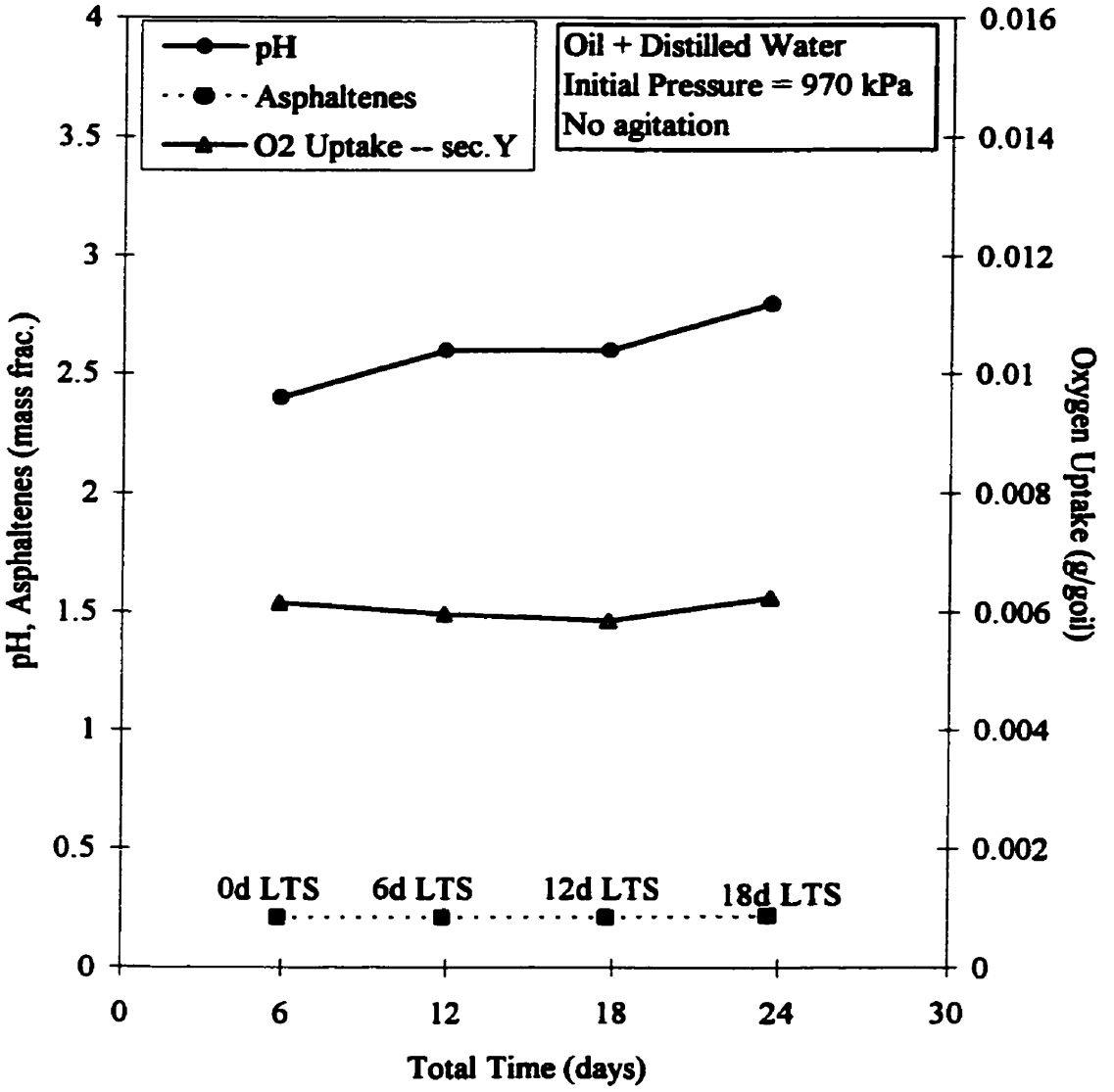

Figure 4.32: Effect of LTS Time on pH, Asphaltenes Contents and Oxygen Uptake (LTS plus ETS Cases)

4.4.3.2 Elevated Temperature Soak (ETS) Reaction Time Effects

Figure 4.33 presents the ETS (at 200 °C) time effect on the viscosity ratios as measured at temperatures of 25, 40 and 70 °C. The tests considered involved varying ETS times with a constant LTS time of 6 days. The specific experimental tests are 1-5, 2-1, 2-2, 2-5, 2-3, and 2-4. It can be seen that a significant decrease in the viscosity ratio is achieved over the first nine days (total run time of 15 days) at the ETS temperature of 200 °C. Beyond this ETS time, the viscosity curves level off. Figure 4.34 summarizes the total oxygen uptake for the 6 runs in question. It is apparent that the oxygen uptake is essentially constant following the initial heating period to the 200 °C ETS temperature. Because this series of reactions was conducted in batch reactors with limited initial oxygen partial pressure, only a finite amount of oxygen was available for each test. In other words, the amount of oxygen uptake is mainly a function of initial oxygen partial pressure. Thus, with the identical oxygen initial pressure and with identical ETS temperatures, the oxygen uptake would be expected to show an asymptotic behavior with regard to ETS time.

The data show that ETS time is significant at a given total oxygen uptake. During the LTS phase of this two-stage process, the chemical bonds of the oil are believed to incorporate oxygen, forming weaker bonds. The higher temperature of the ETS phase supplies the energy required to break the weaker oxygen-carbon bonds (i.e. free radial initialization and propagation reactions). The breaking of these bonds, and the corresponding reduction in size of the oil molecule, is believed to cause the viscosity

ratio reduction seen in Figure 4.33. It appears that allowing enough oxygen into the molecular structures of the oil to initiate the free-radical chain reactions, and then maintaining the run temperature for propagation of these reactions, promotes the cracking reactions and leads to a less viscous products. Over time, all of the weaker bonds formed during the LTS period will break at a given temperature and, after this point, no further reduction in viscosity ratio should be observed.

Figures 4.35 – 4.38 show the effect of ETS time on the asphaltenes contents, pH of the free water phase and coke yield. From these figures, it can be seen that the ETS time has little effect on the asphaltenes content. Coke content increased with time but the yields were less than 0.005 g / 100 g oil. In view of the constant asphaltenes content and small coke formation, the viscosity reduction is thought to be due to the bond breaking in the maltenes fraction.

Figure 4.37 shows that the pH of the free water falls during the initial portion of the ETS stage and then shows an increasing trend with increasing time during the ETS phase. This suggests that the organic acids undergo further decomposition reactions with time. Figure 4.38 shows an increasing trend for the produced CO_2 concentration with the ETS time increase.

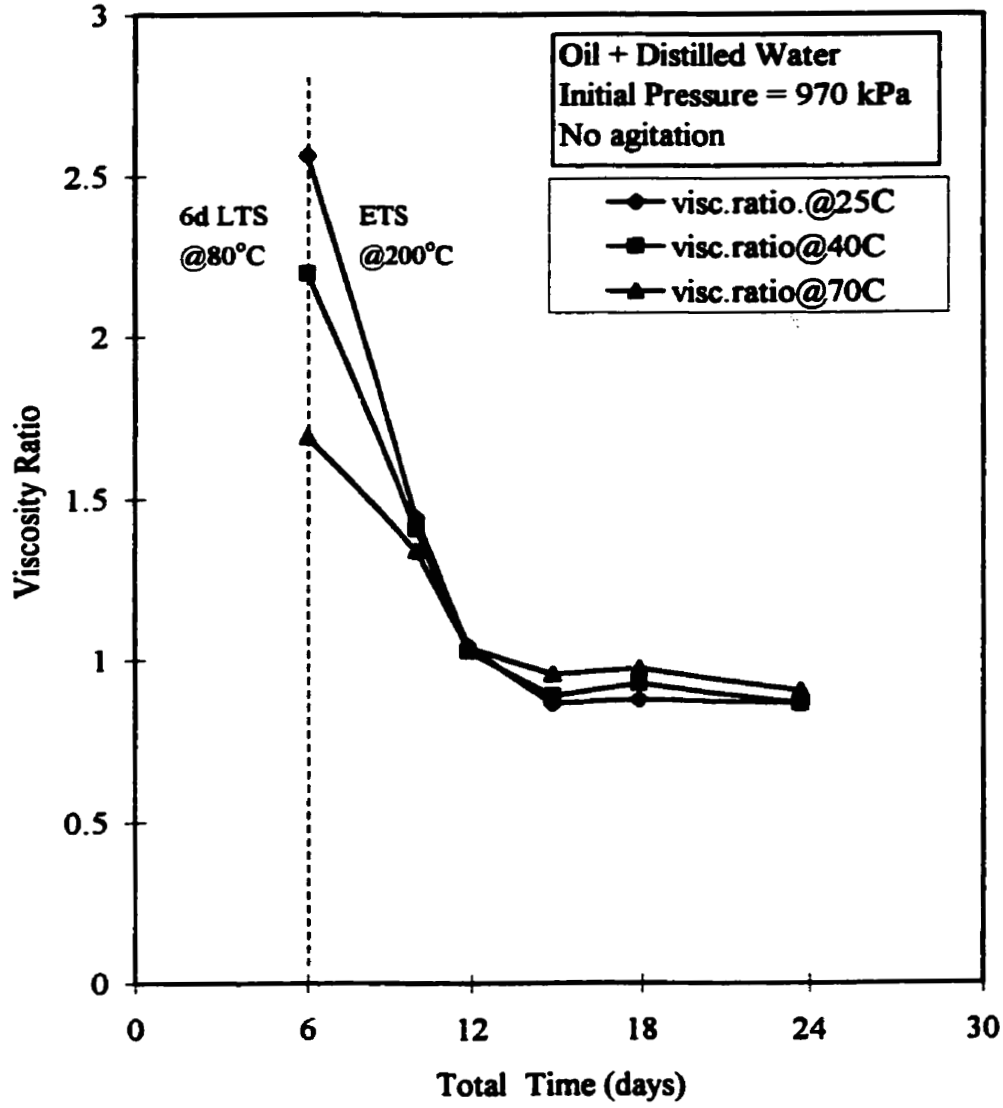

Figure 4.33: Effect of ETS Time on Viscosity Ratio

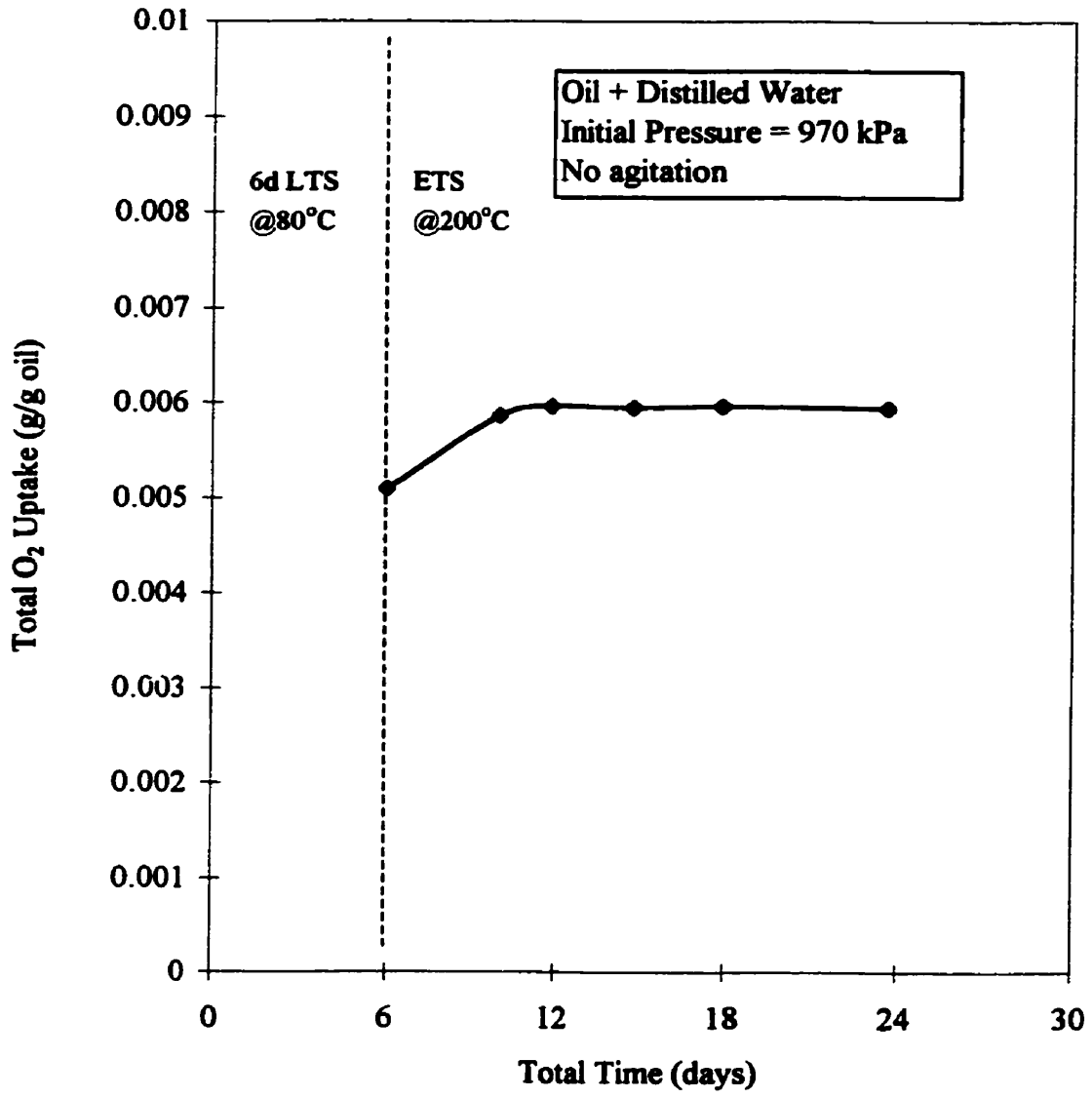

Figure 4.34: Effect of ETS Time on Oxygen Uptake

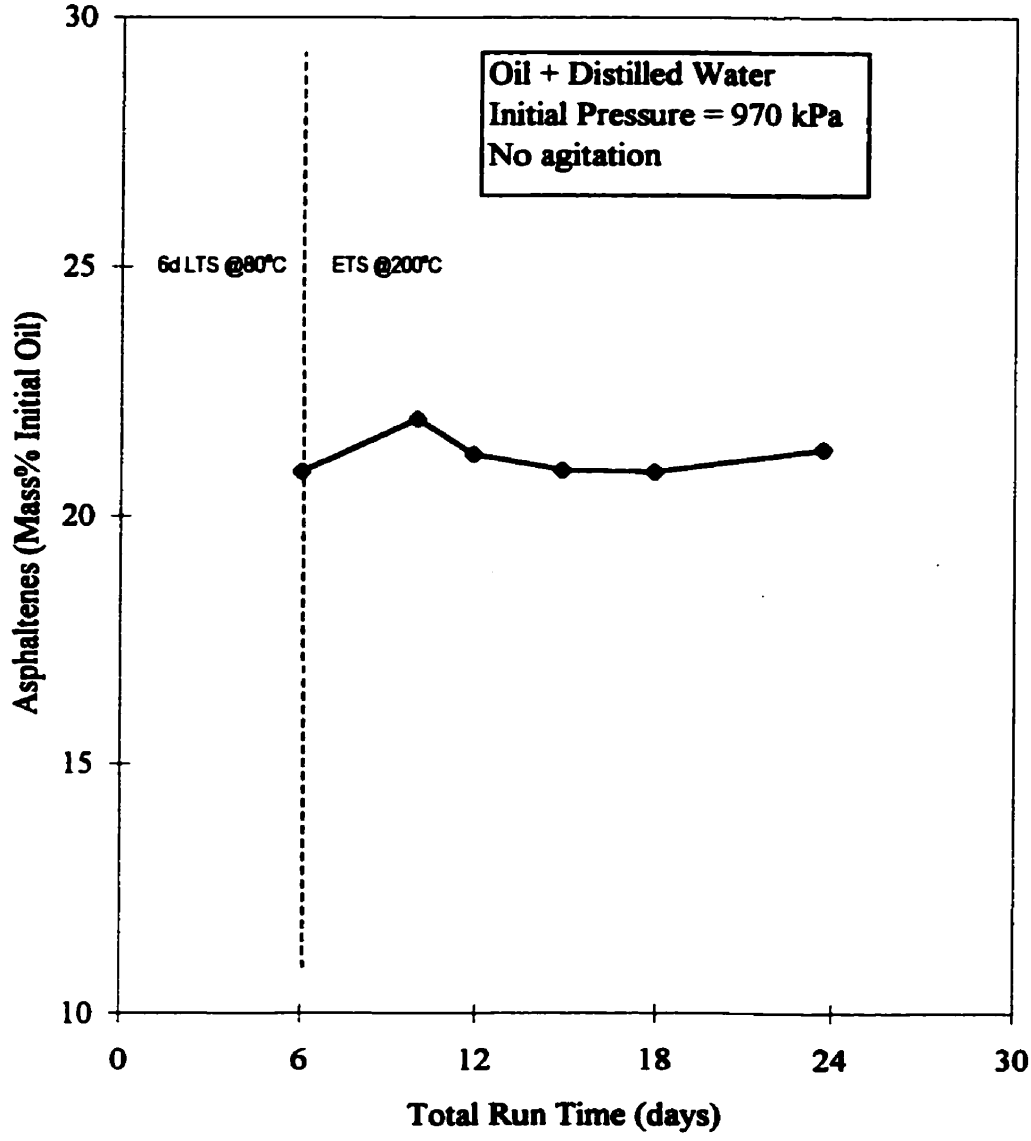

Figure 4.35: Effect of ETS Time on Asphaltenes Content

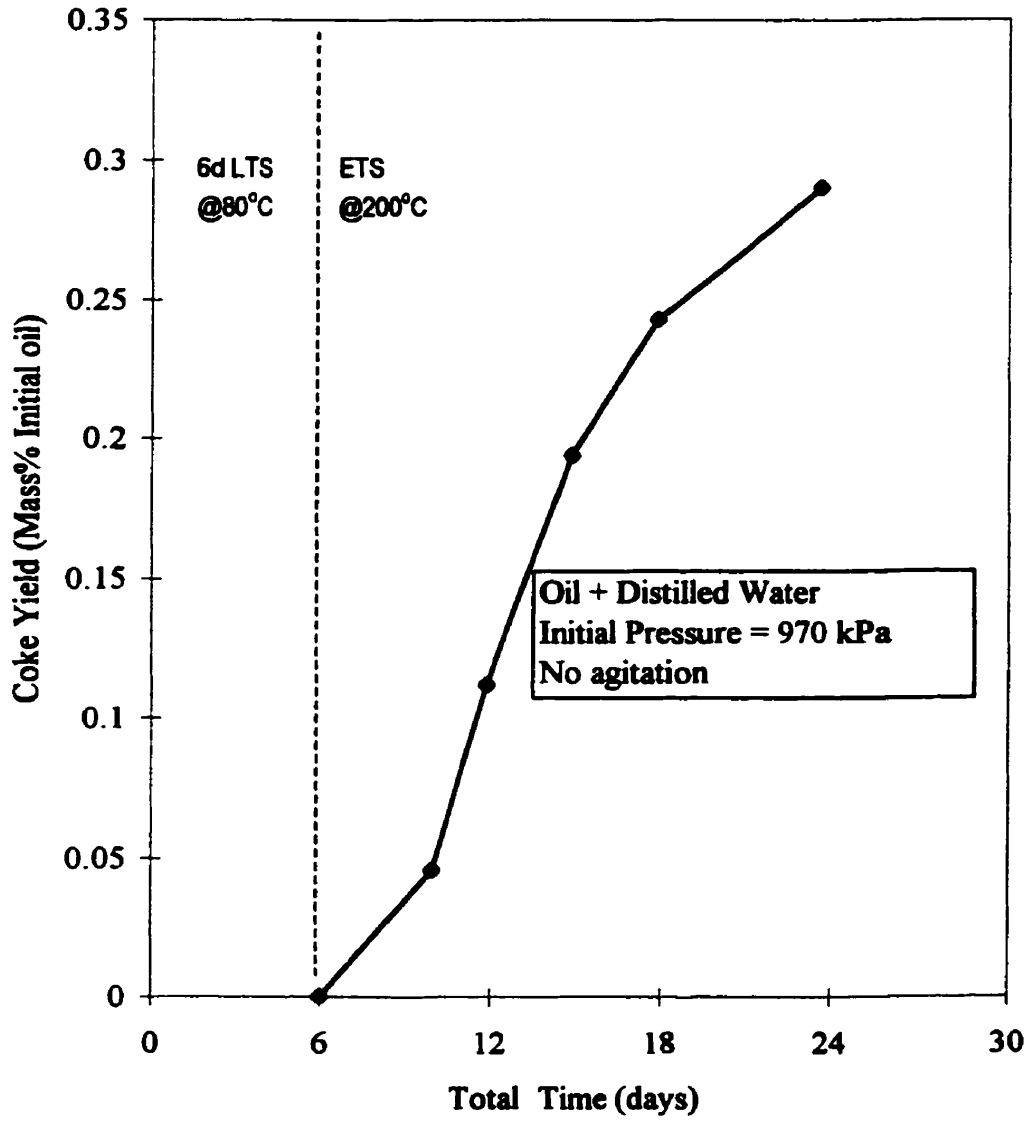

Figure 4.36: Effect of ETS Time on Coke Yield

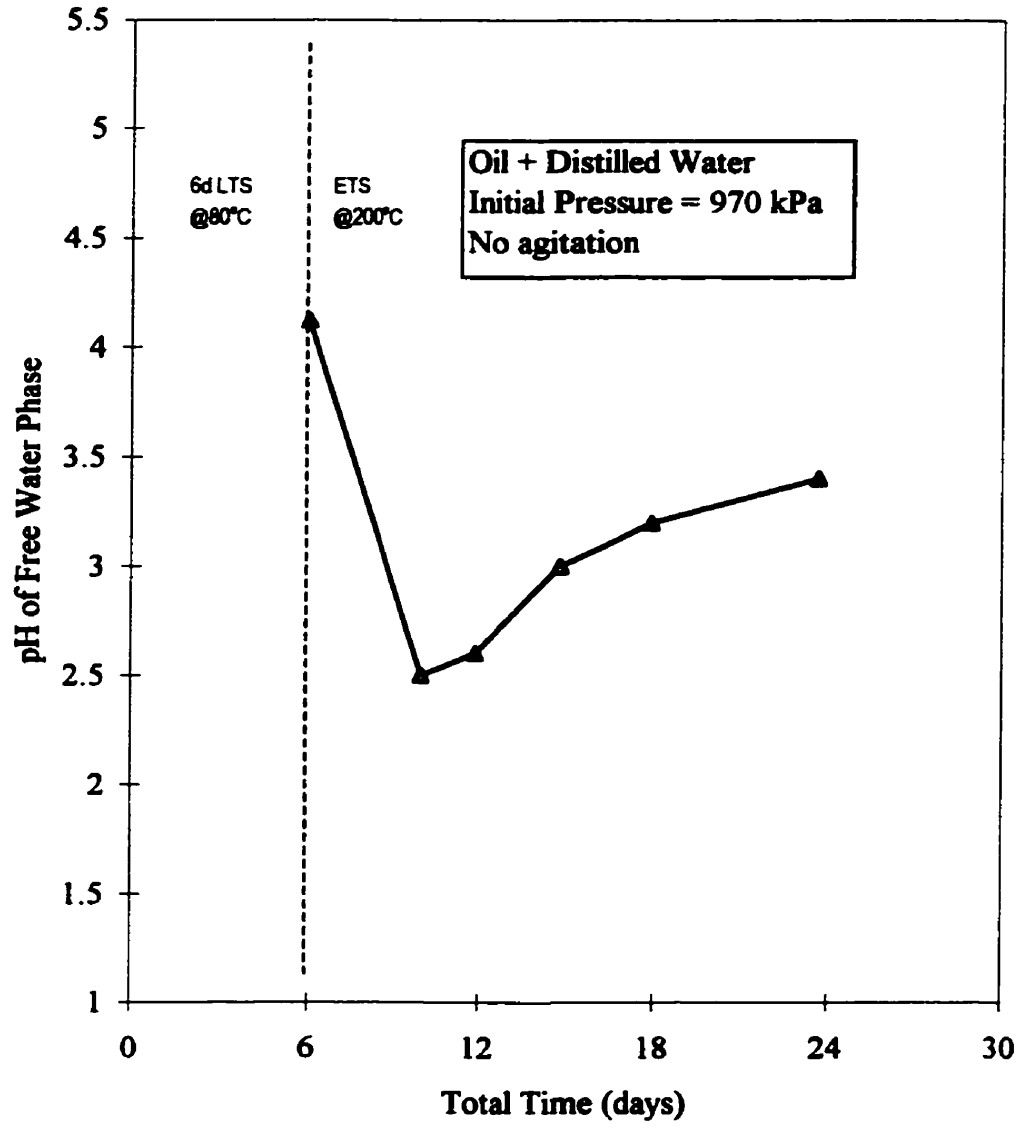

Figure 4.37: Effect of ETS Time on pH of Free Water Phase

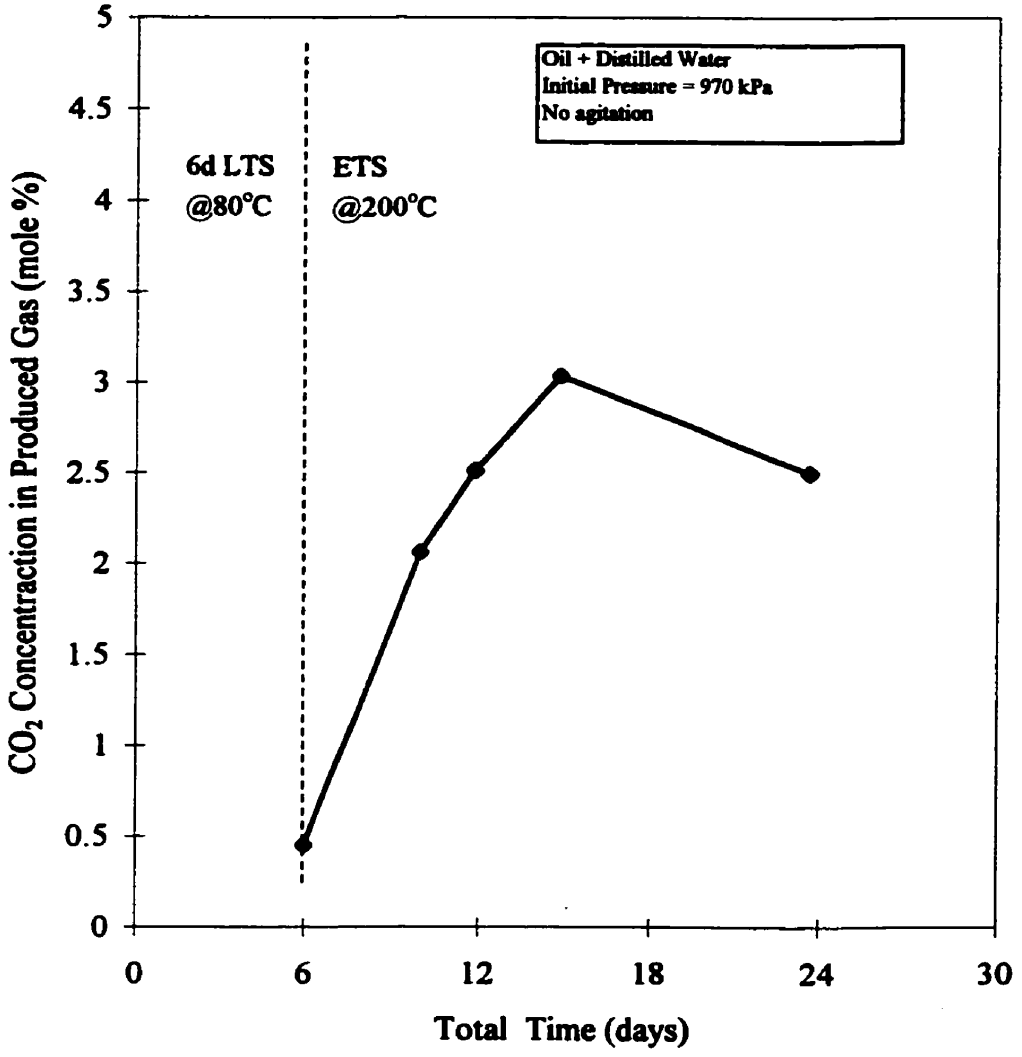

Figure 4.38: Effect of ETS Time on Produced CO_2 Concentration

4.4.3.3 Time Effects in the Presence of Synthetic Athabasca Brine

Effect of LTS Time

Figure 4.39 shows the effect of LTS time on the viscosity ratio for oil in the presence of Athabasca brine. The experimental tests considered are 6-5, 6-1, 6-6 and 6-7. They were performed at the same reaction conditions (i.e. initial pressure of 970 kPa, agitated at 1/3 RPM and 6 day ETS at 200 °C) with varying LTS run time. It can be seen that with the exception of no LTS time (i.e. heating directly to 200 °C), the viscosity ratio is relatively insensitive to LTS time. Note however that the test that was heated directly to the 200 °C ETS temperature (Test 6-5) involved only oxidation reactions occurring at 200 °C. This suggests that in the presence of Athabasca brine and under the same amount of oxygen uptake, the LTS stage seems to oxidize the hydrocarbon, increase the viscosity of the oil and thus is detrimental to the two-step upgrading process.

Effect of ETS Time

Figure 4.40 shows the effect on viscosity ratio of the varying ETS times for tests 6-4, 6-1 and 6-2 involving synthetic Athabasca brine. The experimental tests were performed at the same reaction conditions (oil plus brine, 6 day LTS at 80 °C, 954 kPa, 1/3 RPM agitation) with varying ETS run time. It can be seen that for the same LTS period of six days, a viscosity ratio decrease trend occurs when the ETS time is increased.

4.4.3.4 Time Effects in the Presence of Athabasca Core plus Brine

Figure 4.41 and Figure 4.42 illustrate the effect of varying LTS and ETS times respectively, on the viscosity reduction in the presence of mineral matrix. Figure 4.41 summarizes the experimental tests 5-6, 5-1, 5-7 and 5-8, while Figure 4.42 shows data for tests 5-5, 5-1, 5-2 and 5-3. The general trend with regard to both LTS and ETS time is that of a maximum viscosity for the test performed at 6 day LTS and 6 day ETS (Test 5-1). From the results and the later discussions in section 4.4.5, it seems that the presence of sand promotes bitumen viscosity reduction while brine promotes increases in the viscosity of the bitumen. The maximum viscosity ratio points for 6-day LTS and 6-day ETS would appear to reflect offsetting influences of the mineral matrix and brine.

The trend of the viscosity ratio versus time data for the runs involving sand matrix and brine suggests that the two step oxidation process may have potential as the basis of an in-situ upgrading process. The fact that the brine does influence the viscosity reduction associated with the two step oxidation process further suggests that the addition of metallic salts to the brine should be investigated as a method for enhancing the in-situ upgrading potential of the two step oxidation process.

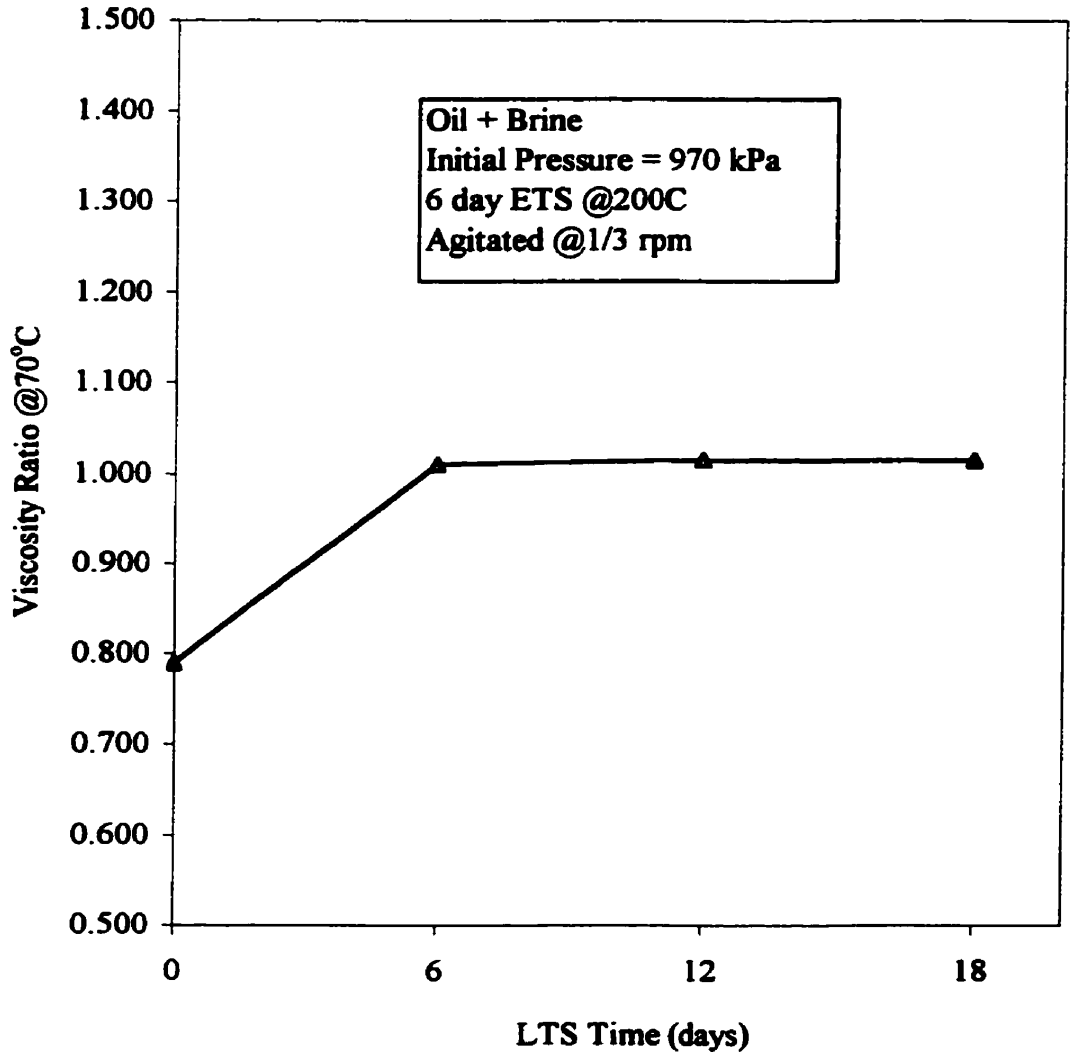

Figure 4.39: LTS Time Effect on Viscosity in Presence of Brine

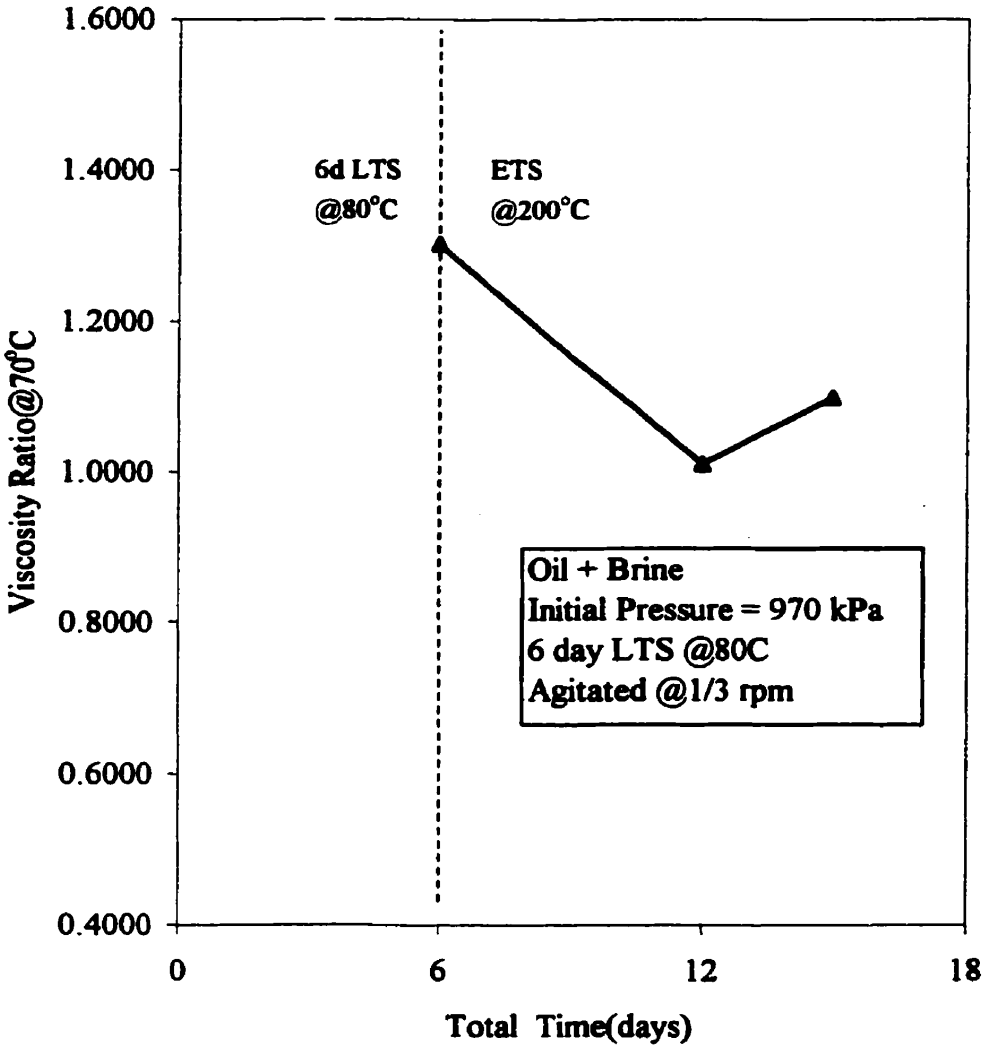

Figure 4.40: ETS Time Effect on Viscosity Ratio in Presence of Brine

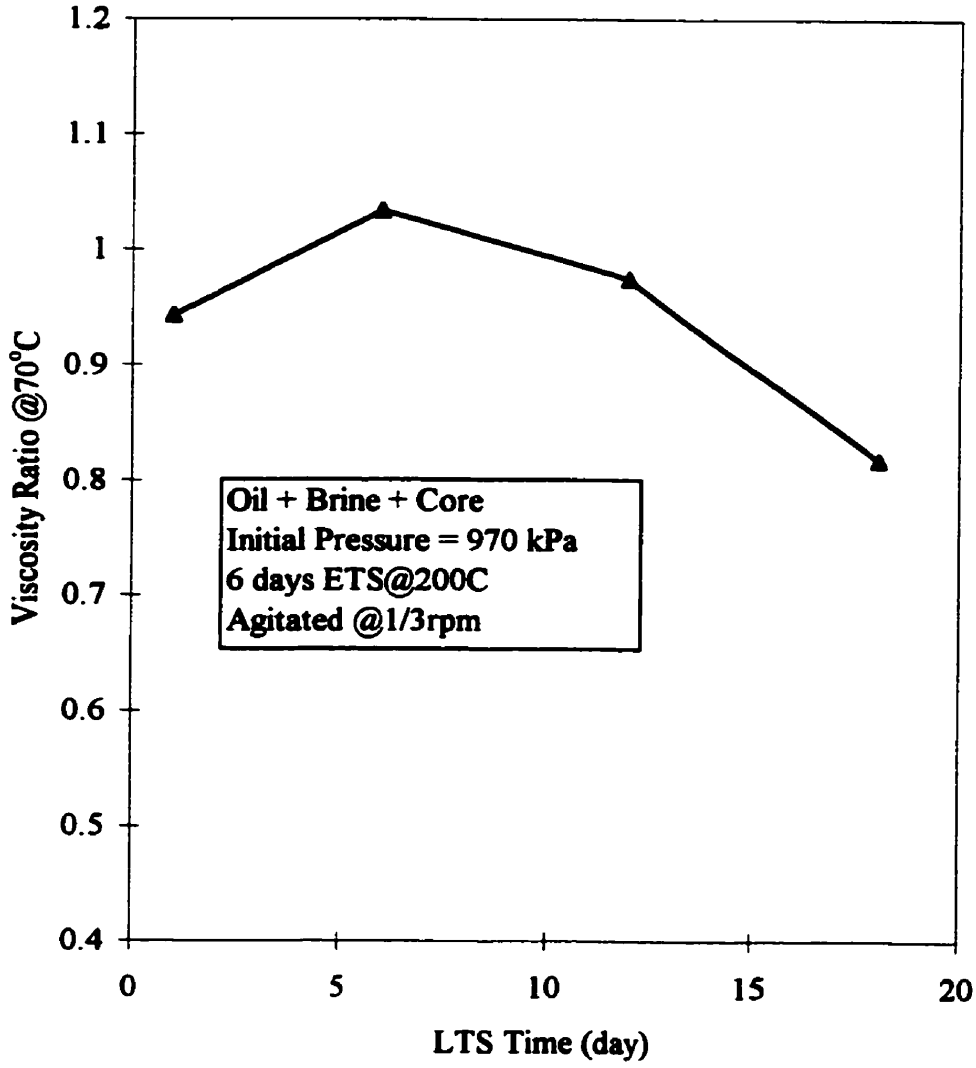

Figure 4.41: LTS Time Effect on Viscosity Ratio in the Presence of Core Matrix

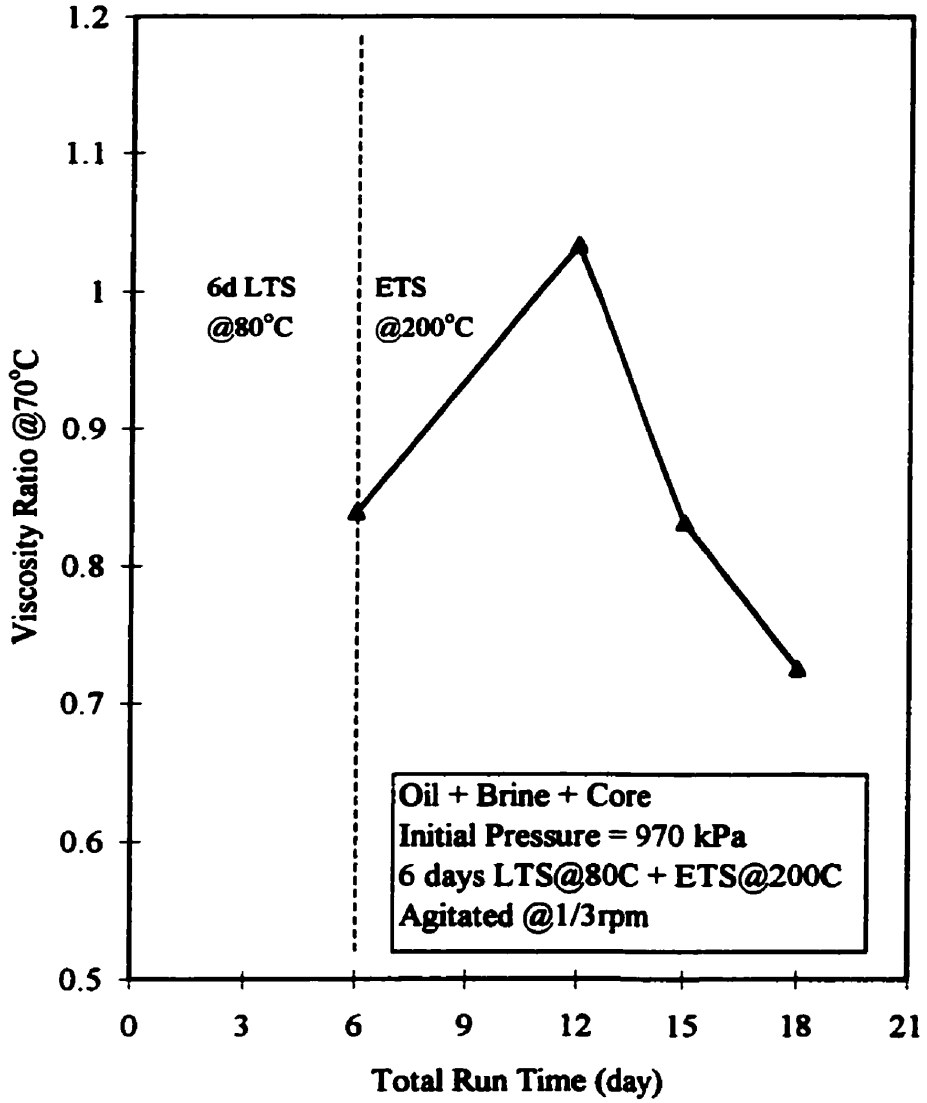

Figure 4.42: ETS Time Effect on Viscosity Ratio in the Presence of Core Matrix

4.4.4 Effect of Brine, Sand Matrix and Agitation on the Compositional Behavior

4.4.4.1 Effect of Brine, Sand Matrix and Agitation on LTS Time Curves

Figures 4.43 – 4.48 summarize the effects of brine, sand matrix and agitation on the physical properties and compositional parameters in response to changes in the LTS period. Comparisons are provided for the four series: oil and distilled water without agitation, oil and distilled water with agitation, oil and brine with agitation and oil, brine and sand matrix with agitation. The synthetic Athabasca brine has a salinity of 1.6% (by mass) and a pH of 8.55. In the experiments in which a core matrix was present, the mineral matrix or sand comprised 71.0 % (by mass), the oil made up 20.4 %, and the remainder or 8.6 % was brine. The nominal masses of oil and brine in the runs involving core matrix were therefore 39 and 16 grams, respectively, as opposed to 50 grams of each in the tests not involving the solid matrix. Agitation was induced by rocking the cells at a speed of 1/3 RPM.

The tests were performed at the same reaction conditions of initial pressure of 970 kPa, LTS at 80 °C and 6 days ETS at 200 °C. Case 1 includes the tests 2-6, 2-2, 2-7 and 2-8 and Case 2 involves tests 3-1 and 3-3, Case 3 includes the tests 6-5, 6-1, 6-6 and 6-7 and Case 4 consists of the tests 5-6, 5-1, 5-7 and 5-8.

Figure 4.43 illustrates the brine, sand matrix and agitation effects on the viscosity ratio at 70 °C (vs. LTS time). Case 1 (distilled water, without agitation) viscosity ratios

suggest little effect of LTS time. Case 2 (distilled water, agitated) implies an effect of agitation on viscosity, which is particularly noticeable at low LTS times. Case 3 (brine, agitated) shows an effect of agitation at low LTS time. It should be noted that the two tests performed at an LTS time of 0 day were heated directly to 200 °C, hence they have not been exposed to oxidation reactions at 80 °C. Case 4 (brine, sand matrix, agitated) indicates an effect of core matrix. At low LTS times, the presence of sand matrix appears to retard the viscosity reduction as compared to those for agitated brine or distilled water. This suggests that the solid matrix has a dampening effect on the mixing during agitation. Core matrix enhances the viscosity reduction at longer LTS times which suggests that the core matrix is impacting the oxidation / cracking reactions through either catalytic or surface area mechanisms.

Figure 4.44 summarizes the changes in the density ratios (at 25 °C) for the four test series. With the exception of the agitated tests involving distilled water, the effect of the two step treatment process is an increased density of the treated oil as compared to that of the original oil.

Asphaltenes contents (Figure 4.45) corresponding to the four tests suggest the same general trends as were identified from the viscosity measurement. The agitated brine test at 18 days would appear to show an abnormally low asphaltenes content but this is a result of coke formation (Figure 4.46). As shown in Figure 4.46, coke yields are generally very low, but the higher coke yields correspond to reduced asphaltenes

contents. This implies a mechanism of asphaltenes conversion to coke which has been previously described by Millour et al. (1987).

Figure 4.47 presents the CO_2 concentration trends. In comparison with the coke yield trends (Figure 4.46), it is apparent that coke yield and CO_2 generation follow similar trends. It can also be seen that the presence of core material greatly enhances the generation of CO_2.

Figure 4.48 shows that pH is strongly affected by the water composition but is insensitive to agitation or LTS time for the conditions evaluated. The runs with brine have higher pH close to the original value of 8.55, while the tests involving distilled water show reduced pH compared to the original value of 6.5. This indicates that, as stated in Chapter 4.3, the brine has a buffering effect on the pH of the effluent waters.

4.4.4.2 Effect of Brine, Sand Matrix and Agitation on ETS Time Curves

Figures 4.49 – 4.55 present comparisons of the effect of brine, sand matrix and agitation on the physical and compositional parameters for different ETS durations. Comparisons are provided for the four classifications described in the previous section. The tests were performed at the same reaction conditions of initial pressure of 970 kPa, 6 days LTS at 80 °C and ETS at 200 °C. Case 1 includes tests 1-5, 1-3, 2-1, 2-2, 2-3 and 2-4, Case 2 contains tests 3-1 and 3-2, Case 3 includes tests 6-4, 6-1 and 6-2, and Case 4 involves tests 5-5, 5-1, 5-2 and 5-3.

Viscosity data (Figure 4.49) for all four test series suggest a trend of decreasing viscosity with increased ETS time. The four runs involving core matrix and brine suggest viscosity improvements at 0 day and longer days (9 days and 12 days) of ETS. The viscosity ratios for the agitated distilled water runs suggest a viscosity improvement due to rocking of the cells.

Density ratio data for at 25 °C (Figure 4.50) show that with the exception of the two runs involving distilled water and agitation, the treated oils are more dense than the original oil. In general, the ETS stage was not effective in reducing the oil density below the levels attained during the LTS period.

Asphaltenes contents (Figure 4.51) shows the same general trends as were observed from the viscosity data. Only the agitated distilled water and brine tests have a trend of decreasing asphaltenes content with ETS time. The presence of solid matrix causes the asphaltenes to behave in a manner similar to the non-agitated distilled water tests. This suggests that the presence of the solid has retarded the benefits of agitation.

Coke yields (Figure 4.52) for Case 1 runs (distilled water) suggest an increase in coke with time but results for the other tests suggest that coke yield may decrease with ETS time. What should be noted is that the decrease in coke is reflected by an increase in asphaltenes for the same test, hence the observation of decreasing coke with increasing ETS time is a reflection of the difficulty in defining coke and asphaltenes (both are determined by solubility on the addition of solvents).

CO_2 data (Figure 4.53) suggest CO_2 concentrations increase with ETS time. Agitation appears to enhance CO_2 production and the presence of core matrix has a very significant effect on the generation of CO_2.

Oxygen concentrations in the post test gas are shown in Figure 4.54. The O_2 concentrations decrease with ETS time, but only the agitated brine runs appear to approach full O_2 utilization.

The pH's of the free water phase are shown in Figure 4.55. In general, pH shows an insensitivity to ETS duration. The runs with brine have pH levels close to that of the original brine value of 8.55, while the runs with distilled water show reduced pH compared to the original value of 6.5. This indicates that, as stated previously, the brine has a buffering effect on the pH of the effluent waters. The data suggest that the pH of the free water falls during the initial portion of the ETS stage and then shows an increasing trend with increasing time during higher ETS times. This suggests that the organic acids undergo further decomposition reactions with time.

4.4.4.3 General Effect of Brine, Sand Matrix and Agitation on the LTS/ETS Process

Agitation

A possible explanation for the agitation effect is that rocking may change the role of the water phase in terms of the nature of the gas-liquid interface. If water is lighter than oil, water sits above the oil in the static cell. If oil is lighter, gas contacts oil directly in the static cell. Figure 4.56 shows the effect of temperature on the density of Athabasca

bitumen (Polikar, 1980) and the distilled water. It can be seen that the density of the Athabasca bitumen is always higher than that of the distilled water in the range of 273 K to 523 K, except that the densities approach each other at the experimental LTS temperature of 80 °C (353 K). Therefore, at the LTS temperature of 80 °C, rocking will increase mixing of the oil and water phase and will most probably increase the interface between the gas and oil phases. The most probable result of the increased mixing between the oil and water phases would be an enhancement in the rate of extraction of oxidized components to the aqueous phase.

At the ETS temperature of 200 °C, the water phase would definitely be above the oil phase (with the possible exception of the runs involving solid matrix), hence rocking would only be expected to have a minor effect on the interfaces between the gas, oil and aqueous phases. Rocking of the cell would certainly promote mixing within the bulk oil phase at 200 °C and to a lesser extent at 80 °C. Mixing would promote renewal of the interface where oxygen transfer occurs, which would in turn promote an increased oxygen concentration within the bulk oil. The difficulty in making a definitive interpretation of the effect of mixing is that sequential reactions are occurring (i.e. oxidation reactions form oxidized hydrocarbon products which can in turn react with oxygen, asphaltenes are formed and they in turn are converted to coke, carbon oxides and other liquid phase hydrocarbons).

Synthetic Athabasca Brine

It was observed that experiments involving agitated oil and brine produced oils with higher viscosity ratios than agitated experiments conducted with distilled water but lower viscosity ratios than static experiments involving distilled water. In addition, in the case of experiments conducted using agitated distilled water, extending the LTS period had the effect of increasing the viscosity ratio, while the agitated experiments involving brine without core showed an increase in viscosity ratio at low LTS times but no significant effect of LTS time for higher LTS durations.

Metals and metallic salts have long been recognised for their catalytic potential in both hydrocarbon cracking and oxidation reaction (Baviere, 1997). Metallic additives cause changes in the nature of the LTS + ETS process. The change appears to depend on the type of oil used and a given additive may affect different crude oils differently. In the above experiments, the Athabasca formation brine seems to catalyze a polymerisation type of reaction more than hydrocarbon chain breaking reactions, and therefore the presence of brine has a negative effect on the heavy oil viscosity reduction process.

Athabasca Core

The mineral matrix of the formation may have a catalytic effect on the free radical initiation reactions and the higher temperature bond-breaking reactions, which result in a viscosity reduction. For Athabasca Oil Sands, the core matrix is predominately quartz with some natural clays present. Clays contribute greatly to the total available surface area for reaction and the presence of transition metals in the clay may also have a

catalytic effect. The extent of viscosity ratio decrease depends on the combination of these effects.

Although the relative amounts of oil and brine used in the experiments involving mineral matrix were different from those used in the sand free tests, the trends shown in the Figures 4.43 to 4.45 are still valuable. It can been seen that the core matrix promotes the generation of carbon dioxide and that it provides a positive catalytic effect in terms of viscosity reduction for both the longer periods of LTS and for the longer exposure time during the ETS. The extent of the influence of mineral matrix on the viscosity reduction is therefore time dependent.

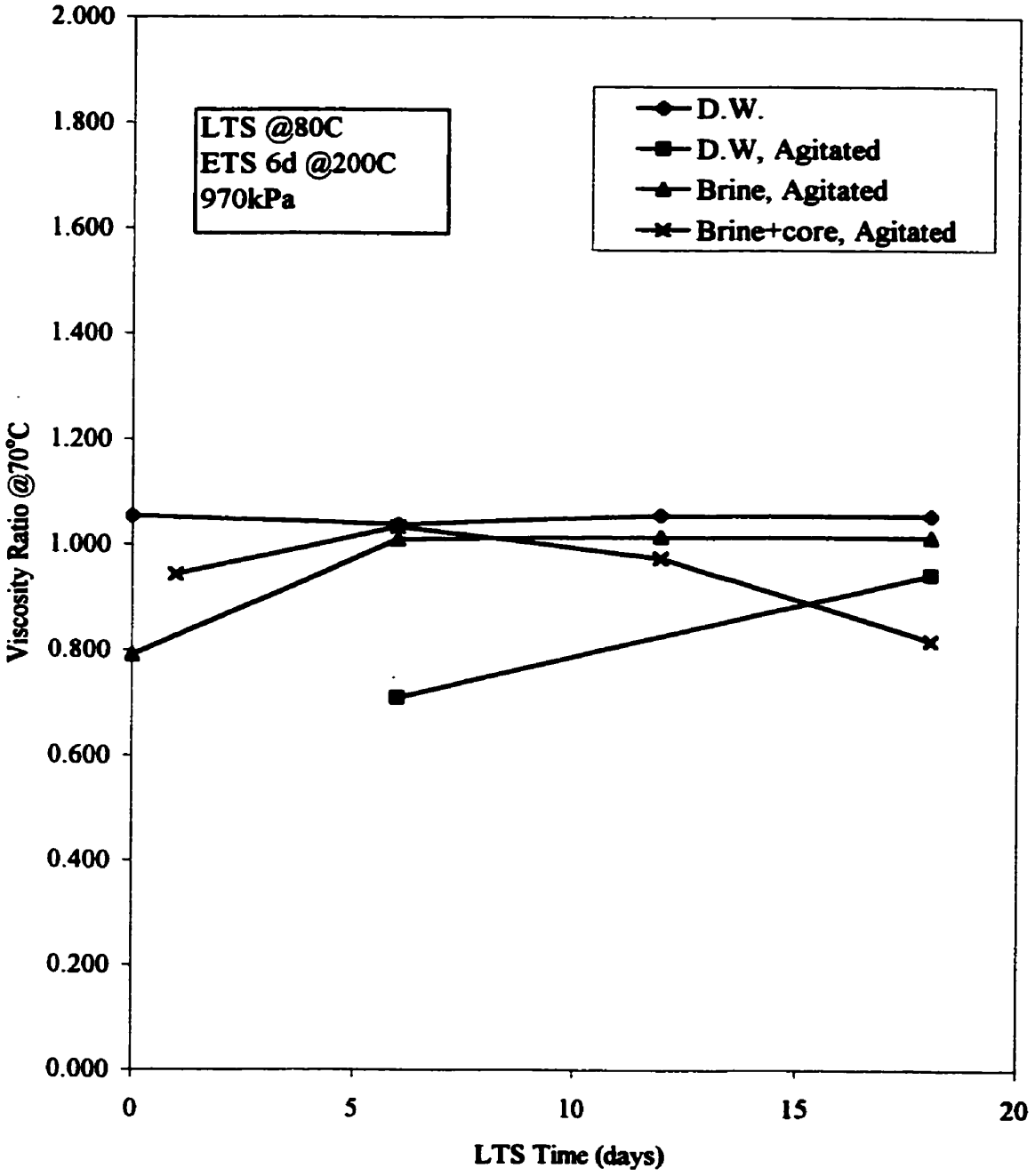

Figure 4.43 Viscosity Ratio vs. LTS Time

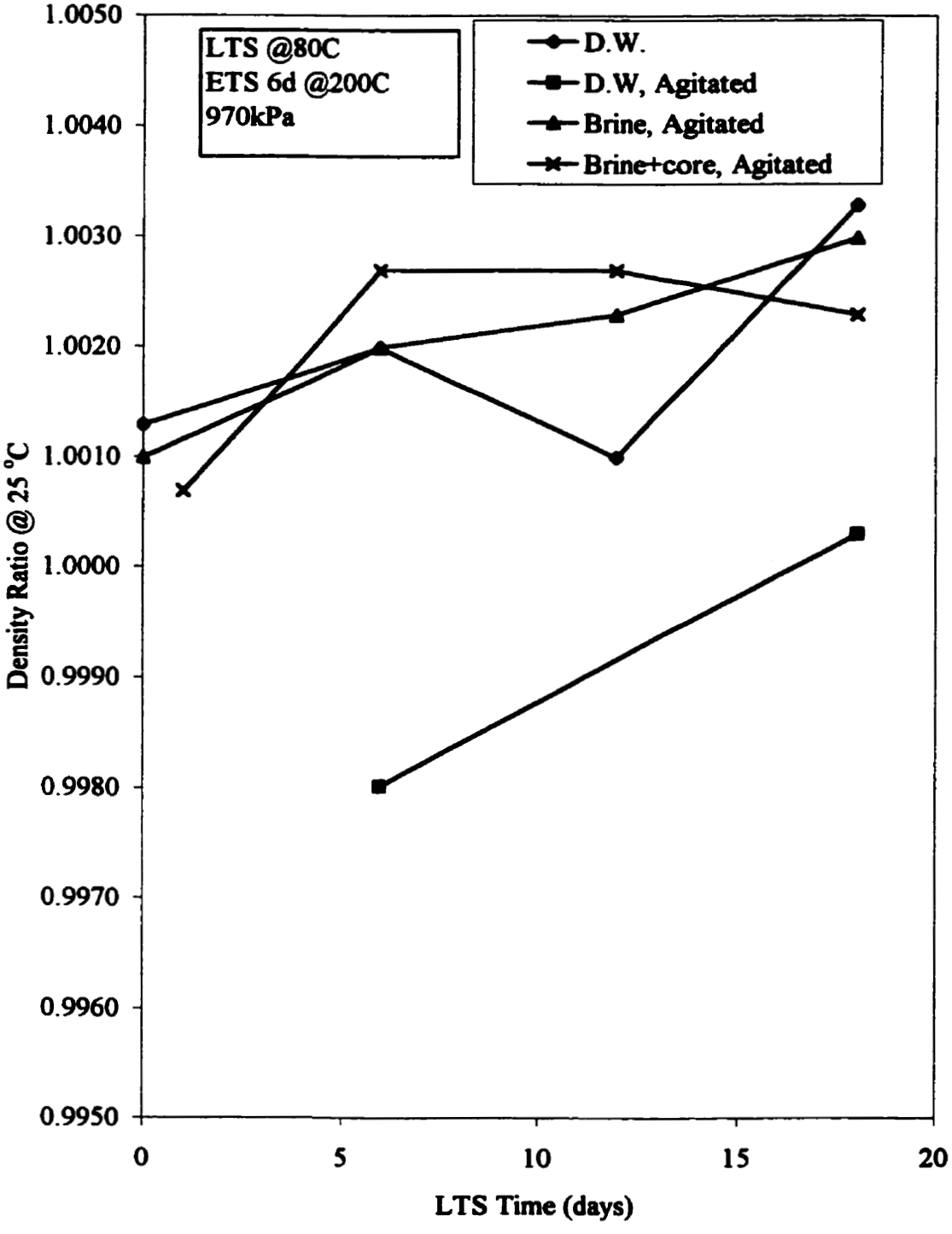

Figure 4.44 Density Ratio vs. LTS Time

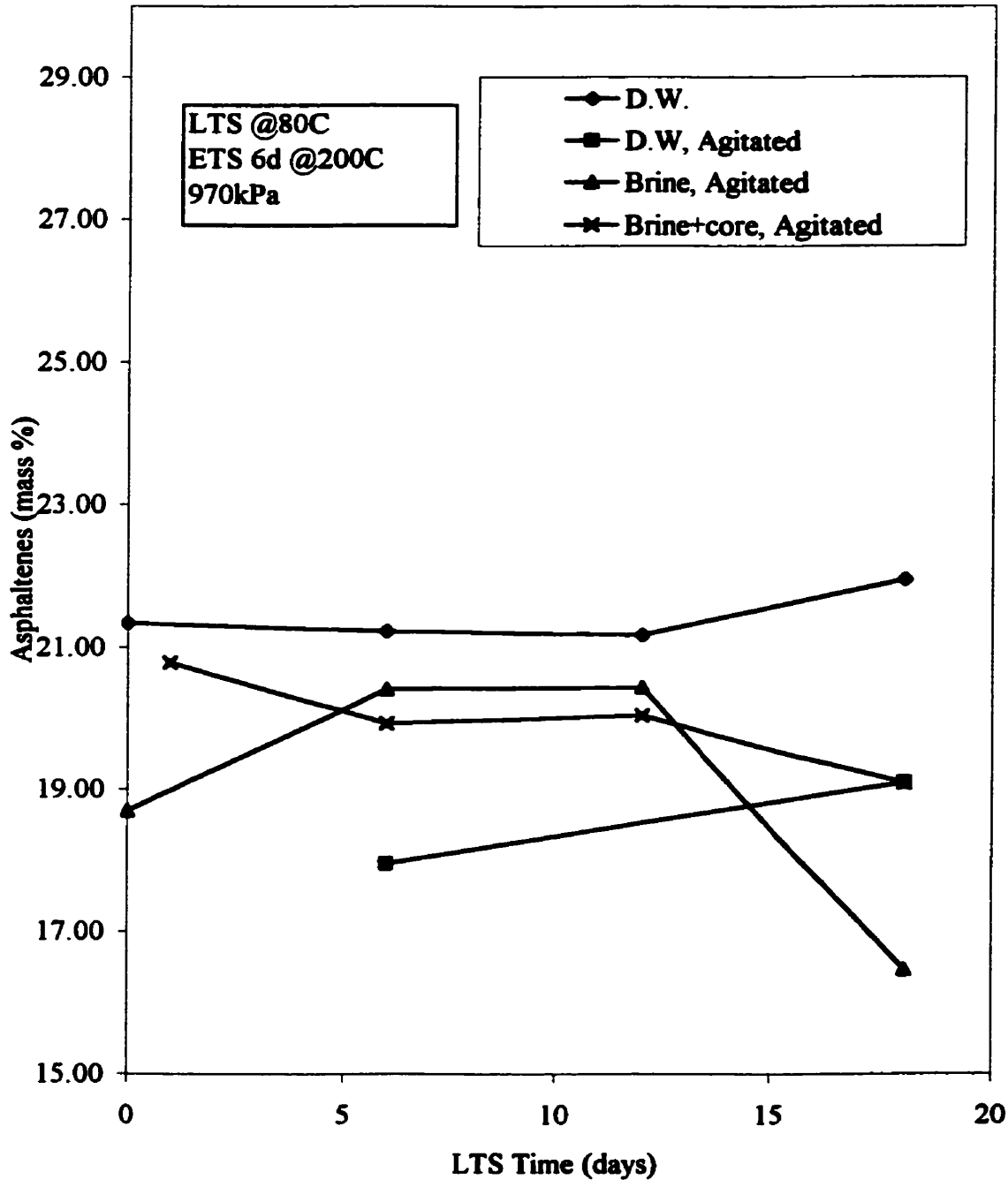

Figure 4.45 Asphaltenes vs. LTS Time

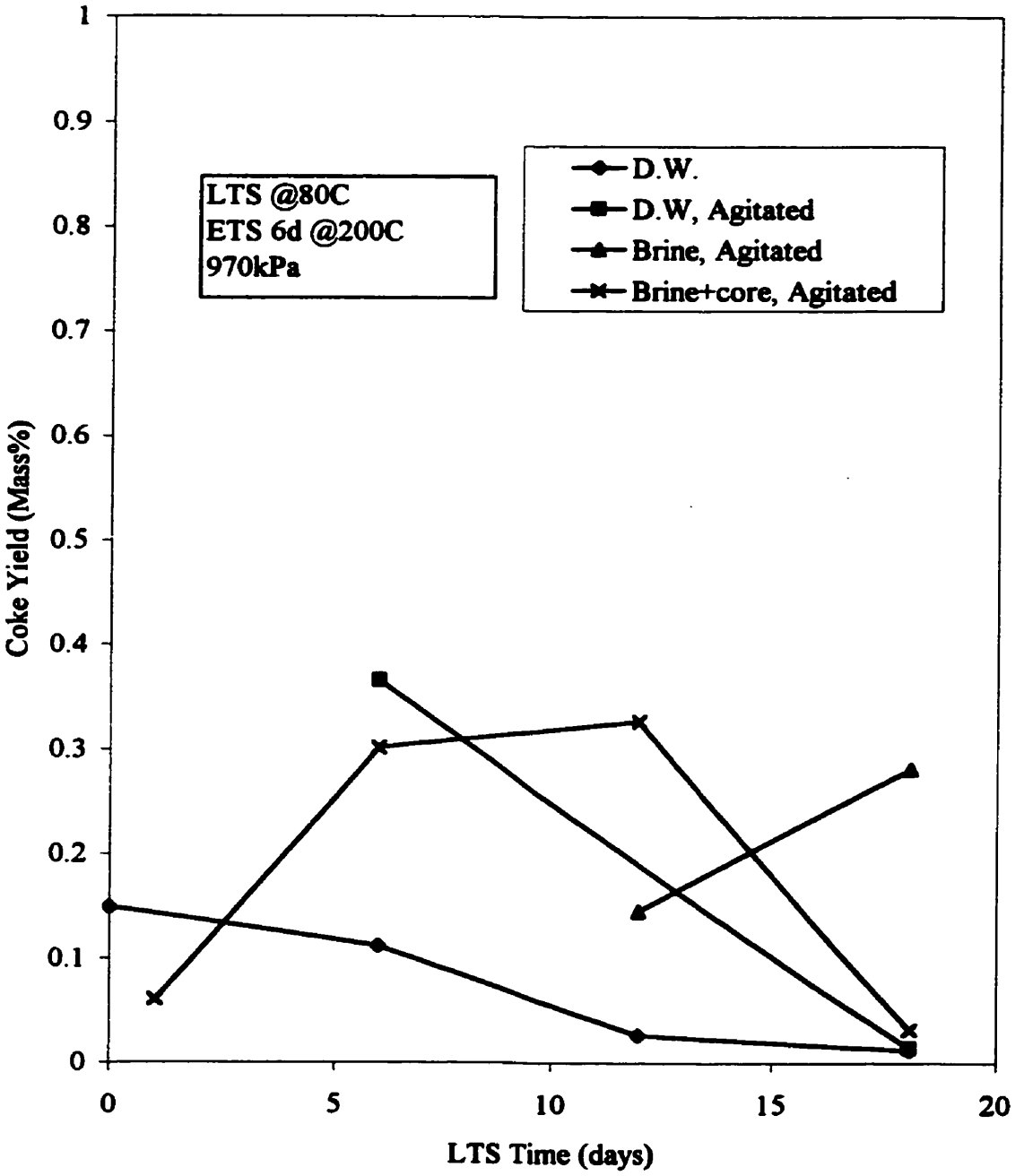

Figure 4.46 Coke Yield vs. LTS Time

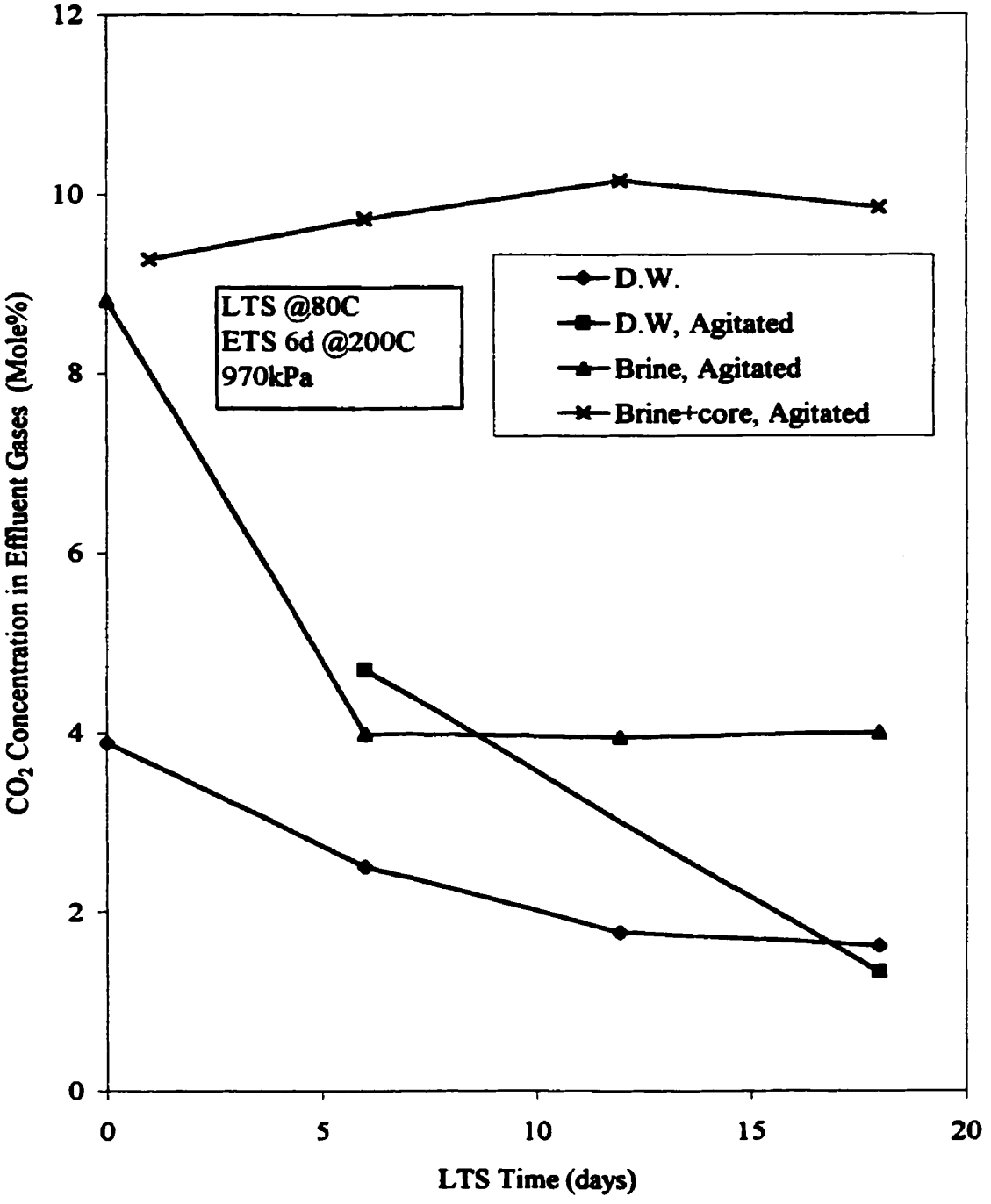

Figure 4.47 CO_2 Concentration in Effluent Gases vs. LTS Time

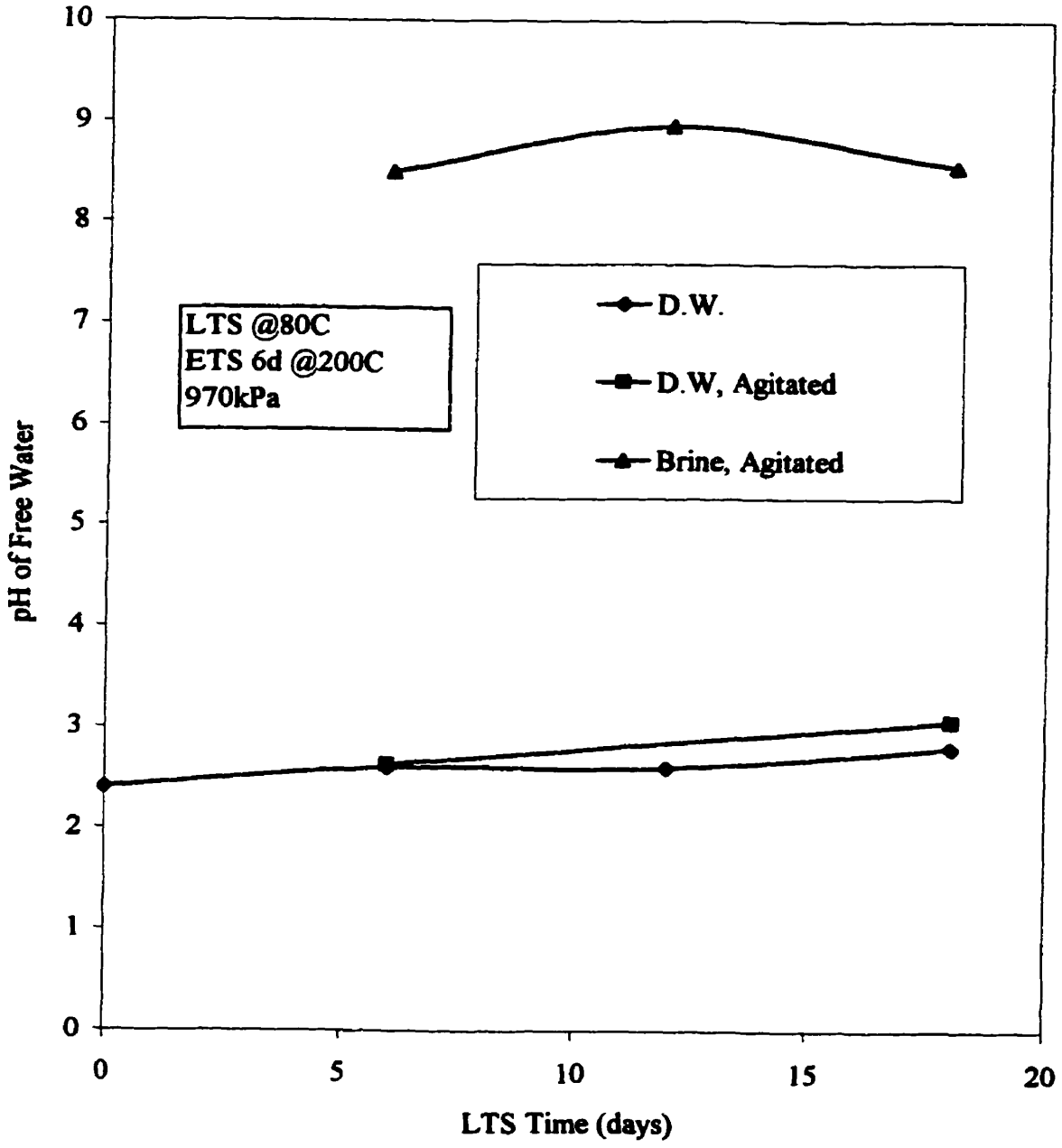

Figure 4.48 pH of Free Water vs. LTS Time

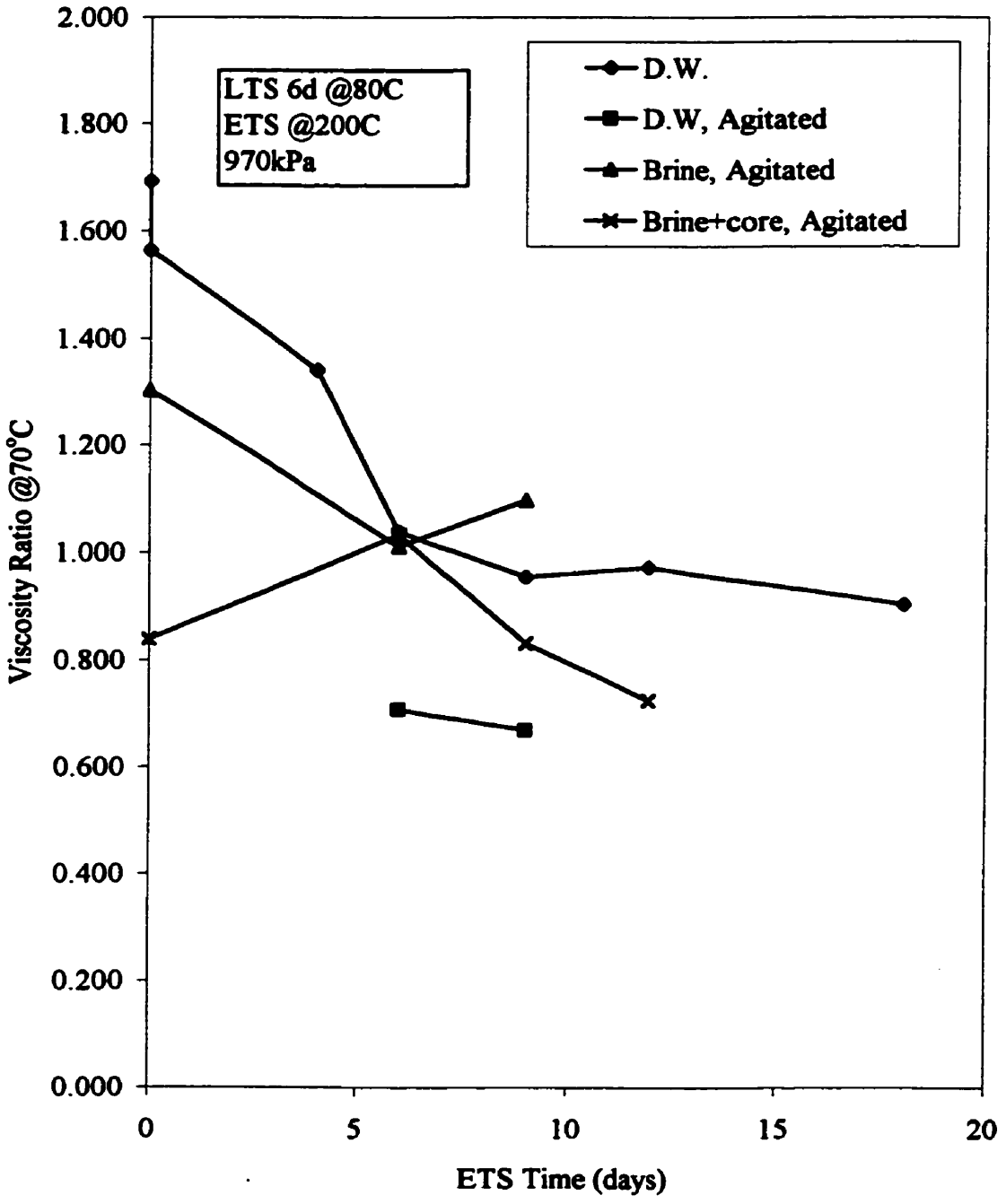

Figure 4.49 Viscosity Ratio vs. ETS Time

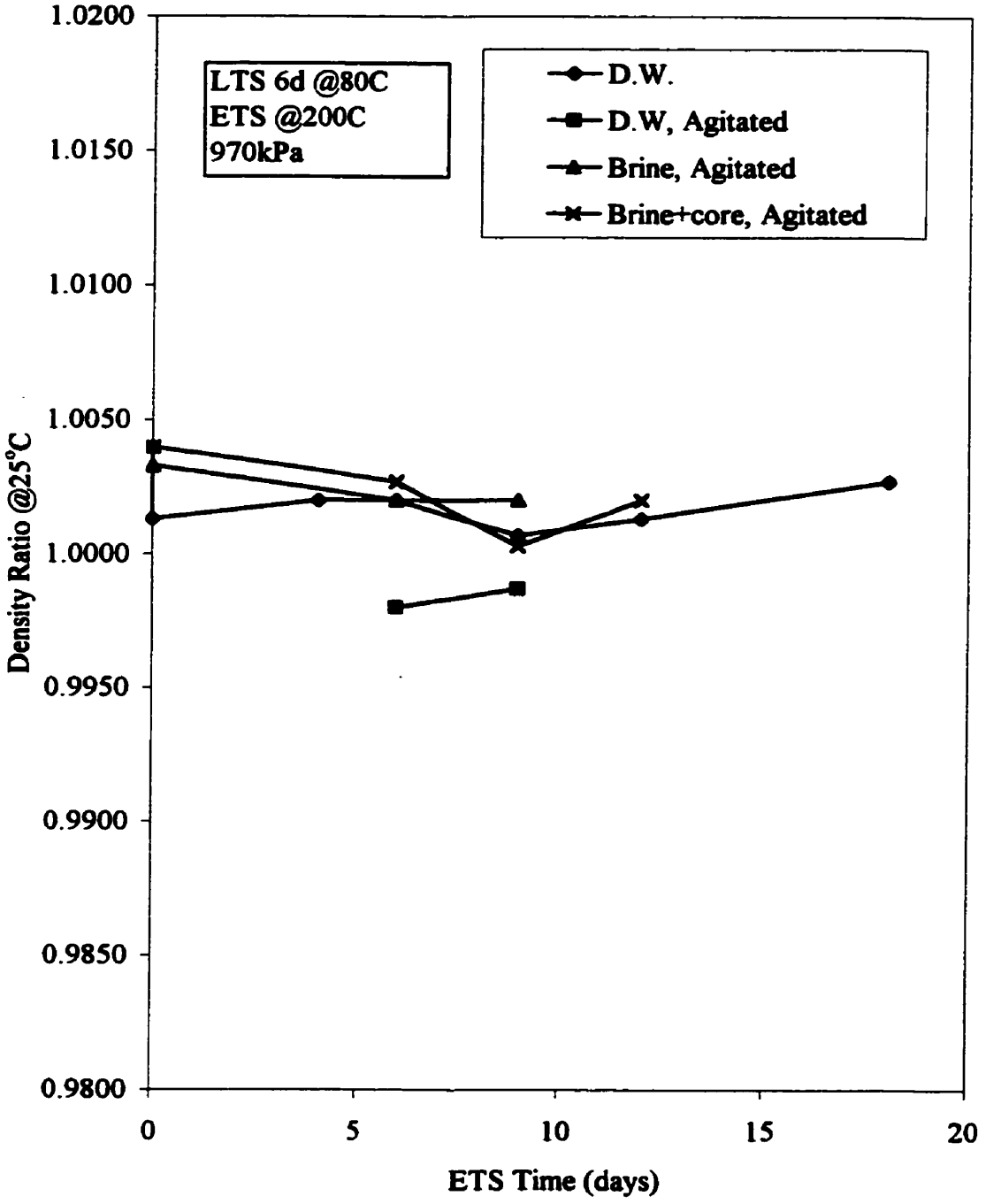

Figure 4.50 Density Ratio vs. ETS Time

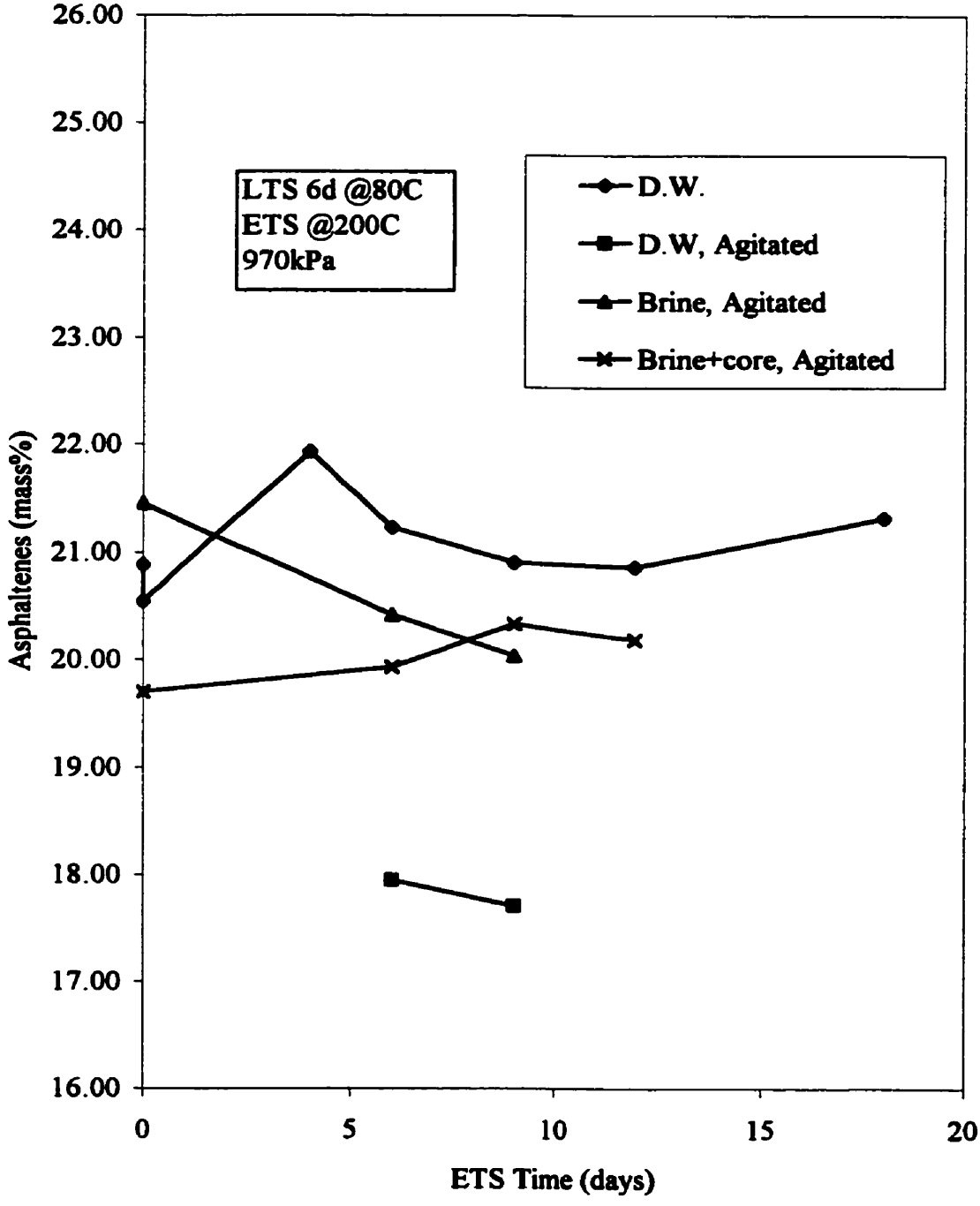

Figure 4.51 Asphaltenes Content vs. ETS Time

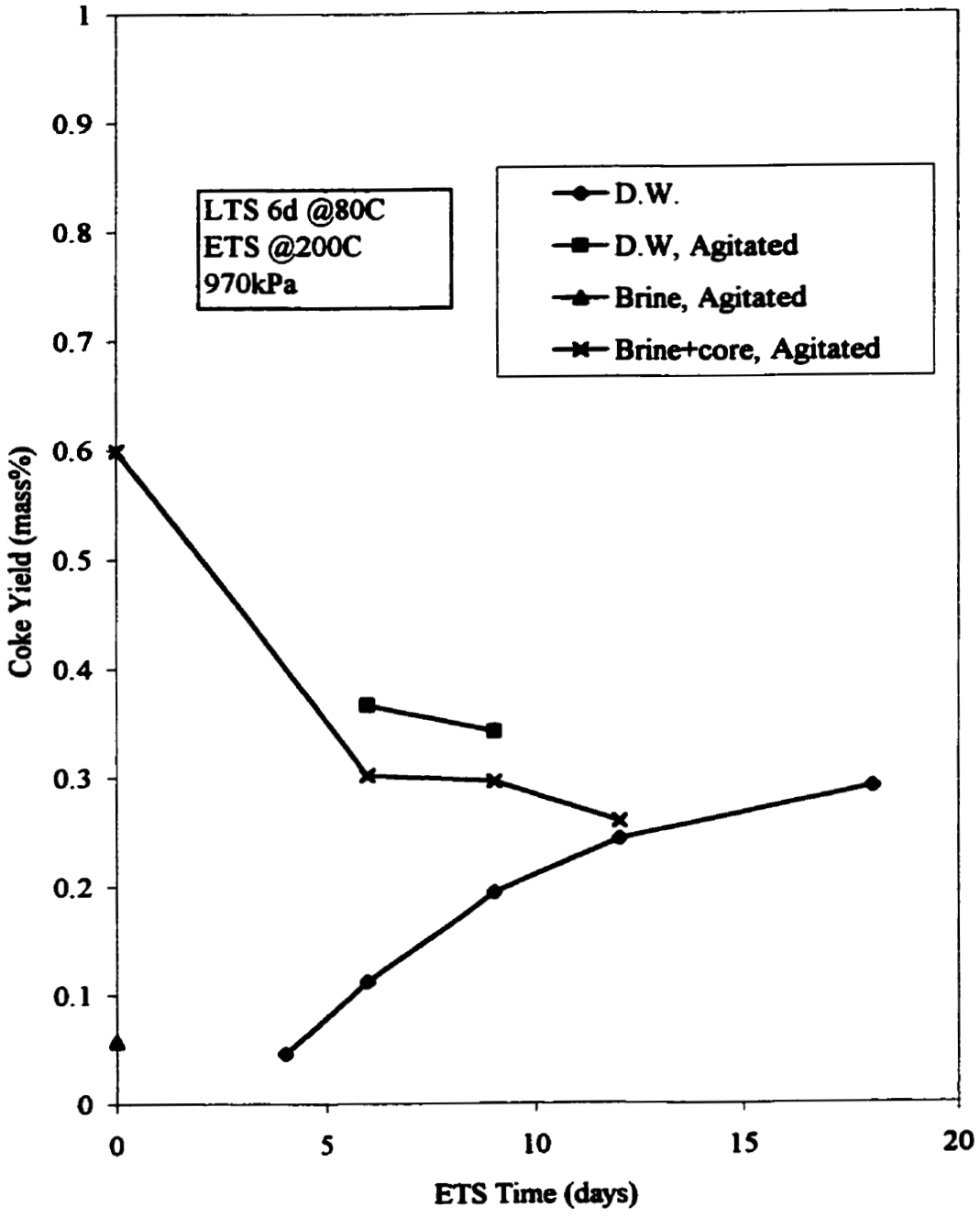

Figure 4.52 Coke Yield vs. ETS Time

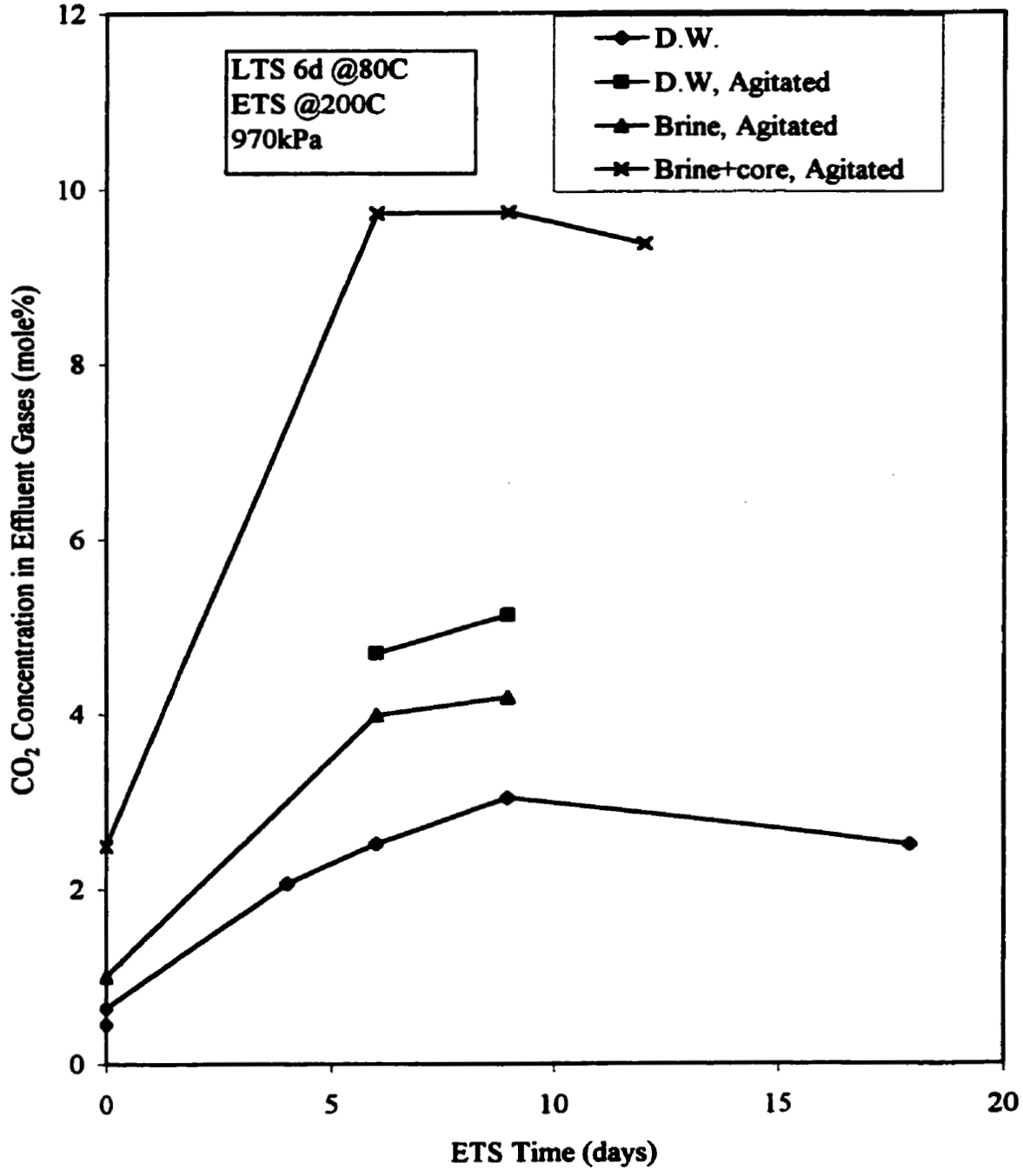

Figure 4.53 CO_2 Concentration in Effluent Gases vs. ETS Time

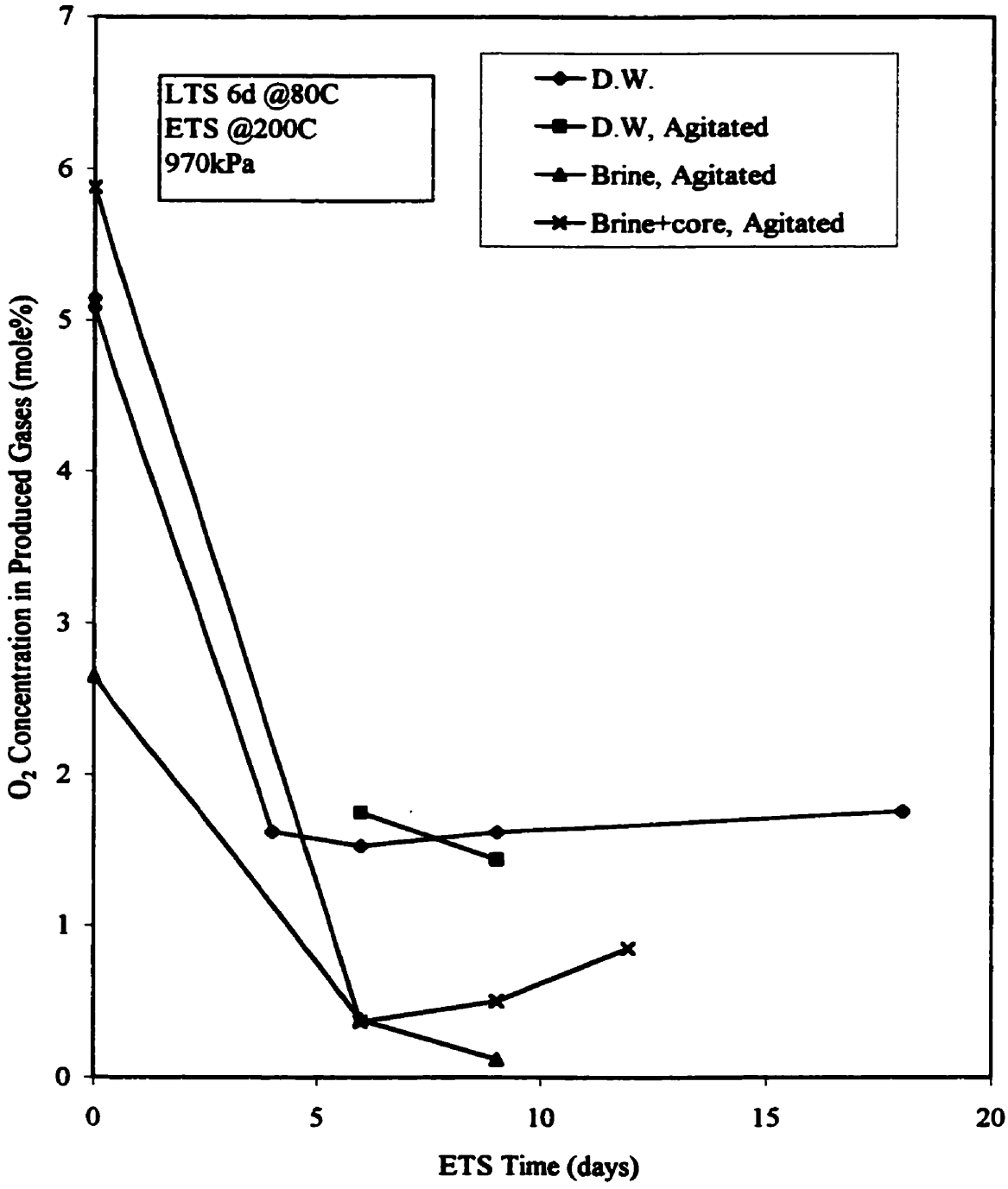

Figure 4.54 O_2 Concentration in Produced Gases vs. ETS Time

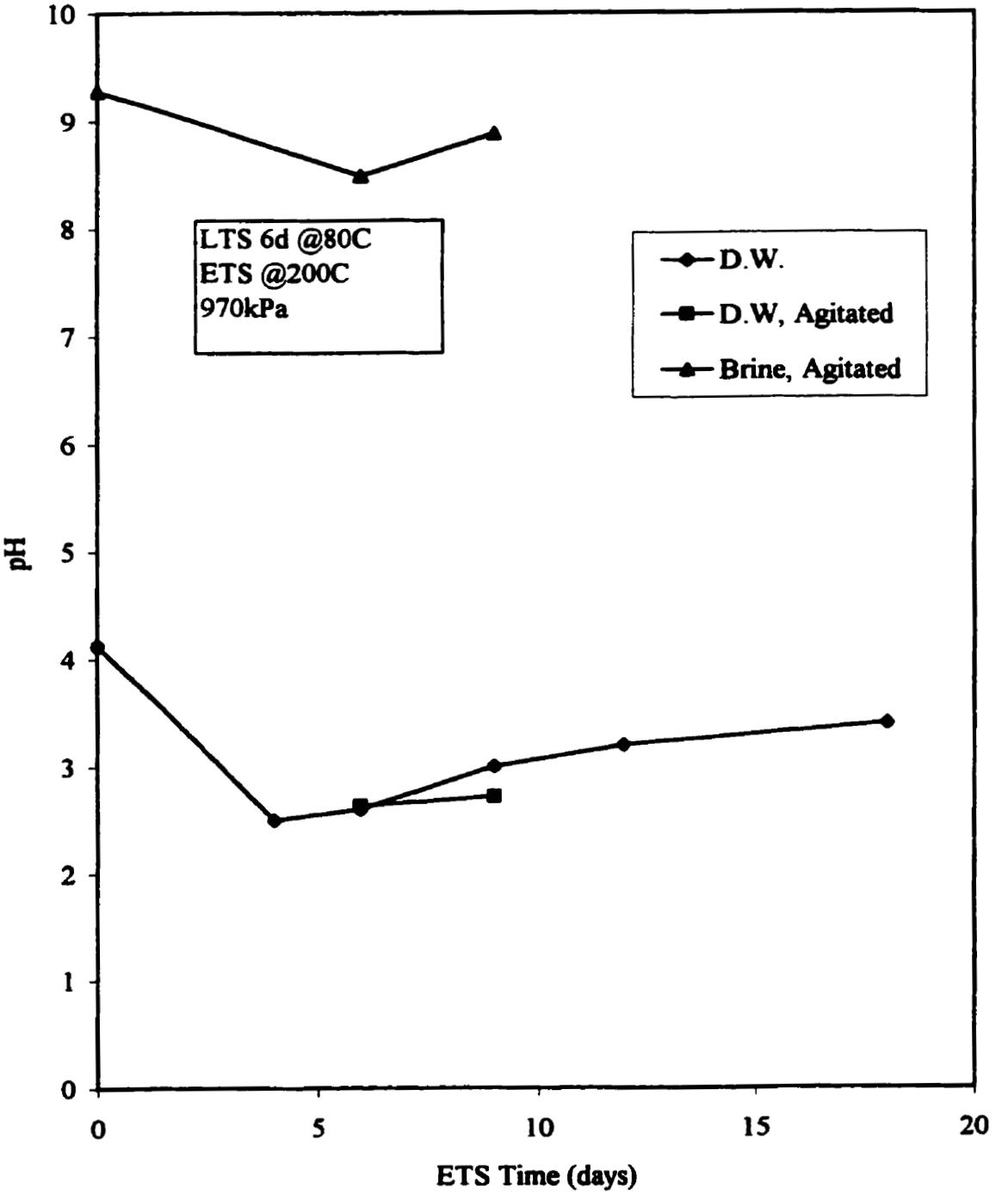

Figure 4.55 pH vs. ETS Time

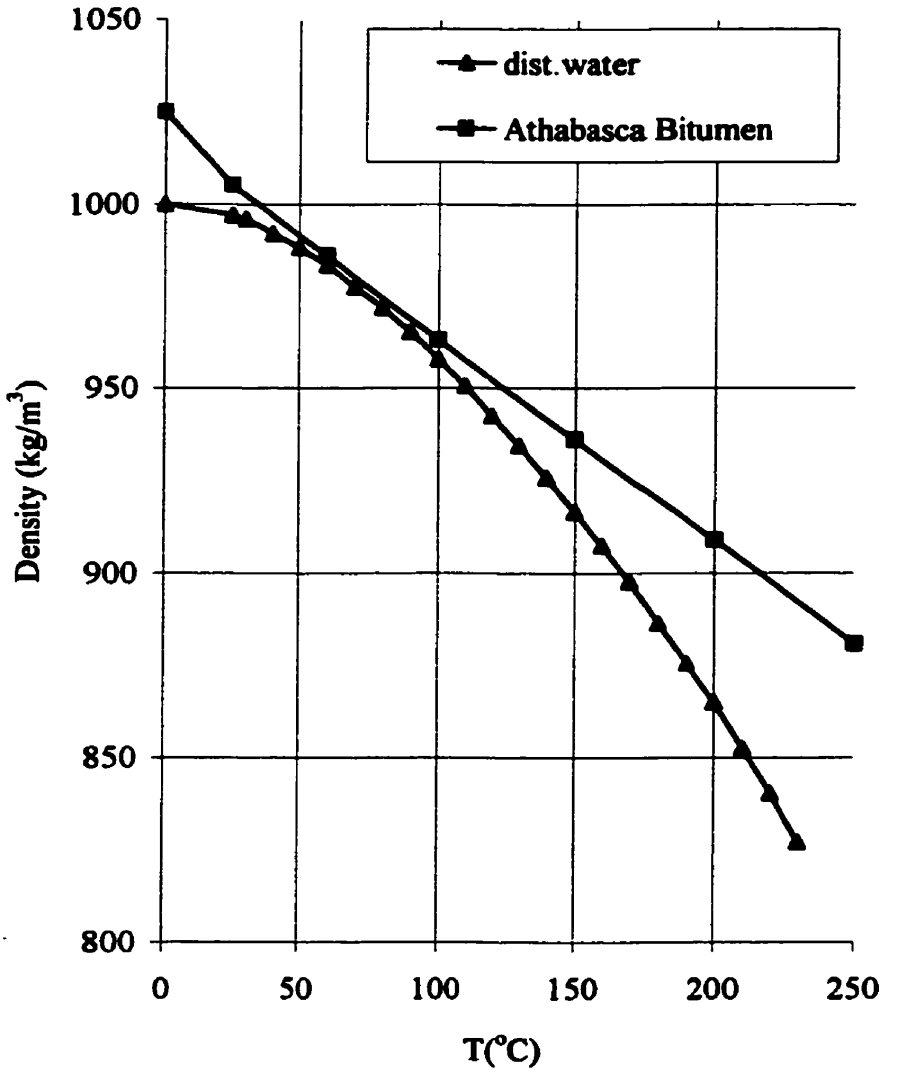

Figure 4.56 Density as a Function of Temperature

4.5. RUN 6-CELL 3

A malfunction in the temperature control (thermocouple function) occurred on the second day of the ETS phase during Test 6-3. Although the thermocouple was fixed the following day and the reactor set back to its original temperature of 200 °C, the sample had seen one hour of 300 °C temperature before the problem was discovered. Figure 4.57 shows the pressure and the temperatures of the reactor wall, gas phase and liquid phase as recorded by the computer data acquisition system. Interestingly, the resultant oil viscosity ratio for this run was 0.479, the lowest in all experiments preformed, which indicates a significant viscosity decrease associated with a short time at the 300 °C temperature level.

The effluent gas analyses for this run showed minute amounts of methane, ethane and propane. The carbon dioxide was the maximum value observed for all of the experiments not involving core matrix. This was the first instance of the production of the three hydrocarbon gases (methane, ethane and propane) in a single experiment. The total amount of these products was 9.1 %, much higher than the other runs not involving core matrix. The increased gas production was a clear indication that thermal cracking had taken place to a greater extent than was observed for the 200 °C or 220 °C ETS tests.

The asphaltenes content of 18.5 % for this case is more than that of the original oil (17.8 %). Thermal cracking appeared to have occurred in the maltenes component, as mentioned in Section 4.3.4. Figure 4.58 shows the carbon number distribution comparison of this after-run sample with the original oil. As shown in Table 4.15, the

fraction of the reacted oil which has a carbon number less than 40 is increased compared to that of the original oil. This is the same behaviour as was observed for the Run 6-5. Both tests suggest that modification of the maltenes fraction is responsible for the viscosity reduction.

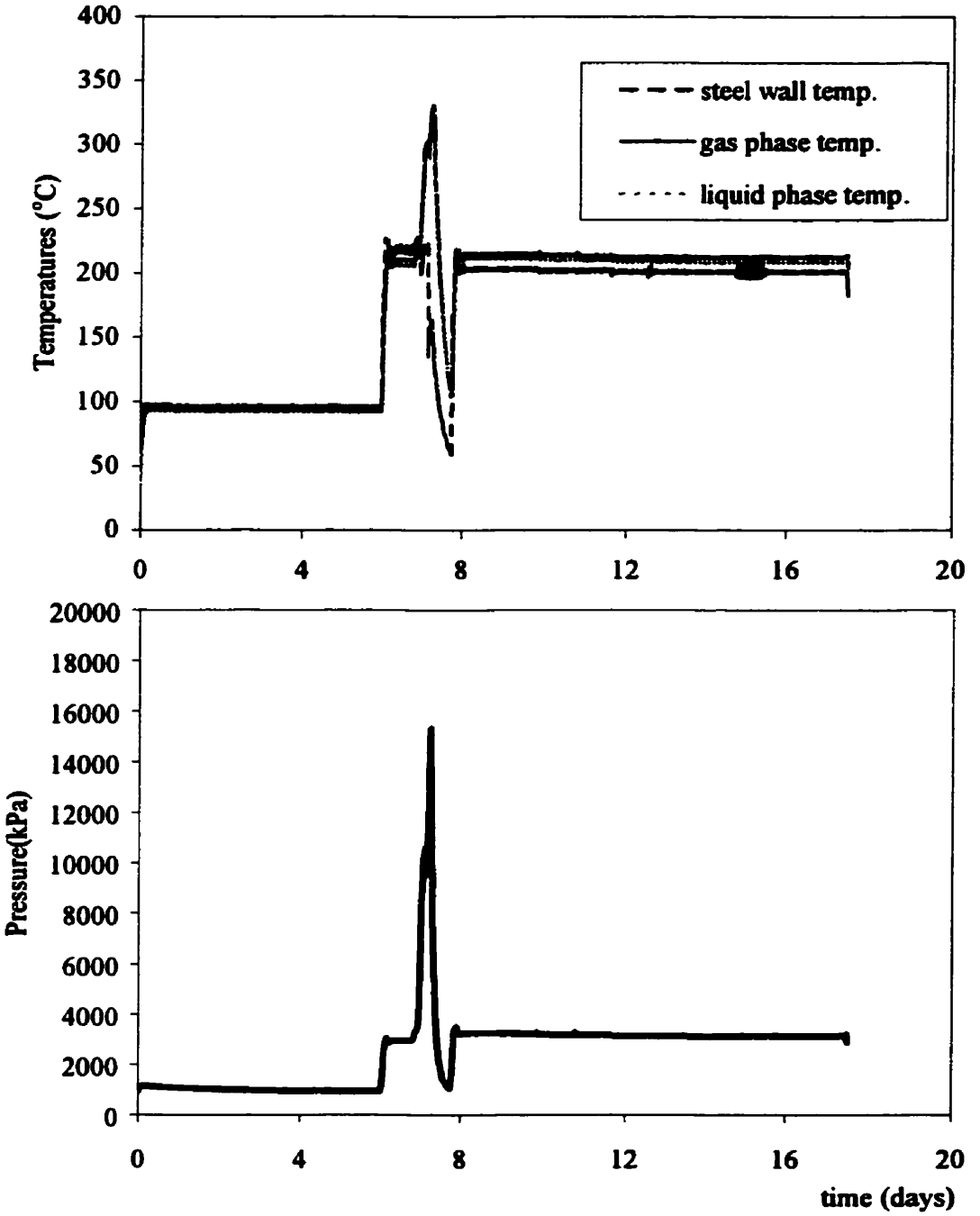

Figure 4.57: Run 6-3 Temperature and Pressure Profile

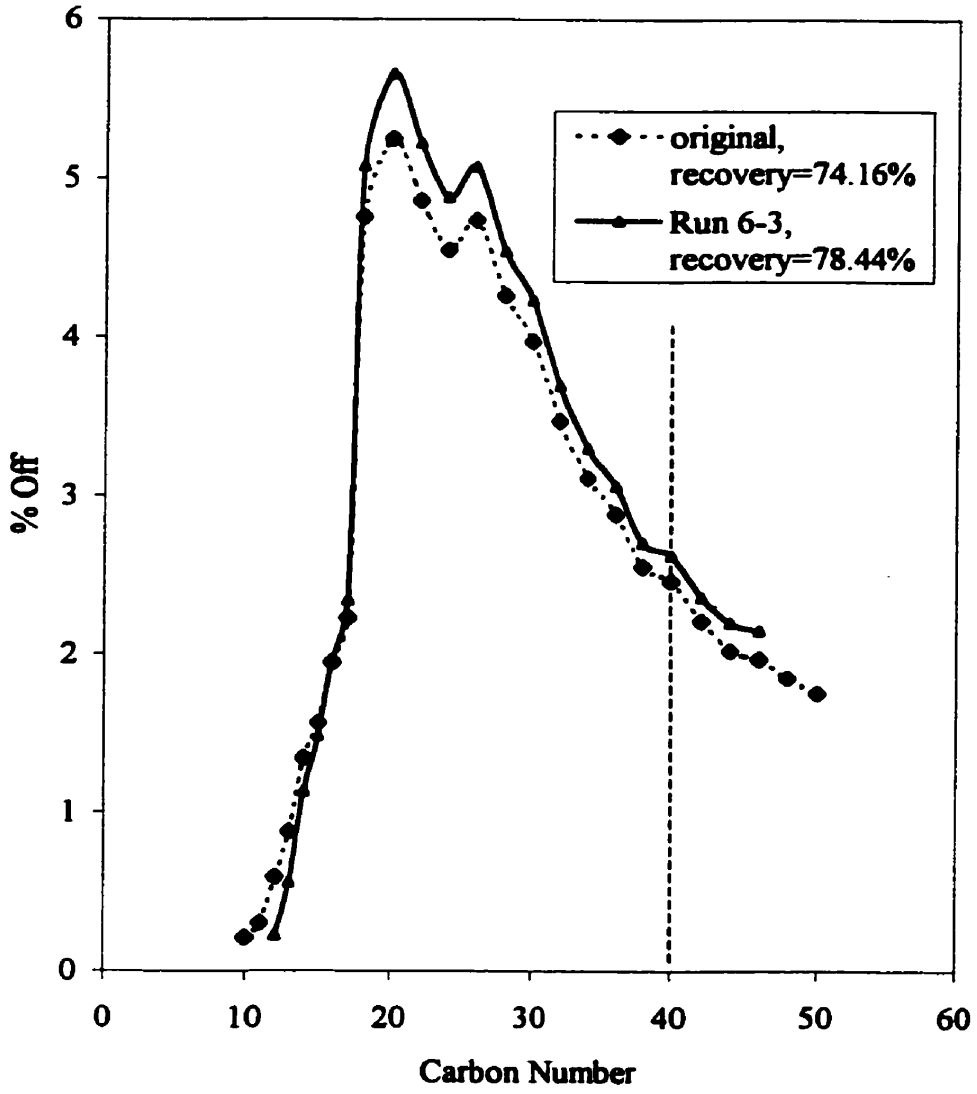

Figure 4.58: Carbon Distribution Comparison of Run 6-3 with the Original

CHAPTER FIVE DATA REPEATABILITY AND RELIABILITY

Data repeatability and confidence is of great concern for any experimental project. In this project, specific actions were taken to minimise potential experimental error.

Firstly, a single barrel of Athabasca crude oil was used throughout the experimental work. The physical properties of the oil were determined and recorded prior to experimental use. It was found that the initial physical properties for the oil were close to previous published values.

Secondly, all measurement devices, including those used during both the experimental and analytical phases, were calibrated regularly. This included the pressure transducers and thermocouples on the rocking cell apparatus, the gas chromatograph, the viscometer, the pH meter and the densitometer.

Finally, standard experimental operating procedures were developed (as described in Chapter 2). Also, the analytical procedures used were developed and proven over the past twenty years by the In-Situ Combustion Research Group at the University of Calgary.

The above actions were found to be adequate to minimise inevitable experimental error. As was described in Section 4.3.3, the asphaltenes behaviour in the reacted oil samples was consistent with that previously published by Millour at al. (1987) and Wichert et al. (1996). Experimental repeatability was also demonstrated in Runs 1-3 and 1-5, in which run conditions were the same for both runs. The viscosity data for both runs were similar, 3050 mPa.s for Run 1-3 and 3300 mPa.s for Run1-5 when measured at 70

°C. The kinetic calculations summarized in Table 4.6 show that these two runs were in good agreement. Consistency of trends for runs conducted at different initial oxygen pressures also gave confidence in the overall accuracy of the methods used to determine the physical properties of the oil samples throughout the whole of the experimental program.

CHAPTER SIX CONCLUSIONS

A systematic experimental investigation for the purpose of developing a unique in-situ process utilizing low-temperature oxidation for upgrading heavy oil has been conducted. Analysis of the results allows the following conclusions to be made:

1. The two step oxidation process achieved viscosity reductions for the reacted bitumen as compared to that of the original oil; however, the asphaltenes content of the modified oil was generally greater than that of the original oil.

2. The majority of the tests showed first order dependence with respect to oxygen partial pressure at the LTS temperature of 80 °C.

3. Total oxygen uptake, which was primarily a function of the initial moles of air charged to the system, had a significant effect on the properties of the reacted bitumen.

4. Oxygen uptake alone did not control the properties of the reacted oil. The duration and temperature of the LTS and ETS periods, as well as the pressure and composition of the aqueous phase and the presence of solid core matrix were important parameters.

5. Viscosity reduction for the oil associated with the bitumen/distilled water system was favoured by low oxygen partial pressure and ETS temperatures in excess of 220 °C.

6. Viscosity reduction of the oil associated with the non-agitated bitumen / distilled water mixtures was promoted by shorter duration LTS oxidation periods (six days)

and longer ETS periods (nine days), and by lower LTS temperatures (80°C) and higher ETS temperatures (220°C or above).

7. The viscosity reduction in experiments conducted with 50 % brine (by mass) was significantly lower than the corresponding viscosity reduction in experiments having a similar proportion of distilled water. This may be a result of excessive oxidation promoted by the high concentration of brine in the system during the LTS period.

8. Systems containing 71 % core, 8 % brine, and 20 % bitumen (all by mass) exhibited a greater viscosity reduction (as compared to brine only tests) at longer LTS periods (18 days) and longer ETS periods (nine days). Sand from the Athabasca Oil Sands appears to have a positive effect on free radical initiation and cracking reactions. It was not possible to determine if these effects were associated with catalytic effects due to the presence of clays or to surface effects. Coke formation was enhanced by the presence of core matrix and this contributed to the viscosity reduction.

CHAPTER SEVEN RECOMMENDATIONS

The trends in the physical and compositional data point out several areas, which require more detailed experimental attention and computer modeling. These areas include:

1) Additional experimental work should be performed at the reaction conditions where the greatest number of instances of viscosity reduction occurred; namely, at shorter duration LTS oxidation periods (six days) and longer ETS periods (nine days), at lower LTS temperatures (80°C) and higher ETS temperatures (220°C), and for oxygen partial pressure of approximately 180 kPa (total initial pressure of 860 kPa when using air).

2) Additional experimental work should be carried out at higher agitation rates to determine the reaction kinetics where the mass transfer effects become negligible. The agitation rates required may be beyond the capabilities of the current apparatus, and a new set-up for supplying high-speed agitation to the system may be needed. Mathematical simulation work of the process would be conducted by using kinetic parameters free of any mass transfer effects.

3) Experimental work should be conducted at higher ETS temperatures (> 220 °C). Higher temperatures may be beyond the capabilities of the current apparatus, necessitating a modified heater assemby.

4) Experimental work involving metallic salts is advisable as the synthetic brine was shown to have an impact on the two stage oxidation process.

5) Additional experimental work is necessary to study the effect of the presence of rock matrix or sand on the reactions; core flooding experiments to examine the reactions taking place under more realistic flow conditions should be undertaken once operating conditions which could be applied in a field situation, are identified.

6) The database from this study with that generated by Wichert (1996) should be combined to develop kinetic models of the oxygen induced cracking process.

7) Thermal cracking in a nitrogen environment should be performed at selected conditions to provide a direct comparison with the oxygen induced cracking behavior. Tests should involve LTS at 80 °C for 0 days and 6 days followed by ETS for 6, 12 and 18 days at temperatures of 200, 220 and 250 °C. The thermal cracking tests should involve oil only, oil plus brine, oil plus brine plus core matrix. Agitation rates would be selected to match those used with the corresponding liquid and solid changes of the current study. Run pressure for the thermal cracking tests would be maintained at 970 kPa (absolute).

8) The effect of total pressure at a given oxygen partial pressure was not investigated in the current study. Different concentrations of oxygen in the gas should be used to confirm the assumption that total pressure is not important.

9) More detailed compositional analysis of the maltenes and asphaltenes fractions (SARA, molecular weight, elemental composition, TGA/DTA/PDSC analysis on asphaltenes) is required to better define the nature of the oxidation reactions.

REFERENCES

Adegbesan, K.O., Donnelly, J.K., Moore, R.G., Bennion, D.W. "Low-Temperature-Oxidation Kinetic Parameters for In-Situ Combustion: Numerical Simulation", SPE Reservoir Engineering, November 1987, pp.573-582.

Babu, D.R., and Cormack, D.E. "Low Temperature Oxidation of Athabasca Bitumen" The Canadian Journal of Chemical Engineering, Vol.61, August 1983, pp.575-580.

Babu, D.R., and Cormack, D.E. "Effect of Low Temperature Oxidation on the composition of Athabasca Bitumen" Fuel, Vol.63, Jane 1984, pp.858-861.

Baviere, M., "Basic Concepts of Enhanced Oil Recovery Processes" Critical Reports on Applied Chemistry", Vol.55, Publ. Elsevier Applied Science, London & N.Y. 1997.

Belgrave, J.D.M, Moore, R.G. and Ursenbach, M.G., "Gas Evolution from the Aquathermolysis of Heavy Oils"; The Canadian Journal of Chemical Engineering, Vol. 72, pp. 511-516, June, 1994.

Castanier, L.M., and W.E. Brigham, "Modifying In-Situ Combustion With Metallic Additives", In Situ, 21(1), 27-45 (1997).

Cram, P.J., and Redford, D.A., "Low Temperature Oxidation Process for the Recovery of Bitumen", The Journal of Canadian Petroleum Technology, July – September, 1977, pp. 72-83.

Dabbous, M.K., and Fulton, P.F., "Low-Temperature-Oxidation Reaction Kinetics and Effects on the In-Situ Combustion Process", Society of Petroleum Engineers Journal, June, 1974, pp.253-262.

Farouq Ali, S.M., and Meldau, R.F., " Practical Heavy Oil Recovery", Textbook, 1999.

Hayashitani, M., Bennion, D.W., Donnelly, J.K. and Moore, R.G., " Thermal Cracking of Athabasca Bitumen", Oil Sand, 1977, pp.233-247.

Hepler, L.G. and Hsi, C., "AOSTRA Technical Handbook on Oil Sands", Bitumens and Heavy Oils, Alberta Oil Sands Technology And Research Authority, 1989.

Hyne, J.B., Greidanus, J.W., Tyrer, J.D., Verona, D., Rizek, C., Clark, P.D., Larke, R.A. and Koo, J.F.K, "Aquathermolysis of Heavy Oils; Proceedings of the Second International Conference", The Future of Heavy Crude and Tar Sands, McGraw-Hill, New York, pp. 404-411, 1984.

Lakatos, I., Bauer, K., Lakatos-Szabo, J., and Szittar, "The effect of In-Situ Low Temperature Oxidation on Chemical and Physical Properties of Heavy Crude Oils", paper presented at the 7th European IOR symposium, Moscow, Russia, October 27-29,1993.

Lake L.W., "Enhanced Oil Recovery", 1989 by Prentice-Hall, Inc.

Lee, D.G., and Noureldin, N.A., " The Effect of Low Temperature Oxidation on the Chemical and Physical Properties of Maltenes and Asphaltenes Derived from Heavy Oil", presented at the Symposium on Hydrocarbon Oxidation, The Division of Petroleum Chemistry, Inc. American Chemical Society, New Orleans, August 30 – September 4, 1987.

Lee, D.G., and Noureldin, N.A., "Effect of Water on the Low Temperature Oxidation of Heavy Oil", Energy and Fuels, Vol. 3, 1989, pp.713-715.

Meyers, K.O., Fassihi, M.R., and Basile, P.F., "Low Temperature Oxidation of Viscous Crude Oils", paper SPE 15648 presented at the 61st Annual Technical Conference and Exhibition of the Society of Petroleum Engineers, New Orleans, October 5-8, 1986.

Millour, J.P., Moore, R.G., Bennion, D.W., Ursenbach, M.G. and Gie, D.N., "An expanded compositional model for low-temperature oxidation of Athabasca Bitumen", The Journal of Canadian Petroleum Technology, Vol.26. May-June, 1987, pp. 24-32.

Millour, J.P., Moore, R.G., Bennion, D.W., Ursenbach, M.G. and Gie, D.N., "A Simple Implicit Model for Thermal Cracking of Crude Oils"; SPE Paper 14226, Presented at the 60th Technical Conference and Exhibition of the Society of Petroleum Engineers, Las Vegas, NV, September 22-25, 1985.

Moschopedis, S.E., and Speight, J.G., " The Effect of Air Blowing on the Properties and Constitution of a Natural Bitumen", Journal of Materials Science, Volume 12, Chapman and Hall Ltd., Great Britain, 1977, pp.990-998.

Noureldin, N.A., Lee, D.G., Mourits, F.M., and Jha, K.N., "Chemical Changes Accompanying the Low Temperature Oxidation of Heavy Oil", AOSTRA Journal of Research, Vol. 3, 1987, pp.155-161.

Polikar, M. (1980), Bulkowski, P. and Prill, G. (1978), Wallace, D. (1978-1983), Fu, C.T., Puttagunta, V.R. and Vilscak, G. (1985), "Internal report of Alberta Reaearch Council".

Speight, J.G., "The Chemistry and Technology of Petroleum", Third Edition, 1999.

Wichert, G.C., "In-Situ Upgrading of Heavy Oils by Low-Temperature Oxidation in the Presence of Caustic Additives", M.Sc.Thesis, The University of Calgary, 1996.

Wichert, G.C., Okazawa, N.E., Moore, R.G., and Belgrave, J.D.M., "In-Situ Upgrading of Heavy Oils by Low-Temperature Oxidation in the Presence of Caustic Additives", paper SPE 30299, presented at International Heavy Oil Symposium, Calgary, June 19-21, 1995.

APPENDIX 1: RAW DATA

Cell #	initial oil input (g)	final oil out (g)	initial water in (g)	final water out (g)	(initl@room T Pressure (psig)	Cell Run Temperature (°C)	Cell Run Time (days)	Comment
1~1	50.00	50.05	50.02	48.59	36.41	80	6	LTS only
1~2	50.02	50.08	50.00	32.4+	68.05	80	6	LTS only
1~3	50.01	49.94	50.02	46.98	122.86	80	6	LTS only
1~4	50.05	49.92	50.02	49.19	251.65	80	6	LTS only
1~5	50.00	49.85	50.02	49.72	127.44	80	6	LTS only
1~6	50.01	50.67	50.01	48.45	125.31	100	6	LTS only
1~7	50.04	49.84	50.04	48.82	125.73	120	6	LTS only
1~8	50.03	48.71	50.00	49.34	124.91	80	5	LTS only
1~9	50.01	49.84	50.03	47.74	126.40	80	12	LTS only
1~10	50.01	49.84	50.02	48.41	129.33	80	18	LTS only

Cell #	density (@25°C)	viscosity (@25°C)	viscosity (@40°C)	viscosity (@70°C)	pH	Asphaltenes	GC Results N_2	O_2	CO_2	CO	CH_4
	g/cm^3	(mPa·s)	(mPa·s)	(mPa·s)		(% mass)	(% mol)	(% mol)	(% mol)	(% mol)	(% mol)
1~1	1.0058	208200	32200	2085	6.25	20.33	-	-	-	-	-
1~2	1.0058	252000	37800	2275	-	20.39	-	-	-	-	-
1~3	1.0064	487000	63500	3050	4.13	20.54	94.28	5.09	0.63	0.00	0.00
1~4	1.0091	1338000	137100	5708	3.73	21.59	92.09	7.47	0.44	0.00	0.00
1~5	1.0091	560800	70910	3300	4.12	20.88	94.40	5.15	0.45	0.00	0.00
1~6	1.0084	528000	69830	3380	3.31	20.93	98.21	0.97	0.82	0.00	0.00
1~7	1.0088	549100	70830	3470	3.04	21.06	98.61	0.43	0.96	0.00	0.00
1~8	1.0091	608000	75120	3572	4.14	21.66	93.26	6.35	0.39	0.00	0.00
1~9	1.0091	621000	78900	3700	2.84	21.44	98.07	1.25	0.68	0.00	0.00
1~10	1.0091	575000	73400	3455	3.45	21.80	98.57	0.69	0.74	0.00	0.00
orig.	1.0051	218700	32250	1950	6.55	17.85	79.28	20.72	0.00	0.00	0.00

Table A1.1: Raw Data From Run #1

Cell #	initial oil input (g)	final oil out (g)	initial water in (g)	final water out (g)	(initl@room T) Pressure (psig)	Cell Run Temperatur (°C)	Cell Run Time (days)	coke (g)	coke (% oil)	Comment
2~1	51.32	51.49	50.10	49.63	125.5	80,200	6,4	0.0236	0.0460	
2~2	50.50	50.72	50.88	49.71	127.3	80,200	6,6	0.0566	0.1121	
2~3	50.66	49.47	50.25	~	128.6	80,200	6,12	0.1231	0.2430	8th day leak
2~4	50.22	50.18	50.82	49.60	128.1	80,200	6,18	0.1458	0.2903	
2~5	50.34	50.51	50.03	49.26	127.7	80,200	6,9	0.0977	0.1941	
2~6	50.07	50.21	50.22	48.78	130.8	80,200	0,6	0.0748	0.1494	
2~7	50.50	50.89	50.08	49.13	125.3	80,200	12,6	0.0133	0.0263	
2~8	50.90	50.62	51.79	50.37	128.6	80,200	18,6	0.0062	0.0122	
2~9	50.74	50.99	50.66	49.66	125.8	80,150	6,6	0.0079	0.0156	
2~10	51.09	51.26	50.42	49.53	129.5	80,175	6,6	0.0000	0.0000	

Cell #	density (@25°C) g/cm^3	viscosity (@25°C) (mPa·s)	viscosity (@40°C) (mPa·s)	viscosity (@70°C) (mPa·s)	pH	Asphaltenes (% mass)	GC results N_2 (% mol)	O_2 (% mol)	CO_2 (% mol)	CO (% mol)	CH_4 (% mol)
2~1	1.0071	315000	45410	2615	2.5	21.93	96.32	1.62	2.06	0.00	0.00
2~2	1.0071	228000	33150	2025	2.6	21.23	95.96	1.52	2.51	0.00	0.00
2~3	1.0064	191500	29850	1895	3.2	20.86	-	-	-	-	-
2~4	1.0078	189000	27900	1760	3.4	21.32	95.75	1.75	2.50	0.00	0.00
2~5	1.0058	189200	28650	1860	3.0	20.90	95.35	1.62	3.04	0.00	0.00
2~6	1.0064	210700	31500	2055	2.4	21.34	94.75	1.36	3.89	0.00	0.00
2~7	1.0061	220500	33650	2060	2.6	21.18	96.53	1.71	1.76	0.00	0.00
2~8	1.0084	190500	29500	2058	2.8	21.96	97.79	0.60	1.61	0.00	0.00
2~9	1.0064	253300	36000	2225	2.5	21.40	92.83	3.92	3.26	0.00	0.00
2~10	1.0074	324500	43330	2640	2.5	22.33	97.41	0.90	1.69	0.00	0.00
original	1.0051	218700	32250	1950	6.55	17.85	79.28	20.72	0.00	0.00	0.00

Table A1.2: Raw Data From Run #2

Cell #	initial oil input (g)	final oil out (g)	initial water in (g)	final water out (g)	(init@room T) Pressure (psig)	Cell Run Temperature (°C)	Cell Run Time (days)	coke (g)	coke (%oil)	Comment
3-1	50.29	50.64	50.64	49.62	126.40	80,200	6,6	0.184	0.3659	air,rock
3-2	50.38	50.71	50.09	48.35	126.90	80,200	6,9	0.172	0.3414	air,rock
3-3	50.46	50.58	50.14	50.22	115.80	80,200	18,6	0.0071	0.0141	air,rock
3-6	50.69	51.00	50.08	49.05	125.10	80,200	6,6	0.0123	0.0243	N_2
3-7	50.87	51.26	50.05	49.26	123.90	80,200	6,9	0.0109	0.0214	N_2
3-8	50.55	50.44	50.76	50.56	124.50	80,200	18,6	0.0064	0.0127	N_2

Cell #	density (@25°C) g/cm^3	viscosity (@25°C) (mPa·s)	viscosity (@40°C) (mPa·s)	viscosity (@70°C) (mPa·s)	pH	GC Results: Asphaltenes (% mass)	N_2 (% mol)	O_2 (% mol)	CO_2 (% mol)	CO (% mol)	CH_4 (% mol)
3-1	1.003084	106300	18670	1380	2.63	17.946	93.560	1.747	4.692	0.652	0.000
3-2	1.003751	100300	16700	1305	2.72	17.708	93.437	1.436	5.127	0.610	0.000
3-3	1.005421	175500	30000	1840	3.06	19.095	97.543	1.134	1.322	0.000	0.000
3-6	1.004085	104200	18050	1250	3.73	16.619	98.840	0.612	0.549	0.000	0.000
3-7	1.003417	96620	16300	1150	6.95	16.769	99.394	0.276	0.331	0.000	0.000
3-8	1.005087	174500	26600	1705	3.53	17.123	99.525	0.259	0.216	0.000	0.000
orig.		218700	32250	1950	6.55	17.850	79.278	20.722	0.000	0.000	0.000

Table A1.3: Raw Data From Run #3

Cell #	initial oil input (g)	final oil out (g)	initial water in (g)	final water out (g)	(init@room T) Pressure (psig)	Cell Run Temperature (°C)	Cell Run Time (days)	coke (g)	coke (%oil)	Comment	
4~1	50.46	49.68	50.52	50.58	1009.1	80,200	6,6	0.409	0.811	air,rock	
4~2	50.3	50.76	50.38	50.07	510	80,200	6,6	0.218	0.432	air,rock	
4~3	50.2	50.77	50.25	48.6	268.6	80,200	6,6	0.180	0.359	air,rock	gas blow out
4~6	50.37	50.69	50.14	49.36	127.4	80,200	18,6	0.000	0.000	N_2	
4~7	50.45	50.74	50.23	49.49	125.9	80,220	6,6	0.152	0.300	air,no-rock	
4~8 N2	50.37	50.74	50.38	50.25	249.3	80,220	6,6	0.193	0.383	air,no-rock	

Cell #	density (@25°C) g/cm^3	viscosity (@25°C) (mPa·s)	viscosity (@40°C) (mPa·s)	viscosity (@70°C) (mPa·s)	pH	Asphaltenes % mass	GC results N_2 % mol	O_2 % mol	CO_2 % mol	CO % mol	CH_4 % mol
4~1	1.0091	745000	92500	4220	1.81	24.68	92.874	0.4362	6.6898	0.5919	0.0000
4~2	1.0064	217500	34000	2075	2.04	21.78	94.617	0.4165	4.9666	0.5352	0.0000
4~3	1.0058	180500	29850	1935	2.82	20.65	0.000	0.0000	0.0000	0.0000	0.0000
4~6	1.0031	105100	18900	1355	7.52	16.41	99.876	0.1240	0.0000	0.0000	0.0000
4~7	1.0044	137800	23300	1575	3.07	18.69	96.570	0.6428	2.7874	0.2518	0.0000
4~8	1.0038	93500	16820	1235	2.79	17.99	93.706	0.5121	5.7823	0.7190	0.0000
orig.	1.0051	218700	32250	1950	6.55	17.85	79.278	20.722	0.0000	0.0000	0.0000
N_2							99.737	0.2627	0.0000	0.0000	0.0000

Table A1.4: Raw Data From Run #4

Cell #	initial oil input (g)	final oil out (g)	initial water in (g)	final water out (g)	(init@room T) Pressure (psig)	Cell Run Temperature (°C)	Cell Run Time (days)	coke sand base (%)	coke oil base (%)	Comment
5-1	38.76	39.09	16.34	~	129.6	80,200	6,6	1.165	4.054	oil+core+brine
5-2	38.76	39.07	16.34	~	127.5	80,200	6,9	1.163	4.049	oil+core+brine
5-3	38.83	39.42	16.37	~	127.8	80,200	6,12	1.153	4.011	oil+core+brine
5-4	38.79	39.6	16.35	~	129.5	80,220	6,6	1.262	4.392	oil+core+brine
5-5	38.8	40.47	16.36	~	132	80,200	6,0	1.250	4.352	oil+core+brine
5-6	38.76	39.62	16.34	~	127.9	80,200	1,6	1.096	3.813	oil+core+brine
5-7	38.77	38.79	16.34	~	124.8	80,200	12,6	1.172	4.079	oil+core+brine
5-8	38.82	38.88	16.37	~	121.3	80,200	18,6	1.087	3.784	oil+core+brine
5-9	38.76	38.66	16.34	~	222.5	80,220	6,6	1.161	4.039	oil+core+brine
5-10	38.83	38.13	16.37	~	125.5	80,200	6,6	1.052	3.660	oil+core+brine

Cell #	density (@25°C) g/cm^3	viscosity (@25°C) (mPa·s)	viscosity (@40°C) (mPa·s)	viscosity (@70°C) (mPa·s)	pH	Asphaltenes (%)	GC Results N_2 % mol	O_2 % mol	CO_2 % mol	CO % mol	CH_4 % mol
5-1	1.0078	208000	33200	2015	~	19.931	89.6976	0.3679	9.7235	0.2110	0.0000
5-2	1.0054	135000.00	24900	1620	~	20.331	89.7595	0.5032	9.7373	0.0000	0.0000
5-3	1.0071	109200.00	19700	1415	~	20.185	89.7806	0.8509	9.3684	0.0000	0.0000
5-4	1.0051	78370.00	15600	1190	~	19.858	89.4053	0.3168	9.9051	0.0000	0.3728
5-5	1.0091	130700.00	26550	1635	~	19.699	91.6331	5.8820	2.4849	0.0000	0.0000
5-6	1.0058	184200.00	30200	1840	~	20.786	89.7803	0.7803	9.2716	0.1677	0.0000
5-7	1.0078	172700.00	30900	1900	~	20.043	89.2731	0.5861	10.1408	0.0000	0.0000
5-8	1.0074	141700.00	25250	1595	~	19.085	87.1806	2.9685	9.8510	0.0000	0.0000
5-9	1.0058	69750.00	13750	1095	~	20.998	90.8892	0.4262	8.2801	0.1518	0.2528
5-10	1.0051	140000.00	23750	1535	~	18.017	93.7101	0.1925	6.0974	0.0000	0.0000
orig.	1.0051	218700.00	32250	1950		17.85	79.2782	20.7218	0.0000	0.0000	0.0000
N_2							99.7373	0.2627	0.0000	0.0000	0.0000

Table A1.5: Raw Data From Run #5

Cell #	initial oil input (g)	final oil out (g)	initial water in (g)	final water out (g)	(init@room T) Pressure (psig)	Cell Run Temperature (°C)	Cell Run Time (days)	Free H_2O phase pH	Asphaltenes %mass	Comment
6-1	50.48	50.60	50.13	48.80	129.0	80,200	6,6	8.49	20.42	brine 1.65%
6-2	50.37	50.52	50.08	48.78	125.9	80,200	6,9	8.88	20.04	brine 1.65%
6-3	50.10	50.52	50.14	48.16	131.0	80,200	6,12	8.70	18.54	brine 1.65%
6-4	50.13	50.38	50.33	48.53	137.0	80,200	1,6	9.28	21.45	brine 1.65%
6-5	50.18	50.38	50.42	50.84	142.0	80,200	6,0	~	18.69	brine 1.65%
6-6	50.68	50.83	50.19	48.60	129.4	80,200	12,6	8.96	20.44	brine 1.65%
6-7	50.49	50.53	50.15	47.80	128.3	80,200	18,6	8.55	16.46	brine 1.65%
6-8	50.38	50.61	50.29	50.53	70.3	80,220	6,6	3.43	17.66	distil.H_2O
6-9	50.39	50.45	50.12	49.73	227.5	80,220	6,6	2.73	24.82	distil.H_2O
6-10	50.43	49.57	50.27	48.89	500.0	80,220	6,6	2.27	23.13	distil.H_2O

Cell #	density (@25°C) g/cm^3	viscosity (@25°C) (mPa·s)	viscosity (@40°C) (mPa·s)	viscosity (@70°C) (mPa·s)	Coke %	GC Results N_2 % mol	O_2 % mol	CO_2 % mol	CO % mol	CH_4 % mol	C2H6 % mol	C3H8 % mol
6-1	1.007	187700	31450	1970	-	95.631	0.3821	3.9870	0.0000	0.0000	0.0000	0.0000
6-2	1.007	223000	36800	2140	0.339	95.461	0.1192	4.1871	0.0000	0.2332	0.0000	0.0000
6-3	1.005	56200	11270	935	0.134	90.602	0.3032	5.1335	0.0000	1.9127	1.8229	0.2256
6-4	1.008	358500	49870	2540	0.057	96.357	2.6482	0.9952	0.0000	0.0000	0.0000	0.0000
6-5	1.006	143500	23500	1540	2.928	90.470	0.7195	8.8103	0.0000	0.0000	0.0000	0.0000
6-6	1.007	188800	31456	1980	0.143	95.508	0.2313	3.9454	0.0000	0.3154	0.0000	0.0000
6-7	1.008	189000	31450	1978	0.278	95.530	0.2579	3.9986	0.0000	0.2137	0.0000	0.0000
6-8	1.005	106500	20500	1425	0.136	93.686	0.6749	5.1320	0.5070	0.0000	0.0000	0.0000
6-9	1.007	280500	44300	5035	0.269	96.222	0.4005	3.1674	0.2103	0.0000	0.0000	0.0000
6-10	1.008	195000	32350	1975	2.347	94.854	0.4700	4.4296	0.2466	0.0000	0.0000	0.0000
orig.	1.005	218700	32250	1950		79.278	20.722	0.0000	0.0000	0.0000	0.0000	0.0000
N_2 orig						99.737	0.2627	0.0000	0.0000	0.0000	0.0000	0.0000

Table A1.6: Raw Data From Run #6

APPENDIX 2: MATERIAL BALANCE CALCULATIONS

Run1 data

Cell #	initial mass oil (g)	final mass oil (g)	oil mass diff. %	initial mass H_2O (g)	final mass H_2O (g)	GC Analysis Results N_2 mass%	O_2 mass%	CO_2 mass%	CO mass%	CH_4 mass%	C_2H_6 mass%	C_3H_8 mass%	coke contents (g)	coke contents mass%	Comments
1~1	50.00	50.05	0.10	50.02	48.59	-	-	-	-	-	-	-	0.0000	0.0000	gas pressure too low
1~2	50.02	50.08	0.12	50	32.4+	-	-	-	-	-	-	-	0.0000	0.0000	cannot analyze GC
1~3	50.01	49.94	-0.14	50.02	46.98	94.28	5.09	0.63	0.00	0.00	0.00	0.00	0.0000	0.0000	
1~4	50.05	49.92	-0.26	50.02	49.19	92.09	7.47	0.44	0.00	0.00	0.00	0.00	0.0000	0.0000	
1~5	50.00	49.85	-0.30	50.02	49.72	94.40	5.15	0.45	0.00	0.00	0.00	0.00	0.0000	0.0000	
1~6	50.01	50.67	1.32	50.01	48.45	98.21	0.97	0.82	0.00	0.00	0.00	0.00	0.0000	0.0000	
1~7	50.04	49.84	-0.40	50.04	48.82	98.61	0.43	0.96	0.00	0.00	0.00	0.00	0.0000	0.0000	
1~8	50.03	48.71	-2.64	50	49.34	93.26	6.35	0.39	0.00	0.00	0.00	0.00	0.0000	0.0000	
1~9	50.01	49.84	-0.34	50.03	47.74	98.07	1.25	0.68	0.00	0.00	0.00	0.00	0.0000	0.0000	
1~10	50.01	49.84	-0.34	50.02	48.41	98.57	0.69	0.74	0.00	0.00	0.00	0.00	0.0000	0.0000	
orig air						79.28	20.72	0.00	0.00	0.00	0.00	0.00			

Cell #	initial temp. °C	initial pressure kPa	initial z factor	initial total gas mol	initial N_2 mol	initial O_2 mol	initial total gas (g)	final temp °C	final pressure kPa	final z factor	final total gas mol	final N_2 mol	final O_2 mol	final CO_2 mol	O_2 uptake g/g oil	final total gas g	gas mass diff. % oil	total oil mass diff. %
1~1	22.2	211	-	-	-	-	-	39.4	189.0	-	-	-	-	-	-	-	-	0.1000
1~2	22.2	469	-	-	-	-	-	31.5	363.4	-	-	-	-	-	-	-	-	0.1200
1~3	22.2	846	0.9921	0.0461	0.0366	0.0096	1.3292	30.9	700.6	0.9968	0.0376	0.0355	0.0019	0.0002	0.0049	1.0656	-0.527037	0.3871
1~4	22.2	1738	0.9851	0.0907	0.0719	0.0188	2.6137	31	1493.0	0.9939	0.0756	0.0696	0.0056	0.0003	0.0084	2.1439	-0.938646	0.6789
1~5	22.2	880	0.9919	0.0478	0.0379	0.0099	1.3775	38.5	721.3	0.9973	0.0377	0.0356	0.0019	0.0002	0.0051	1.0652	-0.624577	0.3246
1~6	22.2	867	0.9920	0.0471	0.0374	0.0098	1.3588	20.8	654.4	0.9963	0.0367	0.0360	0.0004	0.0003	0.0060	1.0334	-0.650712	1.9704
1~7	22.2	861	0.9920	0.0468	0.0371	0.0097	1.3499	21.4	650.3	0.9964	0.0364	0.0359	0.0002	0.0003	0.0061	1.0255	-0.648224	0.2485
1~8	22.2	867	0.9920	0.0471	0.0374	0.0098	1.3588	32	725.5	0.9968	0.0387	0.0361	0.0025	0.0002	0.0047	1.0956	-0.526092	-2.1123
1~9	22.2	873	0.9919	0.0474	0.0376	0.0098	1.3677	22.1	551.0	0.9969	0.0314	0.0308	0.0004	0.0002	0.0060	0.8850	-0.965152	0.6252
1~10	22.2	894	0.9917	0.0485	0.0384	0.0100	1.3973	62.5	802.7	0.9998	0.0384	0.0378	0.0003	0.0003	0.0063	1.0805	-0.633452	0.2935

Table A2.1: Material Balance Spreadsheet for Run # 1

Run2 data

Cell #	initial mass oil (g)	final mass oil (g)	oil mass diff. %	initial mass H_2O (g)	final mass H_2O (g)	GC Analysis Results N_2 mass%	O_2 mass%	CO_2 mass%	CO mass%	CH_4 mass%	C_2H_6 mass%	C_3H_8 mass%	coke contents (g)	coke contents mass%	comment
2~1	51.32	51.49	0.3313	50.1	49.63	96.32	1.62	2.06	0.00	0.00	0.00	0.00	0.0236	0.0460	
2~2	50.5	50.72	0.4356	50.88	49.71	95.96	1.52	2.51	0.00	0.00	0.00	0.00	0.0566	0.1121	
2~3	50.66	49.47	-2.3490	50.25	-	-	-	-	-	-	-	-	0.1231	0.2430	8th day leak, cannot get GC Result
2~4	50.22	50.18	-0.0796	50.82	49.6	95.75	1.75	2.50	0.00	0.00	0.00	0.00	0.1458	0.2903	
2~5	50.34	50.51	0.3377	50.03	49.26	95.35	1.62	3.04	0.00	0.00	0.00	0.00	0.0977	0.1941	
2~6	50.07	50.21	0.2796	50.22	48.78	94.75	1.36	3.89	0.00	0.00	0.00	0.00	0.0748	0.1494	
2~7	50.5	50.89	0.7723	50.08	49.13	96.53	1.71	1.76	0.00	0.00	0.00	0.00	0.0133	0.0263	
2~8	50.9	50.62	-0.5501	51.79	50.37	97.79	0.60	1.61	0.00	0.00	0.00	0.00	0.0062	0.0122	
2~9	50.74	50.99	0.4927	50.66	49.66	92.83	3.92	3.26	0.00	0.00	0.00	0.00	0.0079	0.0156	
2~10	51.09	51.26	0.3327	50.42	49.53	97.41	0.90	1.69	0.00	0.00	0.00	0.00	0.0000	0.0000	
orig air						79.28	20.72	0.00	0.00	0.00	0.00	0.00			

Cell #	initial temp. °C	initial pressure kPa	initial z factor	initial total gas mol	initial N_2 mol	initial O_2 mol	initial total gas (g)	final temp. °C	final pressure kPa	final z factor	final total gas mol	final N_2 mol	final O_2 mol	final CO_2 mol	O_2 uptake g/g oil	final total gas g	gas mass diff % oil	total oil mass diff. %
2~1	22.2	865	0.9920	0.0471	0.0373	0.0098	1.3568	34.0	684.1	0.9969	0.0365	0.0351	0.0006	0.0008	0.0059	1.0360	-0.6251	1.0024
2~2	22.2	878	0.9919	0.0477	0.0378	0.0099	1.3745	29.2	684.1	0.9964	0.0371	0.0356	0.0006	0.0009	0.0060	1.0554	-0.6319	1.1796
2~3	22.2	887	0.9918	0.0481	0.0382	0.0100	1.3874								0.0064			-2.1060
2~4	22.2	883	0.9918	0.0480	0.0380	0.0099	1.3824	29.3	691.0	0.9964	0.0374	0.0358	0.0007	0.0009	0.0059	1.0648	-0.6325	0.8432
2~5	22.2	881	0.9918	0.0478	0.0379	0.0099	1.3785	36.6	717.2	0.9967	0.0377	0.0360	0.0006	0.0011	0.0060	1.0772	-0.5984	1.1302
2~6	22.2	902	0.9917	0.0489	0.0388	0.0101	1.4091	33.0	706.2	1.0021	0.0375	0.0355	0.0005	0.0015	0.0062	1.0740	-0.6693	1.0983
2~7	22.2	864	0.9920	0.0470	0.0373	0.0097	1.3548	40.7	663.4	0.9975	0.0347	0.0335	0.0006	0.0006	0.0059	0.9846	-0.7330	1.5316
2~8	22.2	887	0.9918	0.0481	0.0382	0.0100	1.3874	37.7	687.5	0.9631	0.0375	0.0367	0.0002	0.0006	0.0062	1.0601	-0.6430	0.1051
2~9	22.2	868	0.9920	0.0472	0.0374	0.0098	1.3597	37.2	730.3	0.9966	0.0383	0.0355	0.0015	0.0012	0.0053	1.0977	-0.5165	1.0248
2~10	22.2	893	0.9917	0.0484	0.0384	0.0100	1.3963	39.0	693.7	0.9973	0.0363	0.0354	0.0003	0.0006	0.0062	1.0284	-0.7199	1.0527

Table A2.2: Material Balance Spreadsheet for Run # 2

Run3 data

Cell #	initial mass oil (g)	final mass oil (g)	oil mass diff. %	initial mass H_2O (g)	final mass H_2O (g)	GC Analysis Results N_2 mass%	O_2 mass%	CO_2 mass%	CO mass%	CH_4 mass%	C_2H_4 mass%	C_3H_8 mass%	coke contents (g)	coke contents mass%	initial temp. °C	initial pressure kPa
3~1	50.29	50.64	0.6960	50.64	49.62	93.56	1.75	4.69	0.65	0.00	0.00	0.00	0.1840	0.3659		
3~2	50.38	50.71	0.6550	50.09	48.35	93.44	1.44	5.13	0.61	0.00	0.00	0.00	0.1720	0.3414	22.2	871.7
3~3	50.46	50.58	0.2378	50.14	50.22	97.54	1.13	1.32	0.00	0.00	0.00	0.00	0.0071	0.0141	22.2	875.1
3~6	50.69	51	0.6116	50.08	49.05	98.84	0.61	0.55	0.00	0.00	0.00	0.00	0.0123	0.0243	22.2	798.6
3~7	50.87	51.26	0.7667	50.05	49.26	99.39	0.28	0.33	0.00	0.00	0.00	0.00	0.0109	0.0214	22.2	862.7
3~8	50.55	50.44	-0.2176	50.76	50.56	99.52	0.26	0.22	0.00	0.00	0.00	0.00	0.0064	0.0127	22.2	854.4
N2						99.74	0.26	0.00	0.00	0.00	0.00	0.00			22.2	858.6
orig.air						79.28	20.72	0.00	0.00	0.00	0.00	0.00				

Cell #	initial z factor	initial total gas mol	initial N_2 mol	initial O_2 mol	initial total gas (g)	final temp. °C	final pressure kPa	final z factor	final total gas mol	final N_2 mol	final O_2 mol	final CO_2 mol	final CO mol	O_2 uptake g/g oil	final total gas g	gas mass diff. % oil	total oil mass diff. %
3~1	0.9947	0.0472	0.0374	0.0098	1.3624	31.3	717.2	0.9959	0.0384	0.0359	0.0007	0.0018	0.0003	0.0058	1.1143	-0.4933	1.5551
3~2	0.9947	0.0474	0.0376	0.0098	1.3673	39.7	748.2	0.9964	0.0388	0.0363	0.0006	0.0020	0.0002	0.0059	1.1273	-0.4763	1.4727
3~3	0.9951	0.0436	0.0346	0.0091	1.2584	37.1	653.1	0.9974	0.0347	0.0338	0.0004	0.0005	0.0000	0.0055	0.9792	-0.5532	0.8051
3~6	0.9958	0.0467	0.0371	0.0001	1.0416	31.1	727.5	0.9969	0.0389	0.0384	0.0002	0.0002	0.0000	-0.0001	1.0935	0.1024	0.5335
3~7	0.9958	0.0463	0.0367	0.0001	1.0326	32.9	863.4	0.9967	0.0451	0.0448	0.0001	0.0001	0.0000	0.0000	1.2658	0.4586	0.3295
3~8	0.9958	0.0465	0.0369	0.0001	1.0371	28.9	835.1	0.9965	0.0444	0.0441	0.0001	0.0001	0.0000	0.0000	1.2440	0.4093	-0.6143

Table A2.3: Material Balance Spreadsheet for Run # 3

Run4 data

Cell #	initial mass oil (g)	final mass oil (g)	oil mass diff. %	initial mass H_2O (g)	final mass H_2O (g)	GC Analysis Results N_2 mass%	O_2 mass%	CO_2 mass%	CO mass%	CH_4 mass%	C_2H_6 mass%	C_3H_8 mass%	coke contents (g)	coke contents mass%	initial temp. °C	initial pressure kPa	comment
4-1	50.46	49.68	-1.5458	50.52	50.58	92.87	0.44	6.69	0.59	0.00	0.00	0.00	0.4092	0.8109	22.2	6958.8	
4-2	50.3	50.76	0.9145	50.38	50.07	94.62	0.42	4.97	0.54	0.00	0.00	0.00	0.2175	0.4324	22.2	3517.0	
4-3	50.2	50.77	1.1355	50.25	48.6	-	-	-	-	-	-	-	~	~	22.2	1852.3	gas blow out
4-6	50.37	50.69	0.6353	50.14	49.36	99.88	0.12	0.00	0.00	0.00	0.00	0.00	0.0000	0.0000	22.2	878.6	N2
4-7	50.45	50.74	0.5748	50.23	49.49	96.57	0.64	2.79	0.25	0.00	0.00	0.00	0.1515	0.3003	22.2	868.2	
4-8	50.37	50.74	0.7346	50.38	50.25	93.71	0.51	5.78	0.72	0.00	0.00	0.00	0.1927	0.3826	22.2	1719.2	
N2						99.74	0.26	0.00	0.00	0.00	0.00	0.00					
orig.air						79.28	20.72	0.00	0.00	0.00	0.00	0.00					

Cell #	initial z factor	initial total gas mol	initial N_2 mol	initial O_2 mol	initial total gas (g)	final temp. °C	final pressure kPa	final z factor	final total gas mol	final N_2 mol	final O_2 mol	final CO_2 mol	final CO mol	O_2 uptake g/g oil	final total gas g	gas mass diff. % oil	total oil mass diff. %
4-1	0.9758	0.3530	0.2798	0.0733	10.1795	46.3	6378.8	0.9841	0.2969	0.2758	0.0013	0.0199	0.0018	0.0461	8.6868	-2.9581	2.2233
4-2	0.9835	0.1792	0.1421	0.0372	5.1683	39	3005.3	0.9888	0.1447	0.1369	0.0006	0.0072	0.0008	0.0234	4.1912	-1.9426	3.2895
4-3	0.9900	0.0959	0.0760	0.0199	2.7647	33.5	1380.6	0.9917	0.0698	~	~	~	~	~	~	~	1.1355
4-6	0.9957	0.0475	0.0474	0.0001	1.3313	39.2	871.7	0.9973	0.0446	0.0445	0.0001	0.0000	0.0000	0.0000	1.2477	-0.1660	0.8013
4-7	0.9948	0.0471	0.0373	0.0098	1.3575	35.5	684.8	0.9941	0.0364	0.0352	0.0002	0.0010	0.0001	0.0061	1.0401	-0.6290	1.5042
4-8	0.9906	0.0892	0.0707	0.0185	2.5737	26.9	1370.9	0.9917	0.0709	0.0664	0.0004	0.0041	0.0005	0.0116	2.0651	-1.0097	2.1269

Table A2.4: Material Balance Spreadsheet for Run # 4

Run5 data

Cell #	initial mass oil (g)	final mass oil (g)	oil mass diff. %	initial mass H_2O (g)	final mass H_2O (g)	GC Analysis Results N_2 mass%	O_2 mass%	CO_2 mass%	CO mass%	CH_4 mass%	C_2H_6 mass%	C_3H_8 mass%	coke contents (g/100gsand)	coke contents mass%	initial temp. °C	initial pressure kPa	initial z factor
5-1	38.76	39.09	0.8514	16.67	~	89.70	0.37	9.72	0.21	0.00	0.00	0.00	0.0867	0.3017	22.2	893.7	0.9946
5-2	38.76	39.07	0.7998	16.67	~	89.76	0.50	9.74	0.00	0.00	0.00	0.00	0.0850	0.2958	22.2	879.2	0.9947
5-3	38.83	39.42	1.5194	16.70	~	89.78	0.85	9.37	0.00	0.00	0.00	0.00	0.0743	0.2586	22.2	881.3	0.9947
5-4	38.79	39.6	2.0882	16.68	~	89.41	0.32	9.91	0.00	0.37	0.00	0.00	0.1836	0.6390	22.2	893.0	0.9946
5-5	38.8	40.47	4.3041	16.68	~	91.63	5.88	2.48	0.00	0.00	0.00	0.00	0.1722	0.5992	22.2	910.3	0.9945
5-6	38.76	39.62	2.2188	16.67	~	89.78	0.78	9.27	0.17	0.00	0.00	0.00	0.0174	0.0607	22.2	882.0	0.9947
5-7	38.77	38.79	0.0516	16.67	~	89.27	0.59	10.14	0.00	0.00	0.00	0.00	0.0939	0.3267	22.2	860.6	0.9948
5-8	38.82	38.88	0.1546	16.69	~	87.18	2.97	9.85	0.00	0.00	0.00	0.00	0.0091	0.0317	22.2	836.5	0.9949
5-9	38.76	38.66	-0.258	16.67	~	90.89	0.43	8.28	0.15	0.25	0.00	0.00	0.0823	0.2865	22.2	1534.4	0.9915
5-10	38.83	38.13	-1.803	16.70	~	93.71	0.19	6.10	0.00	0.00	0.00	0.00	0.0000	0.0000	22.2	865.4	0.9948
orig.air						79.28	20.72	0.00	0.00	0.00	0.00	0.00					
orig.N_2						99.74	0.26	0.00	0.00	0.00	0.00	0.00					

Cell #	initial total gas mol	initial N_2 mol	initial O_2 mol	initial total gas (g)	final temp. °C	final pressure kPa	final z factor	final total gas mol	final N_2 mol	final O_2 mol	final CO_2 mol	final CO mol	final CH_4 mol	final O_2 uptake g/g oil	final total gas g	gas mass diff. % oil	total oil mass diff. %
5-1	0.040	0.0319	0.0084	1.1615	40.3	807.5	0.9949	0.0346	0.0310	0.0001	0.0034	0.0001	0.00000	0.00680	1.0235	-0.3562	0.7969
5-2	0.040	0.0315	0.0082	1.1443	39.0	809.6	0.9948	0.0348	0.0313	0.0002	0.0034	0.0000	0.00000	0.00666	1.0305	-0.2937	0.8020
5-3	0.040	0.0315	0.0083	1.1468	27.8	755.8	0.9941	0.0340	0.0305	0.0003	0.0032	0.0000	0.00000	0.00656	1.0042	-0.3673	1.4107
5-4	0.040	0.0319	0.0084	1.1607	40.3	610.3	0.9959	0.0270	0.0241	0.0001	0.0027	0.0000	0.00010	0.00682	0.7973	-0.9369	1.7903
5-5	0.041	0.0325	0.0085	1.1812	36.1	799.9	0.9963	0.0347	0.0318	0.0020	0.0009	0.0000	0.00000	0.00533	0.9946	-0.4809	4.4224
5-6	0.040	0.0315	0.0083	1.1476	36.4	769.6	0.9949	0.0336	0.0301	0.0003	0.0031	0.0001	0.00000	0.00660	0.9907	-0.4047	1.8748
5-7	0.039	0.0308	0.0081	1.1222	30.4	748.2	0.9942	0.0334	0.0298	0.0002	0.0034	0.0000	0.00000	0.00651	0.9903	-0.3403	0.0379
5-8	0.038	0.0301	0.0079	1.0936	20.8	404.1	0.9959	0.0203	0.0177	0.0006	0.0020	0.0000	0.00000	0.00599	0.6028	-1.2644	-1.0781
5-9	0.067	0.0529	0.0138	1.9240	37.2	1475.7	0.9917	0.0612	0.0556	0.0003	0.0051	0.0001	0.00015	0.01122	1.7934	-0.3371	-0.3085
5-10	0.039	0.0390	0.0001	1.0955	38.2	886.1	0.9954	0.0379	0.0355	0.0001	0.0023	0.0000	0.00000	0.00002	1.0979	0.0061	-1.7967

Table A2.5: Material Balance Spreadsheet for Run # 5

Run6 data

the * shows the coke content including some salts

Cell #	initial mass oil	final mass oil	oil mass diff.	initial mass H_2O	final mass H_2O	GC Analysis Results N_2	O_2	CO_2	CO	CH_4	C_2H_6	C_3H_8	coke contents		initial temp.	initial pressure	initial z factor	initial total gas
	(g)	(g)	%	(g)	(g)	mass%	mass%	mass%	mass%	mass%	mass%	mass%	(g)	mass%	°C	kPa		mol
6-1	50.48	50.6	0.238	50.13	48.8	95.63	0.38	3.99	0.00	0.00	0.00	0.00	-	-	22.2	889.6	0.9946	0.0481
6-2	50.37	50.52	0.298	50.08	48.78	95.46	0.12	4.19	0.00	0.23	0.00	0.00	0.171*	0.34*	22.2	868.2	0.9947	0.0471
6-3	50.1	50.52	0.838	50.14	48.16	90.60	0.30	5.13	0.00	1.91	1.82	0.23	0.068*	0.13*	22.2	903.4	0.9949	0.0488
6-4	50.13	50.38	0.499	50.33	48.53	96.36	2.65	1.00	0.00	0.00	0.00	0.00	0.029*	0.06*	22.2	944.8	0.9943	0.0508
6-5	50.18	50.38	0.399	50.42	50.84	90.47	0.72	8.81	0.00	0.00	0.00	0.00	1.475*	2.93*	22.2	979.2	0.9942	0.0526
6-6	50.68	50.83	0.296	50.19	48.6	95.51	0.23	3.95	0.00	0.32	0.00	0.00	0.073*	0.14*	22.2	892.3	0.9946	0.0483
6-7	50.49	50.53	0.079	50.15	47.8	95.53	0.26	4.00	0.00	0.21	0.00	0.00	0.141*	0.28*	22.2	884.8	0.9947	0.0479
6-8	50.38	50.61	0.457	50.29	50.53	93.69	0.67	5.13	0.51	0.00	0.00	0.00	0.069	0.14	22.2	484.8	0.9968	0.0282
6-9	50.39	50.45	0.119	50.12	49.73	96.22	0.40	3.17	0.21	0.00	0.00	0.00	0.136	0.27	22.2	1568.8	0.9913	0.0818
6-10	50.43	49.57	-1.705	50.27	48.89	94.85	0.47	4.43	0.25	0.00	0.00	0.00	1.163	2.35	22.2	3448.0	0.9837	0.1757
orig.air						79.28	20.72	0.00	0.00	0.00	0.00	0.00						

Cell #	initial N_2	initial O_2	initial total gas	final temp.	final pressure	final z factor	final total gas	final N_2	final O_2	final CO_2	final CO	final CH_4	final C_2H_6	final C_3H_8	O_2 uptake	final total gas	gas mass diff.	total oil mass diff.
	mol	mol	(g)	°C	kPa		mol	mol	mol	mol	mol	mol	mol	mol	g/g oil	g	% oil	%
6-1	0.038	0.010	1.392	32.7	714.4	0.9962	0.0381	0.0364	0.000	0.002	0.000	0.000	0.000	0.000	0.0063	1.0917	-0.5942	0.8319
6-2	0.037	0.010	1.361	42	737.9	0.9968	0.0380	0.0363	0.000	0.002	0.000	0.000	0.000	0.000	0.0063	1.0895	-0.5393	0.4984
6-3	0.039	0.010	1.411	41	792.4	0.9955	0.0407	0.0369	0.000	0.002	0.000	0.001	0.001	0.000	0.0065	1.1676	-0.4855	1.1896
6-4	0.040	0.011	1.470	34.5	696.5	0.9971	0.0370	0.0357	0.001	0.000	0.000	0.000	0.000	0.000	0.0062	1.0459	-0.8469	1.2885
6-5	0.042	0.011	1.520	37.1	806.8	0.9949	0.0419	0.0379	0.000	0.004	0.000	0.000	0.000	0.000	0.0068	1.2344	-0.5685	-1.9609
6-6	0.038	0.010	1.396	35.2	726.8	0.9964	0.0384	0.0366	0.000	0.002	0.000	0.000	0.000	0.000	0.0063	1.0975	-0.5882	0.7412
6-7	0.038	0.010	1.385	33.9	722.7	0.9963	0.0383	0.0366	0.000	0.002	0.000	0.000	0.000	0.000	0.0063	1.0975	-0.5690	0.3697
6-8	0.022	0.006	0.815	32	401.3	0.9974	0.0233	0.0218	0.000	0.001	0.000	0.000	0.000	0.000	0.0037	0.6721	-0.2833	0.6035
6-9	0.065	0.017	2.365	29.9	1355.1	0.9935	0.0693	0.0666	0.000	0.002	0.000	0.000	0.000	0.000	0.0107	1.9756	-0.7718	0.6223
6-10	0.139	0.037	5.082	30.7	2817.0	0.9875	0.1398	0.1326	0.001	0.006	0.000	0.000	0.000	0.000	0.0230	4.0167	-2.1126	-1.9396

Table A2.6: Material Balance Spreadsheet for Run # 6